Gut Microbiota Modulate CD8 T Cell Responses to Influence Colitis-Associated Tumorigenesis

by

Amy I-Wen Yu

A dissertation submitted in partial fulfillment
of the requirements for the degree of
Doctor of Philosophy
(Immunology)
in the University of Michigan
2020

Doctoral Committee:

Associate Professor Grace Y. Chen, Co-Chair
Professor Gabriel Nuñez, Co-Chair
Associate Professor Eric C. Martens
Professor Asma Nusrat
Associate Professor Yatrik Shah

Amy I-Wen Yu
aiyu@umich.edu
ORCID: 0000-0002-0219-7359

DEDICATION

媽媽, 爸爸, 謝謝你們不斷的支持我.

I would like to dedicate this dissertation to my family. Thank you for everything.

ACKNOWLEDGEMENTS

I want to thank my dissertation advisor Dr. Grace Chen for her guidance, support, and encouragement. She gave me room to explore and take my project in the directions I wanted, allowing me to grow into an independent scientist. I also want to thank my thesis committee members, Drs. Gabriel Nuñez, Eric Martens, Asma Nusrat, and Yatrik Shah, for their continual support, feedback, and scientific input.

In addition, I would like to thank all the past and present members of the lab as they have provided levity and support whenever needed. I've also had the immense joy of mentoring four undergraduate students; it's been so rewarding to see them grow as people and scientists. I would also like to specifically thank Dr. Sergey Seregin and Jiachen Chen for their guidance and advice in both science and life.

As per usual for science, this project would not have been possible without the generous assistance of others. This project would not have been possible without the Gabriel Nuñez and Eric Martens labs. The Nobuhiko Kamada and Naohiro Inohara labs have also provided scientific support and discussion. Dr. Kathryn A. Eaton assisted with histological scoring, and Dr. Lili Zhao provided statistical support. Thank you to Dr. Hideaki Fujiwara, who helped with intravenous injections, and the rest of the Pavan Reddy lab who have been the best lab neighbor anyone could ask for. Thank you to all the University of Michigan science cores who have provided scientific support. The Immunology Program has also been incredibly wonderful and supportive. Spotify, Netflix, and Hulu have been essential during my time writing this dissertation, especially under shelter-in conditions. This work was supported by the following funding sources: University of Michigan Rackham Research Grants and NIH grant T32 AI007413 (A.I.Y.), and NIH grant R01 CA166879, an American Cancer Society Research Scholar Grant, and the Tom Liu Memorial Golf Tournament Fund from the University of Michigan Rogel Cancer Center (G.Y.C.).

Lastly, I would like to thank my friends and family. Thank you for your unwavering confidence in me. I could not have done this without all of you.

TABLE OF CONTENTS

LIST OF FIGURES

ABSTRACT

The gut microbiome plays important physiological roles, including aiding in digestion of non-digestible starches and fibers, production of nutrients, protection against pathogens, as well as inducing mucosal immune system development. Disturbances to the composition of the gut microbiome are associated with intestinal disease including inflammatory bowel disease (IBD) and colorectal cancer (CRC), where CRC is the third most common cancer in both men and women in the United States. There is increasing evidence that CRC patients have altered microbiomes compared to healthy controls; specific bacteria known to be increased in CRC patients include *E. coli* with the *pks* pathogenicity island, enterotoxigenic *B. fragilis and F. nucleatum*. Additionally, specific microbiota have been shown to modulate host immunity, but the mechanisms by which the gut microbiota can contribute to colon carcinogenesis remain to be fully elucidated.

Our lab is interested in studying the interplay between the gut microbiome and CRC development. Using the azoxymethane (AOM)/dextran sulfate sodium (DSS) mouse model of colitis-associated colorectal cancer (CAC), our lab discovered two colonies of specific pathogen free (SPF) C57BL/6J wild type (WT) mice housed in the same mouse room that develop differential tumor burdens. Mice from the "WT1" colony developed five tumors on average while mice from the "WT2" colony developed 15 tumors on average. The increased tumor susceptibility in WT2 mice can be directly attributed to the gut microbiome as germ-free (GF) WT mice, where GF mice are sterile and have no microbiota, colonized with WT2 bacteria developed more tumors compared to that of GF WT mice colonized with WT1 bacteria. Additionally, 16S rRNA gene sequencing of fecal bacteria from WT1 and WT2 mice revealed distinct microbiomes with certain bacteria consistently associated with high or low tumor numbers.

As the microbiome can promote altered immunity, we further examined SPF WT1 and WT2 immune compositions. Immunologically, naïve and acutely-inflamed (day 12 of AOM/DSS) WT2 mice have increased colon lamina propria (LP) $CD8^+$ $IFN\gamma^+$ T cells compared to WT1 mice as measured by flow cytometry. Bone marrow-derived dendritic cells (BMDCs) stimulated with WT2 bacteria produced increased IL-12, a cytokine that induces increased IFNγ activity by CD8

T cells, compared to BMDCs stimulated with WT1 bacteria. Additionally, introduction of WT2 microbiota promoted an increase in colon LP $CD8^+$ $IFN\gamma^+$ T cells in GF WT and microbiome-depleted SPF WT1 mice. However, in tumor-bearing WT2 mice, there was decreased tumor-infiltrating $CD8^+$ T cells with reduced IFNγ production, where these cells are increasingly exhausted. GF *Rag1*$^{-/-}$ mice as well as SPF *CD8*$^{-/-}$ mice inoculated with WT2 gut microbiota developed fewer tumors than SPF WT2 mice, suggesting that the gut microbiome of WT2 mice increases tumor susceptibility, in part, through an effect on CD8 T cells. Altogether, our data reveals a potential novel role of microbiota in altering colon CD8 T cell function that ultimately impacts colon cancer risk.

CHAPTER 1: Introduction

1.1 Colorectal cancer overview

1.1.1 Colorectal cancer global patterns

Colorectal cancer (CRC) is the third most common cause of cancer and fourth leading cause of cancer-related deaths worldwide (1). While incidence and mortality rates are declining in the United States, Western Europe, and Australia, likely due to increased and improved screening and therapies, CRC incidence rates are rising in Asia, Eastern Europe and South America. This may be attributable to westernization and economic transitioning of countries as a higher incidence of CRC has typically been associated with economically developed countries (1, 2). In addition, there has been a disturbing increase in incidence of young onset colorectal cancer, and in particular, rectal cancer in individuals aged 50 years and younger. This rise in incidence cannot be entirely explained by genetic predispositions, and suggests lifestyle and environment factors potentially play a role (3). Besides genetic predisposition and inflammatory bowel disease (IBD), which account for a small percentage of CRC, risk factors related to dietary and lifestyle habits include smoking, obesity, increased alcoholic consumption, and a diet rich in red meat and reduced in whole grains and dairy (4, 5). Many of these factors can influence or be influenced by the composition of the microbiota (6-11).

In addition, just as different parts of the colon are associated with specific subtypes of CRC, the composition of the gut microbiota also changes with anatomic location, further suggesting a potential link between the microbiota and CRC pathogenesis (2, 12-14). Thus, there is increasing interest in understanding the role of the gut microbiome in dictating CRC risk. Indeed, there is now significant evidence that the gut microbiome composition is altered in patients with CRC and that these perturbations from a healthy state, often referred to as dysbiosis, may contribute to the development and/or progression of CRC.

1.1.2 The microbiome and colorectal cancer

The gut microbiome is comprised of commensal bacteria, Archaea, viruses, fungi, and more. In this thesis, we focus on the role of the bacteria component of the colon microbiome, which consists of trillions of bacteria of at least 1000 different species and plays an important role in the promoting health and intestinal homeostasis (15, 16). For example, gut microbiota are required for the digestion and provision of certain nutrients including resistant starches and vitamins, the development and education of the host immune system, and resistance against colonization by harmful pathogens (16-18).

The gut microbiota is dominated by two phyla, Bacteroidetes and Firmicutes, but also includes Actinobacteria, Fusobacteria, Proteobacteria, and Verrucomicrobia (19, 20). Although there is significant inter-individual heterogeneity in the composition of the gut microbiota such that a "core" microbiome has not been identified, the human microbiome may be stratified into specific enterotypes defined by the relative abundance of certain phylotypes, such as *Bacteroides*, *Prevotella*, and *Ruminococcus* genera, as well as co-occurring bacterial species found in the healthy human gut (7, 19, 21, 22). On the other hand, there is much more similarity in the functional gene content of the gut microbiome and the metabolic pathways they represent between individuals (7). These observations suggest the possibility of using the composition of the microbiota and the metabolites they produce as potential biomarkers or therapeutic targets for disease.

When the microbiome is perturbed, a dysbiotic or imbalanced microbiome can occur which can lead to colon inflammation and intestinal pathology including infectious colitis, IBD, and CRC (23). For instance, multiple studies have shown that IBD and CRC patients have a dysbiotic microbiome community represented by decreased Firmicutes and increased Bacteroidetes bacteria compared to healthy controls. In this chapter, we discuss mechanisms of how specific microbiota promote CRC. Consistently, studies of CRC patients have identified potential metabolic signatures (24, 25).

1.2 Dysbiosis in colorectal cancer

1.2.1 Background

There are a growing number of studies that show differences in the composition of the gut microbiome between individuals who are healthy or have CRC (**Table 1**). Identifying specific bacteria that are found in all cases of CRC, however, has been more of a challenge and may reflect pre-existing inter-individual heterogeneity, the relatively small numbers of patients examined to date, limitations in taxonomic resolution to the species level, differences in the source material used for sequencing analysis (e.g. tissue versus stool), and differences in sequencing method. Most studies evaluating the presence of dysbiosis in CRC patients have been small, case-control studies, typically less than 100 subjects per group, comparing either fecal or tissue samples from CRC patients and normal, healthy controls, some of which were performed with the goal of identifying potential microbial biomarkers of disease. These studies have not showed significant concordance on specific species that are predictive of or are associated with CRC; however, CRC patients generally have altered gut microbiomes, characterized by decreased Firmicutes and increased Bacteroidetes bacteria compared to healthy controls (26-29).

Despite the lack of significant concordance between studies on microbiome differences between CRC and non-CRC control subjects to date, multiple studies have reported an enrichment of *Fusobacterium nucleatum* as well as oral commensal and pathogenic bacteria such as *Porphyromonas* spp., *Prevotella* spp., and *Streptococcus* spp. in CRC patients (30, 31). Although the reason behind this association is poorly understood, it has been posited that the ability of oral bacteria to produce and reside in biofilms enables them to colonize and adhere to the colon epithelium under predisposing conditions (e.g., during inflammation) that result in CRC development (16, 32). Consistently, the presence of biofilms is associated with the development of CRC, particularly in the proximal colon, and consistently, increased colonization of *Fusobacterium* has been observed in right-sided colon cancers (33).

Despite the fact that *Fusobacterium* and other oral microbes are repeatedly identified in colon tumor tissue, one study suggests that the presence of these bacteria is still not predictive of CRC (34). Rather, the depletion of typically beneficial bacteria such as those capable of producing butyrate and other short chain fatty acids (e.g., *Ruminococcoaceae*, *Lachnospiraceae* and *Eubacterium* spp.) were more strongly predictive of CRC (34). A meta-analysis identified eight

taxa whose fecal abundance were significantly associated with carcinomas, namely, *Fusobacterium, Parvimonas, Porphyromonas* and *Peptostreptococcu*s, which are commonly found in the oral cavity, and *Clostridium, Enterobacteriaceae, Escherichia*, and *Ruminococcus*, where decreases in *Clostridium* and *Ruminococcus* are associated with CRC (35). Interestingly, no individual taxa were sufficient to predict for the presence of cancer, suggesting that multiple bacterial populations contribute to cancer susceptibility (35).

Whether the altered microbiomes observed in CRC patients cause the development of CRC or occur as a result of carcinogenesis and cancer progression remains unclear. In a longitudinal study of patients who developed CRC, the reversion of the gut microbiome to that associated with a normal colon in patients after treatment of their colorectal cancer suggests that a CRC-associated microbiome may in fact contribute to disease (36). In addition, studies using germfree (GF) mice strongly suggest that dysbiosis directly contributes to colon tumorigenesis (37). A commonly used mouse model to study the effects of the microbiota on colon carcinogenesis is the azoxymethane-dextran sulfate sodium (AOM/DSS) model of inflammation-associated colon cancer in which mice are treated with the experimental carcinogen AOM followed by multiple rounds of water containing DSS, which causes bacteria-driven inflammation in the colon by disrupting the epithelial barrier (38). This results in the generation of adenomatous polyps, which although are premalignant, can eventually progress into adenocarcinomas, and therefore, have been used as a surrogate marker for cancer (38). AOM/DSS treatment also causes microbiome alterations similar to that of human CRC patients, including reduced species richness and alpha diversity and significant shifts in beta diversity (37). Using this model, it was shown that the colonization of GF C57BL/6 (B6) mice with the microbiome of tumor-bearing AOM/DSS-treated mice resulted in significantly more and larger tumors compared to GF mice colonized with the microbiota of healthy, untreated mice (37). Similarly, conventionalization of GF B6 mice with the fecal microbiome of five CRC patients also resulted in increased tumors, intestinal dysplasia, and inflammation after injection of a single dose of AOM compared to GF mice that were gavaged with stool from healthy controls (39). $Apc^{Min/+}$ mice, which spontaneously develop intestinal tumors due to a mutation in the tumor suppressor gene Apc that occurs in the majority of human CRC, developed more tumors after gavage of fecal contents from CRC patients than from healthy controls (40). The potential carcinogenicity of biofilm-associated microbiota was demonstrated in a study in which GF *Apc* mutant mice developed significantly more tumors when gavaged with

the homogenates of biofilm-positive colon mucosa compared to biofilm-negative colon mucosa (41). However, in one study, GF B6 mice that were gavaged with the stool from either three CRC or three healthy individuals had different susceptibilities to colon tumorigenesis after AOM/DSS treatment that did not correlate with donor cancer status, which may in part be due to incomplete reconstitution of GF mice with human donor microbiota (28). As human-derived microbiota may not interact with the mouse immune system in the same way as an indigenous mouse microbiota, studies involving "humanized" GF mice should still be interpreted with caution although remain one of the few methods to evaluate causality between the microbiome and disease (42, 43).

1.2.2 *Fusobacterium nucleatum*

Fusobacterium spp. were first noted to be enriched in tumors compared to normal adjacent tissue in a small study of six CRC patients (44). This was further confirmed in a larger study of 95 paired tumor and normal tissue from CRC patients in which there was over-representation of the *Fusobacterium* taxon, including *Fusobacterium nucleatum* (45). *F. nucleatum* is a Gram-negative, anaerobic bacterium typically found in the oral cavity and was initially recognized to promote gingivitis and periodontitis (46, 47). Transcriptomic analysis of tumor tissue from 11 matched pairs of CRC and adjacent normal tissue revealed that *Fusobacterium nucleatum* was disproportionately increased in most tumor tissue samples, although it was not more abundant in all cases (48). Increased *Fusobacterum* spp. were also found to be increased in premalignant adenomatous tissue compared to adjacent tissues, suggesting that *Fusobacterium* may be involved in tumor progression. Indeed, oral gavage of *F. nucleatum* into $Apc^{Min/+}$ mice increased the growth and number of tumors that developed (49). Examination of over 1069 cases of CRC from two large U.S. prospective cohort studies, the Nurses' Health Study and the Health Professionals Follow-up Study, revealed detectable *F. nucleatum* DNA in only 13% of cases, although tissue fixation may have affected the detection of *F. nucleatum* in this particular study (50). Interestingly, *F. nucleatum* DNA levels directly correlated with CRC-specific mortality, proximal tumor location, and poor tumor differentiation (33, 51). Furthermore, higher levels of *F. nucleatum* DNA correlated with microsatellite instability (MSI-high) and the CpG island methylator phenotype (CIMP-high), which was also observed in a second retrospective analysis of 246 Asian patients (50). *F. nucleatum* was also more abundant in the tumor tissue of patients who had recurrences, suggesting *F. nucleatum* can promote chemotherapy resistance (52). Altogether, these studies suggest that the presence of *F. nucleatum* in CRC tissue correlates with poorer prognosis. The link between *F.*

nucleatum with microsatellite instability is interesting given that *F. nucleatum* levels are otherwise associated with poor prognostic features since patients with MSI-high tumors tend to have better prognosis. This may reflect the fact that MSI-high tumors tend to be located in the proximal colon which coincides with the preferential location of *F. nucleatum* in biofilms that are dominant on the right side in both tumors and normal adjacent tissue and not on the left (53). Regardless, it remains unclear why *Fusobacterium* preferentially colonizes proximal tumors. How it affects tumor biology is also not fully understood; however, as it has been shown to preferentially bind to CRC cells rather than pre-cancerous adenoma cells and induces their cellular proliferation, it has been suggested that it acts as a cancer promoter rather than as an initiator (54).

1.2.3 Enterotoxigenic *Bacteroides fragilis*

Enterotoxigenic *B. fragilis* (ETBF) is a strain of *B. fragilis* characterized by the expression of the zinc-dependent metalloprotease toxin *B. fragilis* toxin (BFT). ETBF causes inflammatory diarrhea in children and asymptomatically colonizes 20-35% of adults (55). A potential link between ETBF and colon carcinogenesis was suggested by a study in which inoculation of $Apc^{Min/+}$ mice with ETBF, but not non-toxigenic *B. fragilis* (NTBF), increased tumor numbers (56). Subsequently, at least two studies were able to identify enhanced levels of ETBF and the BFT gene (*bft*) in the stool of CRC patients by PCR although the numbers of patients evaluated were small ($\leq$ 100) (57, 58). Interestingly, like *F. nucleatum*, *B. fragilis* and the *bft* gene can be found in biofilms that largely occur in the proximal colon and are also prevalent in patients with familial adenomatous polyposis (FAP), a hereditary condition in which the *Apc* gene is mutated and universally leads to the development of CRC, suggesting the interesting possibility that biofilm formation and aggregation of cancer-associated microbiota may be a precursor to and predictive of malignant transformation (53, 59). In addition, like *F. nucleatum, B. fragilis* was increased in biofilms associated with right-sided CRC (60). Also consistent with the enrichment of *B. fragilis* in right-sided colon tumors, *B. fragilis* is more abundant in MSI-high tumors; however, in a study of 83 individuals with CRC, there was no significant difference in the presence of the *bft* gene between MSI-high and microsatellite stable (MSS) CRC (61).

1.2.4 *Escherichia coli*

Several studies suggest a possible role for *E. coli* in promoting CRC. In one study, 90-92% of CRC patients had tumor-associated bacteria compared to 3% of healthy controls where *E. coli*

was enriched in 62-77% of CRC patients (62). Another study found 71% of CRC patients to have mucosa-associated bacteria where the majority of the gram-negative mucosa-associated bacteria were *E. coli* (63). Finally, in a third study, mucosa-associated *E. coli* were found in 50% of adenocarcinoma samples (64). *E. coli* in the B2 phylogenic group are enriched for the polyketide synthase (pks) genomic island which encodes the genotoxin called colibactin (65).

A role for *pks*+ *E. coli*, specifically, in modulating susceptibility for colon tumorigenesis was discovered in a seminal study by Arthur et al., in which increased *pks*+ *E. coli* was observed in 21 CRC tissue specimens compared to 24 non-CRC controls (66.7% versus 20.8%) (66). The accumulation of this bacterium in tumors may, in part, be due to the presence of chronic inflammation as *pks*+ *E. coli* were also enriched in patients with IBD, a major risk factor for the development of colitis-associated CRC. In mice, Arthur et al. found increased colonization of *E. coli* in conventionalized GF *Il10*$^{-/-}$ mice, which developed spontaneous colitis in SPF conditions, compared to that of conventionalized GF WT mice that do not develop colitis (66). This is consistent with the association of *Enterobacteriaceae* and *E. coli* in IBD and suggests that inflammation promotes the bloom of *E. coli* that occurs prior to frank carcinogenesis (66, 67). More importantly, mono-association of GF *Il10*$^{-/-}$ mice treated with the carcinogen AOM, which results in the development of inflammation-associated colon tumors, with *pks*+ *E. coli*, but not *pks*-deficient *E. coli*, resulted in increased numbers of invasive adenocarcinomas. The ability of *pks*+ *E. coli* to promote colon tumorigenesis was not necessarily due to an effect on inflammation as GF *Il10*$^{-/-}$ mice mono-associated with *pks*-deficient *E. coli* or *E. faecalis*, both of which induced similar levels of colitis as *pks*+ *E. coli*, did not result in any tumors (66). However, in the context of IL-10 deficiency, inflammation is required for the tumor-promoting effects of *pks*+ *E. coli*, as *Il10*$^{-/-}$ mice that were also deficient in T cells (*Il10*$^{-/-}$*;Rag2*$^{-/-}$) are non-colitic and did not develop tumors after AOM treatment despite the presence of similar levels of *pks*+ *E. coli* (68). Subsequent studies using other mouse models, namely, the AOM/DSS, *Apc*$^{Min/+}$, and human xenograft models of colon tumorigenesis also demonstrated a tumor-enhancing effect for *E. coli* in specific pathogen-free (SPF) mice (69, 70).

E. coli of the B2 phylotype is also capable of forming biofilms, which may contribute to their ability to adhere to intestinal epithelium and colonize the gut (71). Consistently, *pks*+ *E. coli* was identified in the biofilms of FAP patients in addition to *B. fragilis* (59). Regardless, it is important to note that *pks*+ *E. coli* has not been consistently observed to be significantly elevated

in all CRC patient cohorts compared to non-CRC controls, and therefore other bacteria likely contribute or are required for full malignant transformation (59, 71). Indeed, in GF genetically-engineered mouse models of CRC, colonization of mice with both *B. fragilis* and *pks+ E coli* alone resulted in significantly greater tumor induction including adenocarcinoma formation compared to either alone (59).

Table 1 Microbiome studies involving stool samples of individuals with colorectal cancer

Study	Country	Sample Sizes	Sequencing	Major Findings
(72)	France	6 CRC patients, 6 healthy controls	V3/V4 region, pyrosequencing	• Bacteroides/Prevotella group bacteria are increased in CRC patients compared to healthy controls
(26)	China	46 CRC patients, 56 healthy controls	V3 region, pyrosequencing	• Bacteroidetes phylum bacteria significantly increased in healthy controls and Proteobacteria phylum bacteria significantly increased in CRC patients • Bacteroides, Roseburia, Alistipes, Eubacterium and Parasutterella genera increased in healthy controls • Porphyromonas, Escherichia/Shigella, Enterococcus, Streptococcus and Peptostreptococcus genera increased in CRC patients • Healthy controls were enriched in OTUs of Alistipes, Phascolarctobacterium, Oscillibacter, unclassified genera of the order Clostridiales, as well as butyrate-producing Roseburia and the Lachnospiraceae family. • CRC patients were enriched in OTUs from Escherichia/Shigella, Klebsiella, Streptococcus, Enterococcus, Peptostreptococcus, Eggerthella, Fusobacterium, and Gemella genera, as well as Citrobacter from the Enterobacteriaceae family
(73)	China	Stool: 21 CRC patients, 22 healthy controls Lumen swabs: 32 CRC patients, 34 healthy controls	V1-V3, pyrosequencing	• Erysipelotrichaceae, Prevotellaceae, Coriobacteriaceae, and Peptostreptococcaceae family bacteria are enriched in CRC patient intestinal lumens compared to healthy controls • Peptostreptococcus, Porphyromonas, Mogibacterium, Anaerococcus, Slackia, Anaerotruncus, Collinsella, Desulfovibrio, Eubacterium and Paraprevotella genera bacteria are enriched in CRC patient stool compared to healthy controls
(27)	USA	47 CRC patients, 94 healthy controls	V3-V4 region, pyrosequencing	• CRC patients have decreased community diversity but no difference in community evenness compared to healthy controls • CRC patients have increased Bacteroidetes and decreased Firmicutes bacteria • In the Firmicutes, the Clostridia family, which include butyrate procuders, are particularly reduced in CRC patients • Fusobacterium, Atopobium and Porphyromonas genera are increased in CRC patients
(74)	China	47 CRC (advanced colorectal adenoma) patients, 47 healthy controls	V1-V3 region, pyrosequencing	• Clostridium, Roseburia, and Eubacterium genera (butyrate producers) are reduced in CRC patients • Enterococcus, Streptococcus, and Bacteroidetes genera are enriched in CRC patients

(75)	USA	11 CRC, 10 healthy controls	V4 region, pyrosequencing	• Several Bacteroides and Prevotella spp. as well as Dialister and Megamonas spp. enriched in healthy controls • Increased representation of Akkermansia in colorectal cancer patients
(29)	USA and Canada	30 CRC (carcinoma) patients, 30 adenoma patients, 30 healthy controls	V4 region, Illumina MiSeq (16S rRNA sequencing)	• CRC patients are enriched for Fusobacterium, Porphyromonas, Lachnospiraceae, and Enterobacteriaceae bactiera and reduced Bacteroides, Lachnospiraceae, and Clostridiales bacteria
(76)	France	53 CRC (carcinoma) patients, 42 adenoma patients, 61 healthy controls	V4 region, Illumina MiSeq (16S rRNA sequencing); Illumina HiSeq (metagenome)	• Bacteroidetes, Fusobacteria, and Proteobacteria are enriched in CRC patients; Firmicutes and Actinobacteria bacteria are reduced in CRC patients • Healthy control metagenomes are enriched for fiber-degrading enzymes and fiber-binding domains • CRC patient metagenomes suggest an increase in degradation of host glycans and amino acid uptake
(77)	Austria	41 CRC patients, 42 adenoma patients, 55 healthy controls	Illumina HiSeq (metagenome)	•Bacteroides and Parabacteroides spp. as well as Alistipes putredinis, Bilophila wadsworthia, Lachnospiraceae bacterium and E. coli enriched in CRC compared with healthy and advanced adenomas. Fusobacterium, Pavimonas micra, Gemella morbillorum and Peptrostreptococcus stomatis elevated in carcinomas and adenomas compared with control •Bifidobactum animalis and Streptococcus thermophilus decreased in feces from adenoma or CRC patients
(34)	USA and Canada	120 CRC patients, 198 adenoma patients, 172 no colonic lesions	V4 region, Illumina MiSeq (16S rRNA sequencing)	• Depletion of Lachnospiraceae and Ruminococcoaceae families (butyrate-producers) in CRC • Higher levels of Fusobacterium, Porphyromonas, Parvimonas, Peptostreptococcus and Prevotella in CRC
(30)	Ireland	59 CRC patients, 21 individuals with polyps, 56 healthy controls	V3/V4 region, Illumina MiSeq (16S rRNA sequencing)	• CRC patients are enriched for Bacteroides, Roseburia, Ruminococcus, Oscillibacter genera and certain genera containing known oral pathogens such as Fusobacterium and Porphyromonas • CRC patients enriched for bacteria in the Prevotella and Pathogen bacteria clusters and positively correlated with CXCL1, SERPINE1, and IL-17a and IL-23 genes • Microbiota composition differed between proximal and distal colon tumors
(78)	China	74 CRC patients, 54 healthy controls	Illumina HiSeq (metagenome)	• Strong association between Parvimonas, Fusobacterium, Solobacterium, and Peptotreptococcus with CRC

1.3 Mechanisms by which gut microbiota contribute to CRC

As discussed above, there are a number of well-studied bacteria that are linked to CRC. Although the mechanisms by which CRC-associated bacteria and dysbiosis in general promotes CRC development remains to be fully elucidated, studies, largely in mice, suggest a mechanism related to an effect on host immune responses, tumor suppressor activity, epithelial transformation and cellular proliferation via the production of bacterial immunostimulatory molecules, microbial metabolites, and genotoxins. These mechanisms are summarized below in **Figure 1**.

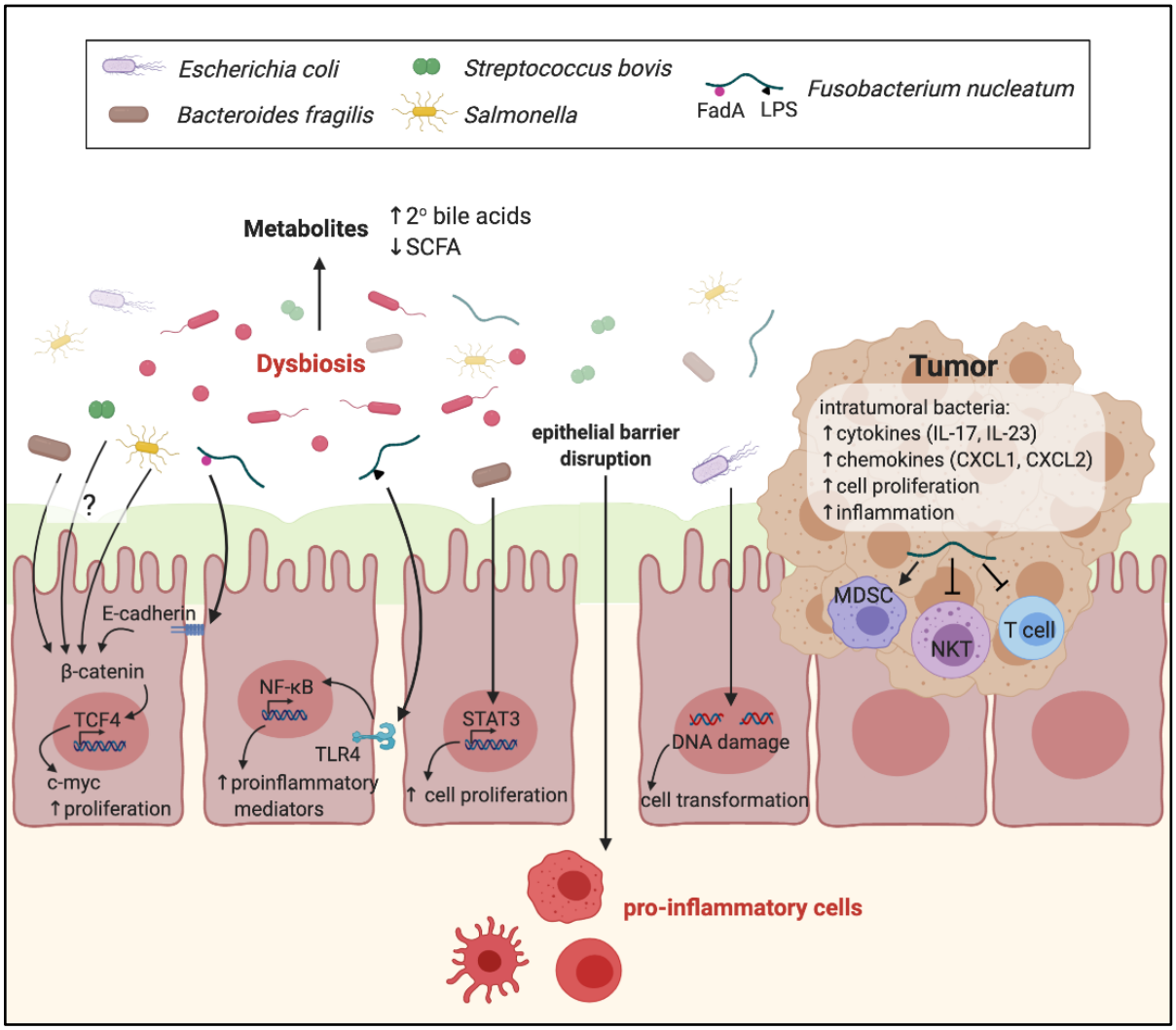

Figure 1 Microbial mechanisms of CRC induction
Specific microbiota can directly promote CRC through mechanisms such as activating Wnt cell cycle signaling (enterotoxigenic *B. fragilis*, *S. bovis*, *Salmonella*, and *F. nucleatum*), promoting inflammatory gene transcription (*F. nucleatum*) and epithelial cell proliferation (*B. fragilis*), and causing DNA damage that lead to mutations and chromosomal instability (*E. coli* with the polyketide synthase pathogenicity island). Furthermore, bacterial metabolites can promote anti- or pro-tumorigenic responses through inhibiting inflammation (SCFAs) or promoting DNA damage and activating cell cycle signaling pathways (secondary bile acids). The specifics of these mechanisms are discussed

in this chapter. CRC, colorectal cancer; LPS, lipopolysaccharide binding protein; SCFA, short chain fatty acid; TCF4, transcription factor 4; NF-κB, nuclear factor kappa-light-chain-enhancer of activated B cells; TLR4, Toll-like receptor 4; STAT3, signal transducer and activator of transcription 3; MDSC, myeloid-derived suppressor cell; NKT, natural killer T cell. The figure image was made with BioRender.com.

1.3.1 Modulation of host immune responses

The gut microbiome is increasingly recognized as having a role in modulating both host immunity and susceptibility to colon tumorigenesis. For example, the gut microbiota can influence frequencies of intestinal lamina propria (LP) immune cells, notably regulatory T cells (Tregs) and T helper 17 (Th17) cells (79-81) which can affect inflammatory responses and tumor susceptibility (56, 82, 83). Recently, certain human gut bacteria have been associated with IFNγ production by CD8 T cells and the promotion of antitumor immunity in mice (84). How these immunomodulatory activities ultimately contribute to colon cancer susceptibility remains to be fully elucidated.

Chronic inflammation is a major risk factor for the development of CRC. An inflammatory response arises when tissue homeostasis is disrupted and is characterized by the recruitment of inflammatory cells to damaged tissue and production of soluble factors to promote tissue repair. These soluble factors promote cellular survival and proliferation, angiogenesis, and matrix remodeling that are required for effective tissue repair and regeneration (85). However, with chronic inflammation that is not self-limited, these same factors can result in the generation of DNA-damaging reactive oxygen species that can initiate tumorigenesis as well as promote a microenvironment that is conducive to tumor growth and survival (85). Thus, patients with IBD, for example, have a substantially increased risk for developing CRC. Inflammation also plays a role in the pathogenesis of sporadic CRCs as elevations in cytokines such as IL-8, IL-17, and IL-23 have been observed in the serum and tissue of CRC patients (86-89). In the context of a breached epithelial barrier, the gut microbiome can further induce inflammation by stimulating innate immune receptors, such as the Toll-like receptors (TLRs) (89). In mice that harbor a mutation in the *Apc* tumor suppressor gene, colon tumors exhibit increased intestinal permeability indicative of a disrupted epithelial barrier, and the presence of intratumoral bacteria is associated with upregulation of IL-17 and IL-23 expression that is TLR-dependent (89). Deficiency in either IL-17 or IL-23 ameliorated tumorigenesis (89). Thus, shifts in the microbial community that result in the accumulation of bacteria that are highly immunostimulatory and pro-inflammatory would be a potential mechanism by which dysbiosis and CRC-associated microbiota can potentiate

tumorigenesis. Consistently, treatment of mice with antibiotics prior to the development of dysbiosis results in reduction in tumor numbers in the AOM/DSS model of colon tumorigenesis (37).

F. nucleatum also interacts with the immune system and stimulates cytokine production through TLR4 and can be sensed by retinoic acid-inducible gene I (RIG-I) (90, 91). In periodontal disease, NK cells can recognize and bind to *F. nucleatum* via the NK killer receptor, NKp46 in humans, or NCR1 in mice, which promotes a TNF-α inflammatory response that promotes disease (92). Although *F. nucleatum* does not instigate or worsen intestinal inflammation in mice, daily gavage of *F. nucleatum* into $Apc^{Min/+}$ mice resulted in expansion of tumor infiltrating myeloid cells, which are capable of promoting tumorigenesis, as well as upregulation of pro-inflammatory genes in tumor tissue similar to what is observed in human CRC tissue (49).

The induction of chronic inflammation is also a potential mechanism by which ETBF promotes tumorigenesis as colonization of WT GF mice with ETBF results in colitis (93). ETBF-colonized $Apc^{Min/+}$ mice also developed inflammation in the colon, resulting in epithelial hyperplasia and neoplasia. Mechanistically, ETBF-colonized $Apc^{Min/+}$ mice had increased colonic IL-17 expression, which, in turn, activates NF-κB signaling in colon epithelial cells to promote the production of the chemokines CXCL1, CXCL2, and CXCL5, which are neutrophil chemoattractants, in the distal colon (56, 94). Consistently, ETBF-colonized mice have increased colon and intratumoral neutrophils that is dependent on IL-17 and CXCL2 signaling (94, 95). Loss of IL-17 signaling either by antibody blockade or by genetic deletion in $Apc^{Min/+}$ mice resulted in suppression of tumors after ETBF colonization (56, 94). In vitro studies using human intestinal epithelial cell lines further show that BFT treatment induces IL-8 chemokine expression, which is increased in IBD patient colons (96-99). Furthermore, IL-8 secretion by BFT-treated HT29/C1 cells is NF-κB-dependent via activation of ERK and p38 MAPK pathways (99, 100).

Although chronically dysregulated inflammation can lead to tumorigenesis, an effective immune response is also important for protecting against cancer development as exemplified by the increased incidence of cancer in immunocompromised patients. Immune responses can lead to the recruitment of immune cells, such as cytotoxic lymphocytes, that can eliminate nascent transformed cells in a process known as tumor immunoediting, or immune surveillance (101). Studies of biopsy samples from colon cancer patients suggest that a robust immune response as

measured by increased infiltration of activated T cells at the site of the cancer is associated with better prognosis and less aggressive behavior of the cancer (102, 103).

Specifically, *F. nucleatum* has been shown to promote an immunosuppressive environment. When measured in colorectal carcinoma tissue, *F. nucleatum* was associated with a lower density of $CD3^+$ T cells (104). Additionally, NK cells are less cytotoxic to *F. nucleatum*-incubated tumor cells compared to tumor cells not incubated with *F. nucleatum* (105). The *F. nucleatum* protein Fap2 interacts with the receptor T cell immunoreceptor with Ig and ITIM domains (TIGIT) on intratumoral NK and T cells to inhibit tumor cell killing (105). Finally, *F. nucleatum*-colonized $Apc^{Min/+}$ mice had increased intratumoral myeloid-derived suppressor cells (MDSCs), which are capable of suppressing CD4 T cells (49). In ETBF-colonized $Apc^{Min/+}$ mice, tumor-infiltrating neutrophils have a transcriptional signature similar to MDSCs, including upregulation of iNOS, and were able suppress CD8 T cell proliferation *in vitro,* suggesting that *B. fragilis* may also affect anti-tumor immunity (95).

Thus, CRC-associated microbiota such as *F. nucleatum* and ETBF may not only accelerate tumorigenesis via upregulating tumor-promoting pro-inflammatory mediators, but also promote a tumor environment that is deficient in anti-tumor activity.

1.3.2 Stimulation of cellular proliferation

In addition to altering inflammatory and immune responses, CRC-associated bacteria can also act directly on the intestinal epithelium to activate pathways involved in cellular proliferation. For example, *F. nucleatum* is known to have adherent and invasive properties via its FadA adhesin (106, 107), which is highly expressed in human adenoma and adenocarcinoma tissues compared to tissue from healthy patients (108). It was shown that FadA binds to E-cadherin (*CDH1*), which is expressed by epithelial cells, enabling *F. nucleatum*'s invasion into the host cell (108). Furthermore, binding of FadA to E-cadherin promotes E-cadherin's phosphorylation and internalization into the host cell, resulting in increased β-catenin translocation into the nucleus and increased transcription of Wnt signaling genes, including the oncogenes *c-myc* and cyclin D1 (108), which are directly involved in cellular proliferation and stem cell activity. Consistently, FadA increases the proliferative activity of multiple human CRC cells *in vitro* and *in vivo* in a FadA-dependent manner (108). FadA also upregulates the expression of the phospholipid-binding protein annexin A1 (*ANXA1*) in CRC cells via E-cadherin, and *ANXA1* can engage β-catenin to activate cyclin D1 to promote cellular proliferation (54).

Other CRC-associated microbiota such as *B. fragilis* and *Salmonella* can affect Wnt signaling to facilitate neoplastic transformation. In the case of *B. fragilis*, treatment of the CRC cell line HT29/C1 with BFT resulted in the cleavage of E-cadherin and activation of β-catenin, resulting in increased *c-myc* transcription and cellular proliferation (109, 110). Additionally, infection by *Salmonella enterica* serovar Typhimurium with the *Salmonella* effector protein AvrA is also associated with activated β-catenin signaling in colon epithelial cells (111). AvrA displays deubiquitinase activity and was able to block the degradation of IκBα and β-catenin, resulting in increased *c-myc* protein expression (112). Consistently, tumors from AOM/DSS-treated AvrA+ *S. enterica* ser. Typhimurium-infected mice displayed increased phosphorylated *c-myc* expression compared to AvrA- *S. enterica* ser. Typhimurium tumors (113).

Bacteria can also stimulate cellular proliferation via mechanisms that do not necessarily involve Wnt signaling. For example, *B. fragilis* colonization of $Apc^{Min/+}$ mice results in upregulated STAT3 signaling, which not only promotes Th17 differentiation, but can also drive epithelial proliferation, such that loss of STAT3 signaling in epithelial cells resulted in significantly fewer tumors (94, 114). *Salmonella* was capable of inducing cellular transformation of mouse embryonic fibroblasts (MEFs) harboring pre-transforming mutations that lead to the inactivation of the tumor suppressor protein p53 inactivation or overexpression of *c-myc* since infection resulted in anchorage-independent soft agar growth and permitted tumor growth in immunocompromised mice (115). This process was dependent on intact MAPK and Akt signaling (115).

1.3.3 Promotion of DNA damage

Another potential mechanism by which CRC-associated bacteria may facilitate the development of CRC is the promotion of DNA damage. In the case of *pks+ E. coli*, which produces the genotoxin colibactin, HeLa cells infected with *pks+ E. coli* exhibited signs of DNA double-stranded breaks and cell cycle arrest (65, 66). This colibactin-associated DNA damage induced DNA repair responses, resulting in cells with chromosomal instability, including chromosomal alterations (e.g. translocations, ring chromosomes, etc.) and abnormal chromosome number (116). *In vitro*, *pks+ E. coli* were able to induce carcinogenic mutations in infected HCT116 (human colon carcinoma), IEC-6 (rat intestinal epithelial) and CHO (hamster ovarian epithelial) cells, revealing the mutagenic and pro-tumorigenic ability of *pks+ E. coli* (116). Rat epithelial cells infected with *pks+ E. coli* also exhibited increased DNA damage compared to cells infected with *E. coli* without the pks pathogenicity island (*E. coli Δpks*) (66). *In vivo*, AOM-treated GF $Il10^{-/-}$

mice monocolonized with *pks+ E. coli* developed more tumors and had increased DNA damage and cell cycle arrest compared to *E. coli Δpks*-monocolonized mice despite no difference in inflammation, strongly suggesting that the tumor-promoting effects of *E. coli* were related to its genotoxic rather than inflammation-promoting effects (66).

1.3.4 Production of metabolites

In addition to pro-tumorigenic activities of gut microbiota, there is growing recognition that microbial-derived metabolites can also affect both health and disease, including CRC. Specific metabolites, such as short chain fatty acids (SCFAs) and secondary bile acids, have received the most attention for their role in modulating immune responses, epithelial homeostasis, and cell signaling that can affect tumor susceptibility.

1.3.4.1 Short chain fatty acids (SCFAs)

Consistent with a potentially significant role for SCFAs in CRC pathogenesis, patients with CRC can have significant reduction in butyrate-producing bacteria (26, 34). Furthermore, risk for CRC is inversely associated with intake of dietary fiber, which is a source of SCFAs via microbial metabolism of resistant starches and other fiber polysaccharides (5). SCFAs, which include butyrate, propionate, and acetate, are generated from the digestion of dietary fibers, such as polysaccharides from plant cell wells, by the gut microbiota, and are then absorbed by host cells (117).

In particular, butyrate is produced by Firmicutes bacteria and is an energy source of epithelial cells and helps maintain colon epithelial integrity (118). Notably, butyrate can inhibit histone deacetylaces (HDACs) in colon epithelial cells and immune cells, which can have anti-tumorigenic effects, including the downregulation of pro-inflammatory cytokines such as IL-6 (119-122). Increased histone acetylation at the *Foxp3* locus results in the differentiation of regulatory T cells (Treg) (80). Consistent with members of Clostridia being relatively high producers of butyrate, Clostridia colonization of GF WT mice promoted colon Treg differentiation in GF WT mice (81). The impact of SCFAs on Treg differentiation may have implications on anti-tumor immunity and response to therapy given its immunosuppressive effect although it remains to be determined whether regulatory T cells play a significant role in colon carcinogenesis. SCFAs, however, can promote intestinal homeostasis as the administration of SCFAs to GF mice made them more resistant to the epithelial damaging-effects of DSS (123). Similarly, butyrate- or

Clostridium-treated mice developed less severe colitis compared to their control counterparts (80, 81). Deficiency in the receptor for butyrate that is expressed on epithelial cells, Gpr109a, resulted in reduced numbers of Tregs and the anti-inflammatory cytokine IL-10 as well as increased susceptibility to DSS-induced colitis (124-127). Furthermore, Gpr109a signaling was also required for butyrate-mediated epithelial expression of IL-18, which is important for promoting epithelial repair and resistance to epithelial-injury induced inflammation (124-127).

Butyrate and SCFAs in general also have anti-tumor effects. Mice deficient in GPR109A, for example, have increased tumor development in both AOM/DSS and $Apc^{Min/+}$ models (127). One mechanism, besides anti-inflammatory activity, is by sensitizing cancer cells to apoptosis. Cancer cells often express Fas, the receptor for Fas ligand (FasL), but are able to evade apoptotic cell death induced by Fas-FasL interactions by effector CD8 T cells and NK cells (128-130). Interestingly, in several human CRC cell lines, the addition of soluble FasL and sodium butyrate to the culture promoted increased CRC cell apoptosis compared to cells that were incubated with sodium butyrate alone (128). Similarly, many cancer cells, including CRC cells, are able to evade apoptotic death induced by tumor necrosis factor-related apoptosis-inducing ligand (TRAIL) and its receptors, including the death receptors DR4 and DR5 (131-133). TRAIL-resistant human colon cancer cell lines KM12C, KML4A, and KM20 were incubated with TRAIL, and with or without sodium butyrate. Cells that received sodium butyrate displayed increased TRAIL-mediated cell death (134). Other mechanisms have been proposed including downregulation of pathways involved in cellular proliferation, induction of antioxidant pathways, and effects on microbiome composition (135, 136). However, microbial regulation of SCFA levels is unlikely to be the main contributor to colon cancer risk as fecal SCFA levels were not found to be predictive of either adenomas or carcinomas (137).

1.3.4.2 Secondary bile acids

On the other hand, secondary bile acids have been shown to have pro-tumorigenic effects. Primary bile acids are secreted by the liver into the gastrointestinal tract where they aid in lipid digestion (138). Bile acids have anti-microbial properties and can modify the gut microbiome composition (138, 139). Primary bile acids pass through and are mostly reabsorbed by the small intestine without microbial alterations (140). However, about 5% of total bile acids are not reabsorbed and enter the large intestine and undergo modification by the gut microbiome via bile acid hydrolases to generate secondary bile acids (138, 140). High fat diets, which lead to increased

bile acid levels, are a risk factor for CRC, and high levels of secondary bile acids have been measured in CRC patients (141-143). Interestingly, a meta-analysis of eight fecal metagenomic studies of CRC encompassing 386 cancer cases and 392 tumor-free controls demonstrated a significant enrichment of the *bai* operon, which encodes bile acid converting enzymes involved in secondary bile acid production, in the stool of CRC patients (25).

Two well-studied secondary bile acids that have been linked to CRC are deoxycholic acid (DCA) and lithocholic acid (LCA). They can induce reactive oxygen and nitrogen species (ROS and RNS) production by human colon tissue and human adenocarcinoma cells (144-147). ROS and RNS induce DNA damage, and DCA and LCA have been shown to induce DNA breaks in human adenocarcinoma cell lines and human colon tissue (145, 147, 148). Bile acids can activate multiple pathways, including Wnt, EGFR, and NF-κB, which in turn, can stimulate the proliferation of CRC cells as well as induce tumor formation in mice (149-156). Administration of secondary bile acids has also been associated with changes in the gut microbiome, which may contribute to tumor promotion as gavage of feces from DCA-treated mice into $Apc^{Min/+}$ mice resulted in increased tumorigenesis (151).

1.4 Conclusion and Goals

Since the advent of 16S rRNA and metagenomic sequencing technologies and the establishment of germfree mouse models, significant advances have been made in our understanding of the role of the gut microbiome in the pathogenesis of colorectal cancer. It has now become apparent that the presence of CRC is associated with significant shifts in the microbial community compared to healthy individuals. The exact nature and timing of these changes and whether these changes directly cause colorectal cancer in humans remain active areas of intense research and would require a concerted effort by the scientific community to embark in large population studies that are prospective in nature and involved the longitudinal analysis of stool or mucosal tissue samples.

It has become generally accepted that colon carcinogenesis is a multi-step process that requires the accumulation of genomic mutations that precipitate cellular transformation and that the gut microbiota, which can act either as tumor promoters or tumor suppressors by modulating inflammation. Inflammation, in turn, can also allow the bloom of harmful pathobionts that

outcompete and deplete potential beneficial bacteria to further facilitate tumor progression. Thus, it has become tantalizing to speculate that identification of specific bacteria associated with CRC and/or preneoplastic lesions (e.g., adenomas) would allow the establishment of microbial biomarkers to assess colorectal cancer risk or identify strategies to manipulate the microbiome or target specific microbes and their products for cancer chemoprevention.

While there are a growing number of studies investigating the interactions between specific microbiota, host immunity, and CRC, most studies have been done in genetically susceptible mice. Additionally, while some gut microbiota species have been shown to promote different immune cell subsets, namely T cells, in the context of CRC, further studies are needed to examine how the gut microbiota may alter other immune cell subsets. There also remains an overall gap in knowledge of how consortia of specific gut microbiota might alter host immune or carcinogenic responses, which is likely more physiologically analogous than studying the role of an individual bacterial species. Moreover, the role of microbial metabolites in host immune responses or CRC burdens needs to be further examined.

In this project, we remove host genetic differences to specifically study how microbiota alone can alter CRC susceptibility by utilizing two C57BL/6 wild-type (WT) mouse colonies which have significantly different microbiomes. Furthermore, these two WT colonies present with different tumor burdens in a chemically-induced model of colitis-associated colon cancer (CAC). Using this system, we seek to identify which gut bacteria contribute to tumor burden differences and how. Specifically, in Chapters 2 and 3, we identify microbiome differences that promote tumor burden differences and explore possible mechanisms. In Chapter 4, we investigate how these microbiome differences alter host immunity which ultimately leads to dissimilar CRC outcomes. Our findings propose several new avenues of study which are discussed in Chapter 5. Overall, this dissertation furthers our understanding of how the gut microbiome affects host immunity in the context of CAC, where the gut microbiome has preventative and therapeutic potential.

CHAPTER 2: Microbiome Differences Between Two C57BL/6 Mouse Colonies Promote CRC Tumor Burden Differences

2.1 Introduction

We have previously demonstrated that alterations in the gut microbiome can directly contribute to tumorigenesis (37). In this study, we use the azoxymethane (AOM)/dextran sulfate sodium (DSS) model of inflammation-associated colon tumorigenesis (38, 157) in which mice are given an intraperitoneal injection of the carcinogen AOM followed by three rounds of chemical water containing 2% DSS. DSS compromises the intestinal barrier, resulting in increased epithelial permeabilization and inflammation (158). In this model, tumors develop by weeks 8-10 (37, 159) (**Figure 2.1**). Although this model is driven by epithelial injury and inflammation and has been used to understand the pathogenesis of IBD-associated colon cancer, there are features of this model that also recapitulate sporadic colorectal cancer including the predominance of tumor mutations that dysregulate Wnt signaling (160, 161), which occurs in the majority of human CRC, as well as the progression from adenomas to adenocarcinomas (162). AOM/DSS treatment also results in microbiome alterations similar to that observed in human CRC patients such as reduced species richness and alpha diversity as well as significant shifts in beta diversity (37).

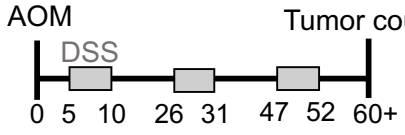

Figure 2.1 Timeline of AOM/DSS-induced colon tumorigenesis Age-matched C57BL/6 mice were treated with 10mg AOM/kg weight followed by three five-day rounds of 2% DSS. Mice were sacrificed at least one week after the last cycle of DSS, and tumors were counted.

2.2 Materials and Methods

2.2.1 Mice

All SPF mice were housed in the University of Michigan Rogel Cancer Center Mouse Facility. SPF WT1 mice were originally purchased from Jackson Laboratory and bred in-house at the University of Michigan (UM). SPF WT2 mice were generated from WT littermates (*Nod1*$^{+/+}$) of backcrosses between Jackson Laboratory B6 mice and transgenic *Nod1*$^{-/-}$ mice (>F8) and subsequently established as a separate wildtype colony on a different rack from WT1 mice to minimize cross-contamination of WT1 and WT2 microbiomes. Tails from WT1 and WT2 mice were sent to DartMouse™ for SNP genotyping using the Illumina Infinium Genotyping Assay. *CDX2-Cre Apc*$^{fl/fl}$ mice were bred in house, and 7-8 week-old *CDX2-Cre Apc*$^{fl/fl}$ mice were used. Germ-free (GF) WT and GF Swiss Webster mice were also used. GF WT mice originate from Jackson Laboratory B6 mice and were bred and housed at the University of Michigan Germ-free Mouse Facility. Animal studies were conducted under protocols approved by the University of Michigan Committee on the Use and Care of Animals.

2.2.2 Inflammation-induced colon tumorigenesis

6-10 week-old SPF WT1 and WT2 mice were injected intraperitoneally with 10mg azoxymethane (Sigma) per kg mouse weight. After five days, mice were treated with three cycles of 2% dextran sulfate sodium (MP Bio, m.w.=36,000-50,000) given for five days in the drinking water followed by 16 days of regular drinking water. Mice were sacrificed between days 60-70 after AOM injection (**Figure 2.1)**. This time range does not significantly affect tumor numbers between mice of the same group (**Figure 2.2**). For tumor counting, colons were flushed of stool with PBS, longitudinally cut open, and grossly counted using a magnifier and measured with calipers. For **Figure 2.9** involving conventionalized GF mice, GF WT mice were 9-12 weeks old and GF SW mice were 5 weeks old when they were gavaged. Four weeks after colonization, all GF WT groups were treated with two rounds of 2% and a final round of 1.5% DSS water due to increased mortality of GF+WT2 microbiota after two DSS rounds; GF Swiss Webster mice received three rounds of 1.5% DSS water to ensure survival.

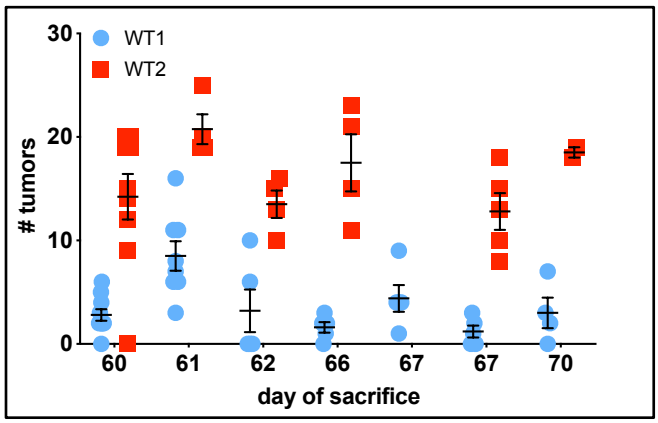

Figure 2.2 No significant tumor burden differences are measured between days 60-70 of AOM/DSS
The tumor counts of WT1 and WT2 controls of seven different AOM/DSS experiment are shown. Mice sacrificed between days 60-70 of AOM/DSS. No differences in tumor burdens are measured between different days of sacrifice within this range. Data are mean ± SEM.

2.2.3 Bacteria preparation for oral gavage

Whole SPF stool and cecal contents were isolated from young adult SPF WT1 and WT2 mice. Specifically, stool and cecal contents were collected under strictly anaerobic conditions (85% N_2, 10% H_2, 5% CO_2) in a Coy anaerobic chamber immediately after euthanasia and homogenized in anaerobic PBS. Mice received 150µl of homogenate. Homogenates were aliquoted into Eppendorf tubes (one tube/donor) to ensure homogenates remained anaerobic before gavage. One tube was frozen for later 16S rRNA sequencing.

Homogenates were also plated onto either brain-heart infusion (BHI, BD) agar supplemented with 10% horse blood (Quad Five), chopped-meat carbohydrate broth (CMCB) agar (163), or YCFA agar (164). Plates were cultured at 37°C anaerobically for 48 hours. Cultivable bacteria were resuspended from plates using anaerobic PBS and gavaged into GF WT mice. Mice received 150µl of homogenate. One tube was frozen for later 16S rRNA sequencing.

2.2.4 MC38 subcutaneous tumor model

$1x10^6$ MC38 cells were injected into the flank of 7-8 week old SPF WT1 or WT2 mice. Tumors were measured over time with a caliper to determine growth speed. All mice were sacrificed on the same day once some tumors reached 20mm in diameter (approximately day 21). Endpoint subcutaneous tumors were cut out from the flank and weighed.

2.2.5 AOM-only model

10mg AOM/kg mouse weight was intraperitoneally injected weekly into 7-11 week old SPF WT1 or WT2 mice for six weeks. Six months after the first injection, mice were sacrificed for tumor counting; colons were flushed of stool with PBS, longitudinally cut open, and grossly counted using a magnifier and measured with calipers.

2.2.6 ELISA

Stool was collected on day 0, 12, 26 or 60 of AOM/DSS and homogenized in PBS at 100 mg/ml. Homogenates were diluted to a range of 1:100 to 1:100000 and lcn-2 was measured using the Lcn-2/NGAL ELISA kit (R&D Systems) according to manufacturer's instructions.

2.2.7 Histological scoring

Histological assessment of H&E sections was performed in a blinded fashion by board-certified veterinary pathologist Kathryn A. Eaton using a previously described scoring system with some modifications (165). Briefly, a point scale was used to denote the severity of inflammation (0=none, 1=mild and mucosa only, 2=moderate infiltration of mucosa or extension to submucosa, 3=severe in mucosa and submucosa, and 4=transmural), severity of epithelial loss (0=none, 1=mild or basal 1/3 of glands, 2=moderate or basal 2/3 crypts, 3=severe where only surface epithelium remains, 4=ulceration/erosion), and quantification of adenoma/carcinoma (0=none, 1=single focus, 2=multiple foci). Each parameter was then multiplied by a factor reflecting the percentage of the colon involved (none, 25% or less, 26-50%, 51-75%, and 76-100%), and then summed to obtain the overall score.

2.2.8 qPCR

DNA was isolated from stool using the DNeasy PowerSoil Kit (Qiagen) and used for quantitative PCR using SYBR Green on the ABI 7900HT. Primer sequences used:

qPCR primer: Eub F	5'-AGAGTTTGATCCTGGCTC-3'
qPCR primer: Eub R	5'-TGCTGCCTCCCGTAGGAGT-3'

2.2.9 Isolation of bacterial DNA and 16S rRNA sequence analyses

16S rRNA analysis was performed with fecal samples that had been collected from 6-12 week old mice on the day of AOM injection and were frozen at -20 or -80° C. Bacterial DNA was isolated using the PowerSoil-htp 96 Well Soil DNA isolation kit (Qiagen) with the epMotion 5075

manually with the DNeasy PowerSoil Kit (Qiagen). The V4 region of the 16S rRNA gene was amplified using custom barcoded primers, sequenced with the Illumina MiSeq Personal Sequencing platform, and processed using the mothur software package to reduce sequencing errors and remove chimeras as previously described (Kozich et al., 2013; Schloss et al., 2009). Sequences were aligned to the SILVA 16S rRNA sequence database (Pruesse et al., 2007). Sequences were grouped based on their taxonomic classification or clustered into operational taxonomic units (OTUs) using a 97% similarity cutoff. Parallel sequencing and processing of a mock community allowed us to determine a sequencing error rate of 1.38%. Dissimilarity in community structure between samples was calculated using the θ_{YC} (thetaYC) distance metric. ThetaYC distances between the samples were used for two-dimensional ordination analysis by non-metric dimensional scaling (NMDS). Microbial alpha diversity was calculated using the inverse Simpson index and the observed number of OTUs (richness) (37). Analysis of MOlecular VAriance (AMOVA) was used to determine significance between community structure differences of different groups of samples. LEfSe and Metatstats in mothur were used to determine statistically differential OTUs between group (166, 167). All FASTQ sequences can be obtained from the Sequence Read Archive at NCBI (BioProject number PRJNA557261).

2.2.10 Statistical analyses

Continuous data are shown as mean ± SEM. Sample sizes can be found in the Figure Legends. Statistical analyses were performed using GraphPad Prism7, R and mothur software. Statistically significant differences were determined by Mann-Whitney when only two groups are compared (e.g., tumor numbers, fecal Lcn-2 levels). Differences in bacterial community structure were analyzed using Analysis of MOlecular VAriance (AMOVA) in mothur (168). P-values below 0.05 were considered statistically significant and are represented as follows: *$p<0.05$.

2.3 Results

2.3.1 Two WT mouse colonies develop different tumor burdens after AOM/DSS treatment

In our previous study (37), we observed C57BL/6 (B6) wildtype (WT) mice with higher tumor numbers after AOM/DSS treatment than what we have typically observed (165, 169).

Specifically, when we compared the two mouse colonies, "WT1" mice (165, 169) developed five tumors on average, whereas "WT2" mice (37) developed 15 tumors on average (**Figures 2.3A and 2.3B**). Not only do WT2 mice develop more tumors, they developed larger tumors, and also lost more weight after each round of DSS treatment compared to WT1 mice (**Figures 2.3C and 2.3D**). Additionally, on day 12 during the acute inflammatory response to the first round of DSS (day 12), WT2 mice developed significantly more colonic inflammation based on levels of stool lipocalin-2, a surrogate marker for intestinal inflammation (170) and histologic scoring (**Figures 2.3E and 2.3F**).

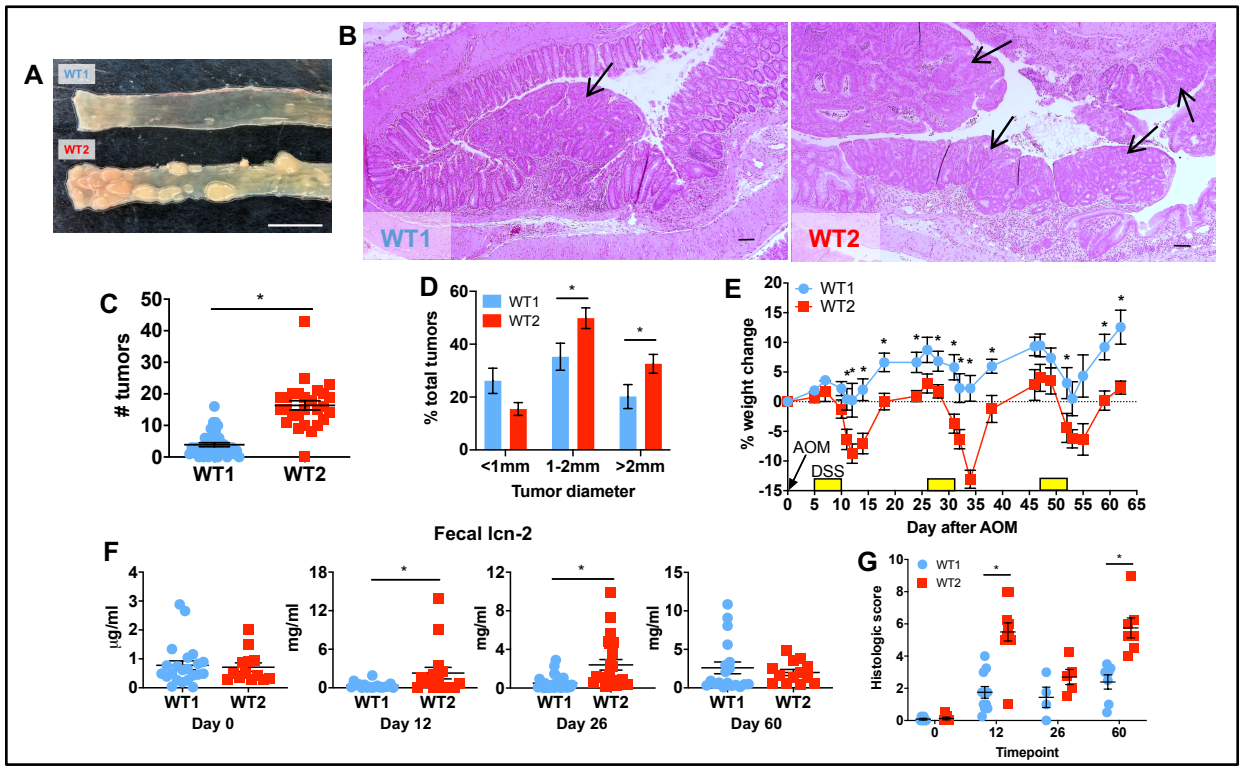

Figure 2.3 Two colonies of C57BL/6 WT mice have different colon tumor burdens in the AOM/DSS model of inflammation-associated colon tumorigenesis

A) Representative photo of WT1 and WT2 tumors at day 60 (tumor endpoint) of AOM/DSS treatment. Scale bar is 1cm.

B) Representative micrographs of H&E stains of WT1 and WT2 colon tissue at the tumor endpoint at 40x magnification. Tumors are denoted by black arrows. Scale bar is 100µm.

C and D) Tumor numbers (**C**) and sizes (**D**) at the tumor endpoint are shown. WT1 n=42 and WT2 n=36.

E) Representative graph of percent weight change during AOM/DSS treatment compared to day 0. n=5 mice/group.

F) Stool lipocalin-2 levels were measured by ELISA on days 0, 12, 26, and 60 of AOM/DSS treatment. D0: WT1 n=22 and WT2 n=13, D12: WT1 n=18 and WT2 n=17, D26: WT1 n=29 and WT2 n=23, D60: WT1 n=19 and WT2 n=13.

G) Severity and extent of inflammatory cell infiltration, epithelial loss and dysplasia of WT1 and WT2 mice on days 0, 12, 26, and 60 of AOM/DSS treatment were assessed by histological scoring. D0: n=6/group, D12: n=11/group, D26: WT1 n=4 and WT2 n=5, D60: n=7/group.

Data are mean ± SEM and are pooled from or representative of at least two experiments. *p<0.05 by Mann-Whitney

Both WT1 and WT2 mice are in the B6 background. WT1 mice include WT B6 mice bought directly from Jackson Laboratories or pups from in house breeding cages of Jackson WT B6 mice. The WT2 mouse colony was generated from breeding littermate WT (*Nod1*$^{+/+}$) pups from backcrosses of *Nod1*$^{-/-}$ mice to WT1 mice (both on a B6 background) where *Nod1*$^{-/-}$ mice develop high tumor numbers similar to WT2 mice in a microbiome-dependent manner (165). We hypothesized that the potentially dysbiotic microbiome of *Nod1*$^{-/-}$ mice was transferred to *Nod1*$^{+/+}$mice during backcrossing events. To confirm, we analyzed the microbiome composition of *Nod1*$^{-/-}$ and *Nod1*$^{+/+}$ (aka WT2) mice through 16S rRNA sequencing of stool-extracted DNA. Community-level microbiome differences, or beta-diversity, was visualized by NMDS ordination in **Figure 2.4A** using thetaYC distances, which represents structure dissimilarities between two communities, as calculated by the Yue & Clayton dissimilarity index (171). *Nod1*$^{-/-}$ and *Nod1*$^{+/+}$ mice have similar microbiomes, as the coordinates, each representing the overall microbiome composition of a single mouse, cluster together in overlap. Additionally, by Analysis of MOlecular Variance (AMOVA), which measures whether overall structural differences, or bacteria in this case, are statistically different between groups, these two mouse groups do not have significantly different microbiome compositions.

To determine whether there are genetic differences between WT1 and WT2 mice, we sent tails to DartMouse™. They performed preliminary SNP genotyping analysis and determined that both of our WT1 and WT2 colonies are ~98% homozygous B6 for all 5,307 SNP linkage markers compared to their Jackson C57BL/6J control, but that there are genetic differences even between mice within each colony (**Figure 2.4B**).

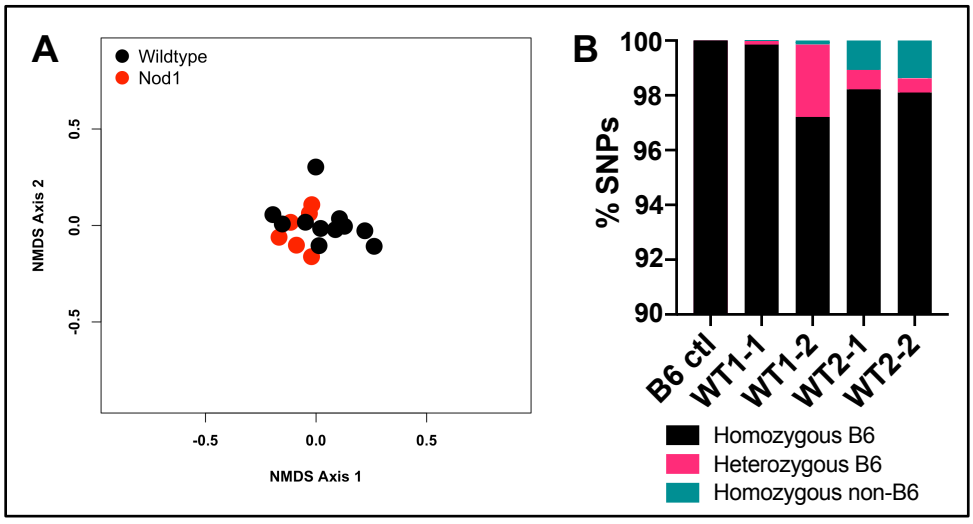

Figure 2.4 WT2 mice have similar microbiomes as *Nod1*$^{-/-}$ mice and are genetically similar to WT1 mice
A) NMDS plot showing microbiome similarity of *Nod1*$^{-/-}$ mice and their *Nod1*$^{+/+}$ littermates (aka WT2 mice). Data was generated by Joseph Zackular.
B) SNP genotyping results of representative WT1 and WT2 mice compared to the B6 control. Data was generated by DartMouse™.

2.3.2 The two WT mouse colonies have different microbiome compositions and metabolic profiles

To examine microbiome differences between the two colonies, we performed 16S rRNA sequencing on stool-extracted DNA from untreated WT1 and WT2 mice. Although no difference in species richness, or the observed number of species, was measured between the gut microbiomes of the two colonies, WT2 microbiomes have increased alpha diversity, which is comprised of species richness and species evenness, compared to WT1 microbiomes (**Figures 2.5A and 2.5B**). Beta diversity was visualized by NMDS ordination. Two separate clusters, representing the microbiomes of WT1 and WT2 mice, show that WT1 and WT2 colonies have distinct microbiome compositions (**Figure 2.5C**). Consistently, the gut microbial community structures of WT1 and WT2 mice were dissimilar as shown as thetaYC distances, where a distance of 1 means highly dissimilar and microbiome compositions compared within a group typically have a distance of 0.5; the thetaYC differences were significant as calculated by AMOVA (**Figure 2.5D**).

Furthermore, when we examined specific bacterial differences between WT1 and WT2 microbiomes, certain bacterial families are differentially abundant. Notably, WT1 mice have increased *Anaeroplasmataceae*, *Erysipelotrichaceae,* Clostridiales and *Sutterellaceae* bacteria while WT2 mice have increased *Prevotellaceae* and *Helicobacteraceae* bacteria (**Figure 2.5E**).

In this study, operational taxonomic units (OTUs) are sequences of 97% similarity which classify to the genus level. To identify OTU differences that are significantly associated with WT1 or WT2 microbiomes, we used linear discriminant analysis (LDA) effect size (LEfSe) analysis (166) (**Figure 2.5F**). Consistent with our relative abundance data in **Figure 2.5E**, as determined by an LDA score minimum cutoff of 4, WT1 mice are enriched in a member of the *Erysipelotrichaceae* family, and WT2 mice are enriched in a member of the *Prevotellaceae* family, where increased *Prevotellaceae* are also measured in human CRC patients (26, 72).

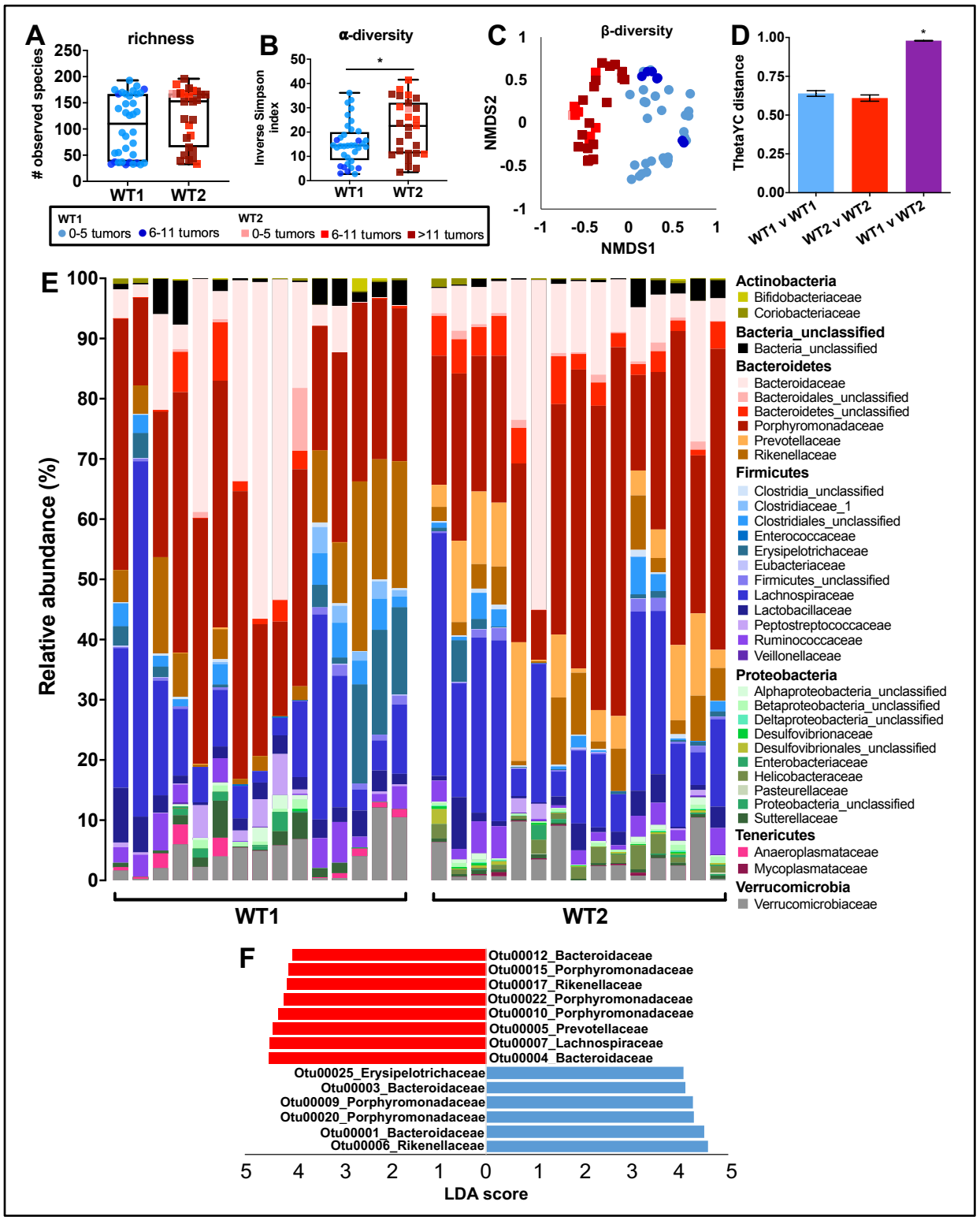

Figure 2.5 WT1 and WT2 mice have significantly different gut microbiome compositions
A-C) 16S rRNA sequencing of naïve WT1 and WT2 fecal microbiota was performed, and richness (**A**) and alpha-diversity (**B**) were measured. Beta-diversity (**C**) is shown as NMDS plot. *p<0.05 by Mann-Whitney
D) Microbiome composition dissimilarity based on thetaYC distances. *p<0.05 by AMOVA
E) Relative bacteria family abundances of naïve WT1 and WT2 mice. n=15/group.

F) The most differentially abundant OTUs between WT1 (blue) or WT2 (red) microbiomes were determined by LEfSe pairwise analysis. OTUs with LDA scores over 4 are shown.
Data are pooled from at least five experiments; WT1 n=51 and WT2 n=45 unless otherwise noted.

It is also known that different microbiota can produce different metabolites that can affect immunity and tumorigenesis. To determine if microbiome differences between our two B6 WT colonies may also alter metabolite production, we performed Phylogenetic Investigation of Communities by Reconstruction of Unobserved States (PICRUSt) analysis on stool-extracted 16S rRNA DNA sequences from naïve WT1 and WT2. PICRUSt is a bioinformatics software that can predict the functional content of the metagenome from 16S rRNA sequences (172). In other words, the bacteria present in sample, as determined by 16S rRNA sequencing, can be used to predict the functional genes that are differentially enriched between groups. The output from PICRUSt can be analyzed by the same statistical tests in mothur that are used for differential OTU analyses. By LEfSe, pathways that are predicted to be upregulated in WT1 mice include branched-chain amino acid (AA) degradation and butyrate metabolism; pathways that are predicted to be upregulated in WT2 mice include several AA metabolism and biosynthesis pathways as well as vitamin biosynthesis pathways (**Figure 2.6**).

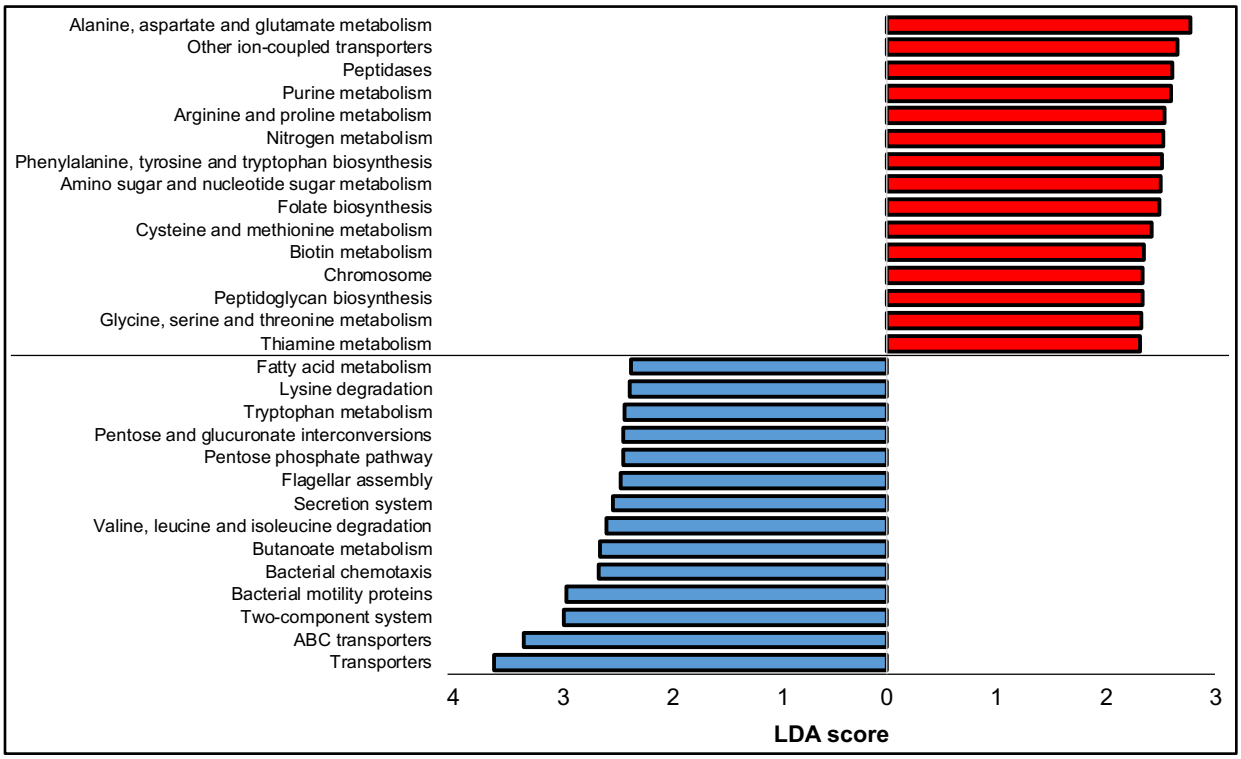

Figure 2.6 Predicted metagenomic differences between naïve WT1 and WT2 mouse microbiomes
Gene pathways that are predicted to be different between WT1 mice (blue) and WT2 mice (red) based on their microbiome compositions. Pathways with an LDA score over 2.3 and p-value<0.05 are shown. n=12 mice/group.

2.3.3 Gut microbiome differences between WT1 and WT2 mice directly contribute to colon tumor burden differences

We have previously shown that treating WT2 mice with an antibiotic cocktail starting two weeks before and throughout AOM/DSS treatment resulted in few to no tumors, further suggesting the microbiome plays a role in increased tumorigenesis in WT2 mice (37). To more rigorously determine whether the microbiome differences between WT1 and WT2 colonies are directly responsible for the differences in tumor phenotype, we gavaged anaerobically-prepared stool and cecal homogenates of SPF WT1 or WT2 mice into GF WT mice. After four weeks of colonization, GF WT mice had comparable stool bacteria levels compared to SPF control mice as measured by qPCR using universal bacteria primers (**Figure 2.7**). We further analyzed the microbiome compositions of the colonized GF WT mice. Relative abundances of bacterial families of mice colonized with SPF intestinal contents resembled that of the SPF intestinal content donors (**Figure 2.8A**). For instance, GF WT mice colonized with SPF WT2 bacteria (WT2>GF WT) had increased *Prevotellaceae* bacteria compared to GF WT mice colonized with SPF WT1 bacteria (WT1>GF WT). Donor microbiome compositions were not significantly different from respective colonized GF WT mice as determined by thetaYC measurements and AMOVA (**Figures 2.8B and 2.8C**). Additionally, WT1>GF WT mice had significantly distinct microbiome compositions compared to WT2>GF WT (**Figures 2.8B and 2.8C**). Altogether, this suggests that successful microbiome transfer can be achieved with this method.

Furthermore, to determine whether cultivable bacteria from SPF WT1 or WT2 microbiomes also contribute to tumor susceptibility, stool and cecal homogenates were plated onto: 1) brain-heart infusion (BHI) agar supplemented with 10% horse blood, 2) chopped-meat carbohydrate broth (CM) agar (163), and 3) YCFA agar (164). These general purpose media were used to maximize the growth of a broad spectrum of bacteria including the Bacteroidetes, Firmicutes, and Proteobacteria phyla among others. After 48 hours at 37ºC under anaerobic conditions, bacterial colonies from all three media were resuspended and pooled in anaerobic PBS and gavaged into GF WT mice. Four weeks after colonization, microbiomes were analyzed for colonization transfer success. While the cultivable bacteria are similar in species with the SPF

inputs, expectedly, they differ in abundances (**Figures 2.8A and 2.8D**). However, GF WT mice colonized with cultivable SPF WT1 microbiota (cult WT1>GF WT) have bacteria similar to SPF WT1 mice (**Figure 2.5E**), with increased abundances of *Lachnospiraceae* and *Anaeroplasmataceae* compared to GF WT mice colonized with cultivable SPF WT2 microbiota (cult WT2>GF WT) (**Figure 2.8D**). Cult WT2>GF WT mice had increased *Prevotellaceae* and *Helicobacteraceae* bacteria compared to cult WT1>GF WT mice (**Figure 2.8D**), consistent with what we have observed in SPF WT2 mice (**Figure 2.5E**). Additionally, GF WT mice colonized by cultivable SPF bacteria had microbiomes similar to their respective cultivable bacteria inputs, and cult WT1>GF WT mice had significantly distinct microbiome compositions compared to cult WT2>GF WT mice as measured by thetaYC distances and AMOVA (**Figures 2.8E and 2.8F**).

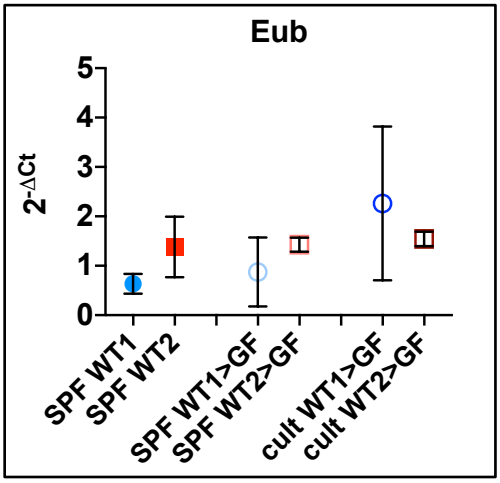

Figure 2.7 Colonized GF mice have comparable stool bacteria levels as SPF mice
DNA was isolated from stool collected from colonized GF WT mice four weeks after gavage. qPCR using Eubacteria primers was used to measure total bacteria. Data are mean ± SEM. n=2/group.

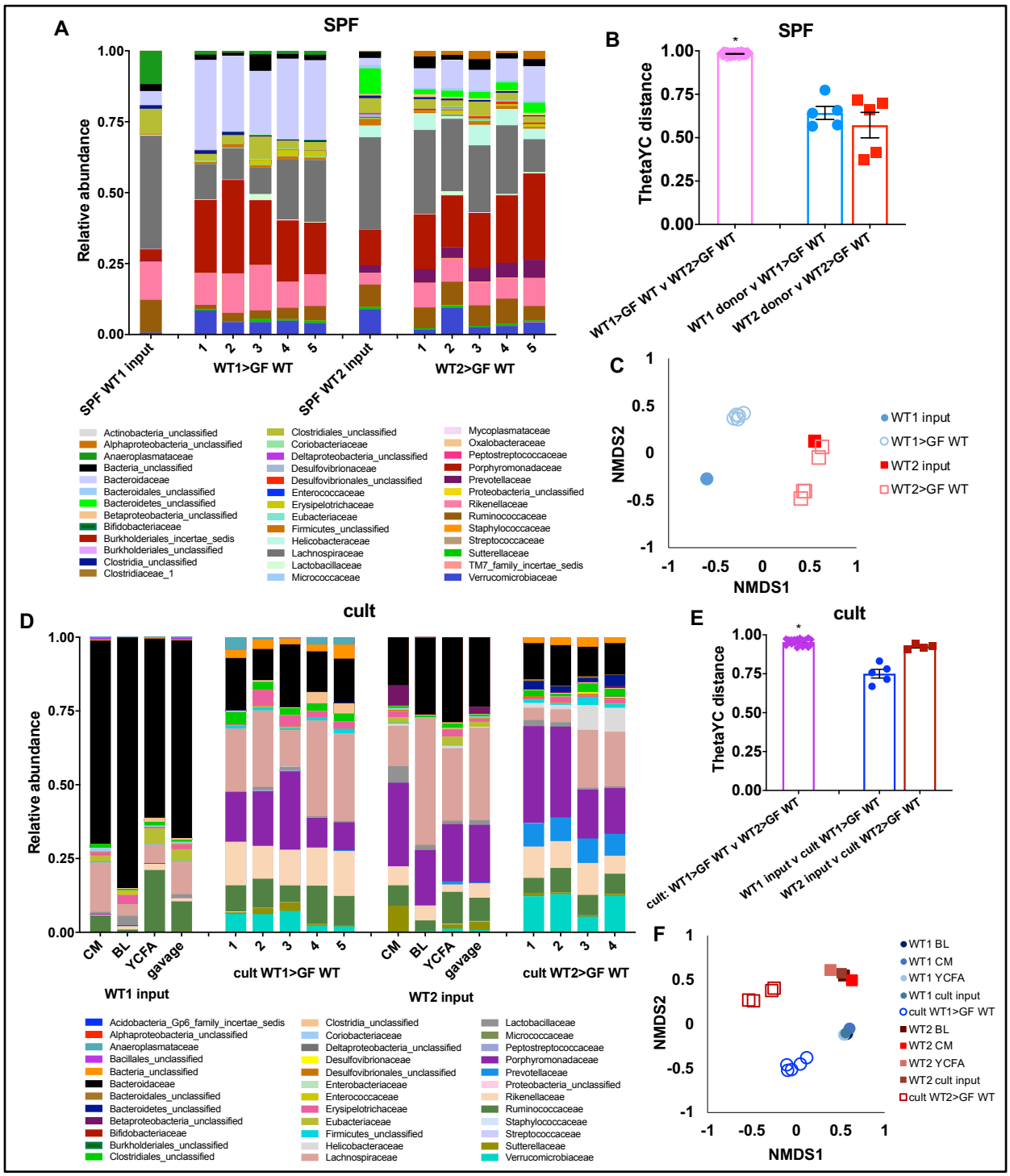

Figure 2.8 GF WT mice colonized with SPF intestinal contents or cultivable SPF intestinal bacteria have microbiomes that resemble that of the donor microbiomes after four weeks of colonization

A-C) GF WT mice were gavaged with whole anaerobically-prepared SPF stool and cecal contents. The microbiomes of colonized GF WT mice were analyzed four weeks after colonization. Relative abundances (**A**), thetaYC distances (**B**) and an NMDS plot (**C**) of microbiome similarity between donors and colonized GF WT are shown.

D-F) Anaerobically-prepared SPF intestinal contents were also plated onto three different media plates. Cultivable bacteria that grew were gavaged into another group of GF WT mice. Their microbiomes were also analyzed four

weeks after colonization. Relative abundances (**D**), thetaYC distances (**E**) and an NMDS plot (**F**) of microbiome similarity between donors and colonized GF WT are shown.
Data are mean ± SEM. n=4-5/group, *p<0.05 by AMOVA

As determined in **Figure 2.4B**, WT1 and WT2 mice are not 100% genetically identical, and it is possible that genetic differences may contribute to the observed tumor susceptibilities. To determine if microbiome differences alone can contribute to tumor burden differences, four weeks after colonization, GF WT mice colonized with SPF intestinal contents or cultivable bacteria were treated with AOM/DSS to induce tumors. WT1>GF WT developed significantly fewer and smaller tumors compared to WT2>GF WT, suggesting that microbiome differences between SPF WT1 and WT2 mice are sufficient to promote tumor burden differences regardless of any inherent genetic differences between the SPF WT colonies (**Figures 2.9A-C**). Interestingly, cult WT2>GF WT also developed more tumors compared to cult WT1>GF WT, but developed significantly fewer and smaller tumors compared to SPF WT2>GF, suggesting some bacteria that are promoting tumor differences are cultivable (**Figures 2.9A-C**).

Furthermore, to determine if microbiome differences could promote tumor burden differences when host genetic differences are present, we gavaged anaerobically prepared SPF WT1 or WT2 stool and cecal contents into GF Swiss Webster (SW) mice, which are an outbred mouse strain where individuals are genetically dissimilar. After four weeks of microbiome colonization, colonized GF SW mice were treated with AOM/DSS to induce colon tumors. At the end of AOM/DSS, GF SW mice colonized with SPF WT2 microbiota developed significantly more tumors compared to GF SW mice colonized with SPF WT1 microbiota (**Figure 2.9D**). This suggests that even with host genetic differences, WT1 and WT2 microbiota are sufficient to induce tumor burden differences.

Altogether, these data suggest that the different tumor susceptibilities of WT1 and WT2 mice can be attributed to gut microbiome differences and that the absence or presence of specific bacterial populations, some of which may be cultivable, can determine tumor outcomes.

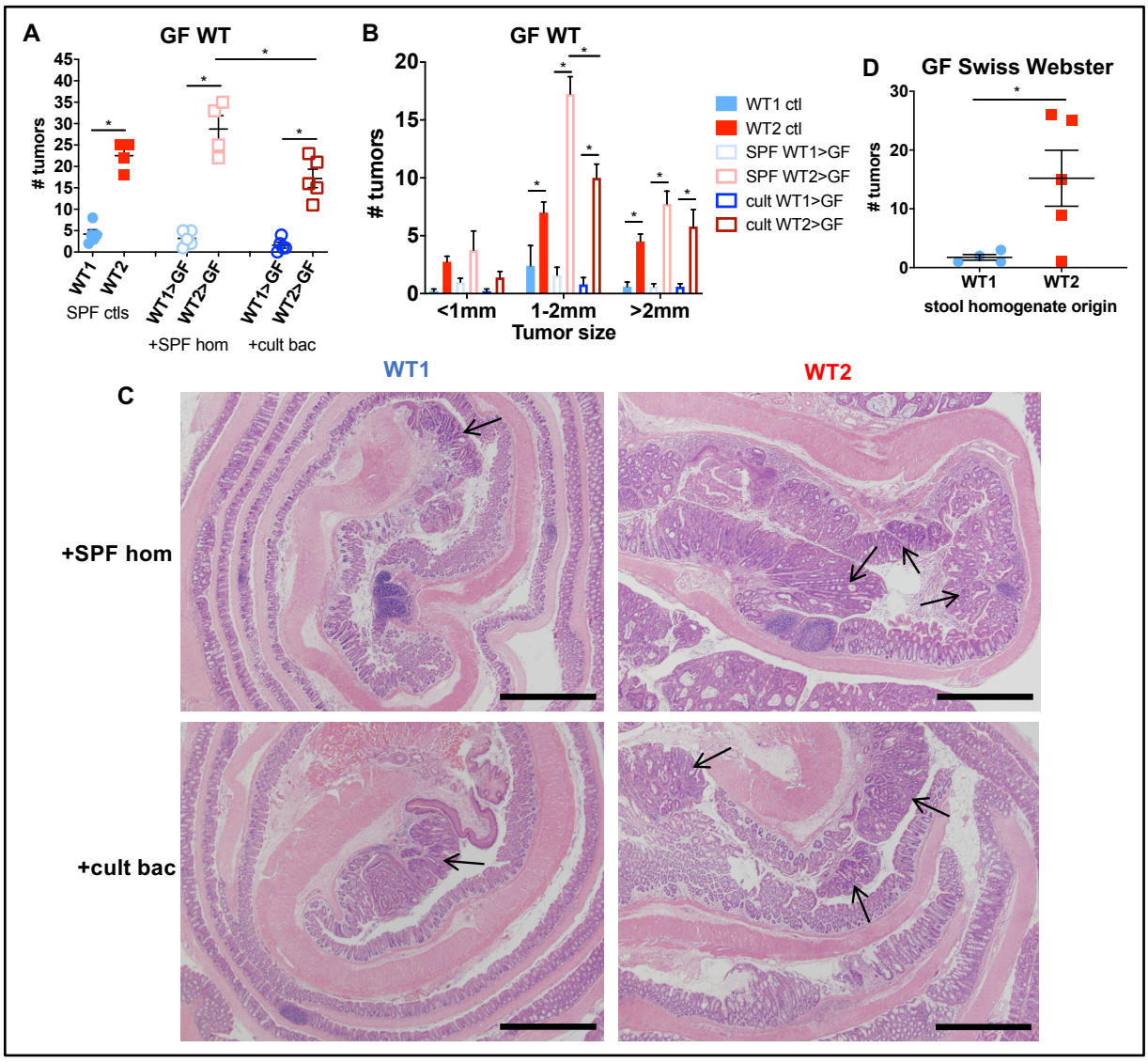

Figure 2.9 Gut microbiome differences of WT1 and WT2 mice directly contribute to differences in tumor susceptibility

A and B) Tumor numbers (**A**) and sizes (**B**) of AOM/DSS-treated GF WT mice that were colonized with SPF WT1 or WT2 whole stool and cecal homogenates or anaerobically cultivable WT1 or WT2 stool and cecal bacteria for 4 weeks. Tumors were counted 10 days after the last DSS round. n=4-5/group.

C) Representative micrographs of H&E stains of colonized GF WT colon tissue at the tumor endpoint at 40x magnification. Tumors are denoted by black arrows. Scale bar is 1mm.

D) SPF intestinal contents were gavaged into 5 week-old GF Swiss Webster mice. Four weeks after colonization, mice were treated with AOM/DSS. Mice were sacrificed and tumors were counted on day 66. n=5/group.

Data are mean ± SEM. *p<0.05 by Mann-Whitney

2.3.4 Gut microbiome differences promote tumor burden differences in an inflammation-dependent way

To determine if the tumor burden differences promoted by the two microbiome compositions were inflammation-dependent, we tested three additional mouse models of colon cancer that are not solely driven by inflammation: 1) AOM-only model, 2) subcutaneous MC38 tumor model, and 3) *CDX2-Cre Apc*$^{fl/fl}$ genetic model.

The AOM-only model is driven by carcinogen-induced oncogenic mutations. Mice were intraperitoneally injected with the carcinogen AOM weekly for six weeks. Six months after the first injection, mice were sacrificed for tumor counting. No differences in colon tumor numbers between WT1 and WT2 mice were measured (**Figure 2.10A**).

In the MC38 model, MC38 colon adenocarcinoma cells, which are syngeneic to C57BL/6 mice, are subcutaneously injected into the flank of experimental mice. Small tumors appear within a week, and growth can be measured over time. No differences in MC38 tumor growth (**Figure 2.10B**) or endpoint tumor size (**Figure 2.10C**) were measured between SPF WT1 and WT2 mice.

The tumor suppressor *APC* is mutated in the majority of colorectal cancers (173). *CDX2-Cre Apc*$^{fl/fl}$ mice are a genetic model of colon cancer where *APC* is deleted in intestinal epithelial cells as a result of the *CDX2* promoter. In our mouse rooms, these mice develop spontaneous colon tumors starting at two months old. To determine if WT2 microbiota can promote increased tumorigenesis compared to WT1 microbiota in this model, we treated *CDX2-Cre Apc*$^{fl/fl}$ mice with an antibiotic cocktail and antifungal water for one week before gavaging these mice with anaerobically-prepared SPF WT1 or WT2 stool and cecal homogenates for three consecutive days. Eleven weeks later, mice were sacrificed for colon tumor counting. No differences in overall tumor numbers were measured (**Figure 2.10D**), but tumors from *CDX2-Cre Apc*$^{fl/fl}$ mice with WT2 microbiota were generally larger in size (**Figure 2.10E**). However, as these mice were already 7 weeks old at the time of microbiome transfer, it is possible they had already developed small tumors.

Altogether, these three models show that the WT2 microbiome promotes increased colon tumorigenesis in an inflammation-dependent manner. However, in the genetic *CDX2-Cre Apc*$^{fl/fl}$ model, WT2 microbiota may promote increased tumor sizes after tumors have been established.

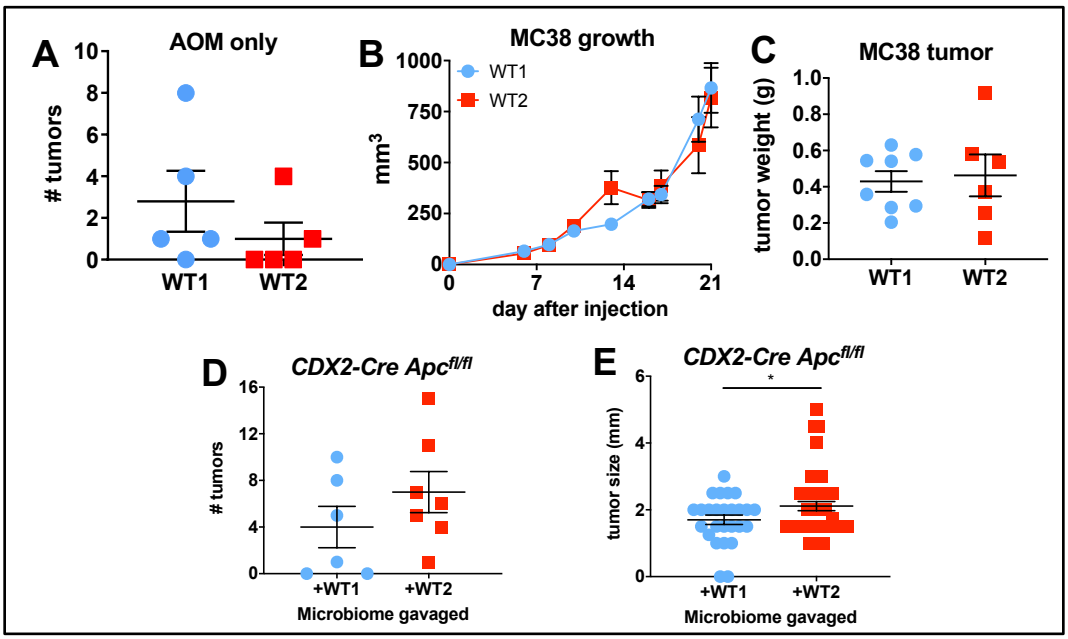

Figure 2.10 The tumorigenic effects of WT2 microbiota are inflammation-dependent
A) WT1 and WT2 mice were injected once a week with AOM for six consecutive weeks. Colon tumors were counted six months after the first AOM injection. Data are mean ± SEM. n=5/group.
B and C) 1x10^6 MC38 cells were subcutaneously injected in the flanks of SPF WT1 and WT2 mice. Tumor growths (**B**) were measured at intervals over 21 days; n=5/group. Mice were sacrificed on day 23 after cells were injected, and subcutaneous MC38 tumors were weighed (**C**); n=7-8/group. Data are mean ± SEM and representative of or pooled from at least two experiments.
D and E) SPF WT1 and WT2 microbiomes were gavaged three times over consecutive days into microbiome-depleted *CDX2-Cre Apc$^{fl/fl}$* mice. Eleven weeks after the last gavage, mice were sacrificed for colon tumor counting. Total tumor numbers (**D**) and tumor sizes of all tumors (**E**) are shown. Data are mean ± SEM. n=6-7/group, *p<0.05 by Mann-Whitney

2.4 Discussion and Future Directions

In Chapter 2, we described a unique model where two genetically WT mouse colonies develop significantly different inflammation-associated colon tumor burdens which can be directly attributed to microbiome differences between the two colonies. WT1 mice develop an average of 5 tumors and WT2 mice develop an average of 15 tumors. Even before tumors are induced, microbiomes of WT2 mice resembled that of IBD patients and CRC patients. We also showed that gavage of anaerobically-prepared SPF intestinal contents was able to successfully colonize germ-free mice where microbiomes of colonized mice resembled the donor microbiome composition. We also determined that some of the bacteria that promotes tumor burden differences are cultivable. Using three colon cancer models that are not driven by inflammation, we further

determined that the microbiome differences between WT1 and WT2 mice promoted tumor burden differences in an inflammation-dependent way.

It is known that mice of the same genotype can have different phenotypes in different facilities or even in different mouse facilities at the same institution (174, 175). For instance, *Il10*$^{-/-}$ mice develop spontaneous colitis in certain facilities but not in others, and have varying degrees of colitis severity, dependent on the microbiome composition (176, 177). Mice from different vendors are also known to have different microbiota (178-180). There has also been growing concern in recent years about reproducibility in research (181). Differences in microbiota between mouse rooms and facilities could confound phenotype results and may contribute to contradictory experimental results. While there is no way to resolve microbiome differences between facilities causing different experimental outcomes, for studies in fields where the microbiome contributes to disease, including microbiome composition sequences in research paper publications can help with experimental normalization and interpretation.

As described in **Section 1.3.4**, microbiome-produced metabolites can impact colorectal tumorigenesis. Here, we showed that not only do the two colonies have significantly different microbiomes, the metagenome of these mice are also different based on predictive PICRUSt analysis (**Figure 2.6**). A future direction of this finding would be metabolomics analyses on metabolites extracted from stool from the two colonies. We plan to determine which metabolites are significantly differentially abundant between the two colonies and if these metabolites can be commercially bought, we can directly test whether they play a role in protecting against or promoting colon tumors. To this end, we started a collaboration with Dr. Robert Quinn at Michigan State University to begin processing stool samples for metabolomics analyses.

In **Figure 2.10**, we show that the WT2 microbiome's effects on increased tumorigenesis is dependent on inflammation; of note, *CDX2-Cre Apc*$^{fl/fl}$ mice were 7 weeks old when they received antibiotic and antifungal water. However, in our mouse facility, *CDX2-Cre Apc*$^{fl/fl}$ mice develop spontaneous tumors typically by week 8. Therefore, in this particular experiment, these mice likely already had tumors at the time of SPF WT1 or WT2 microbiome gavage, where the gavaged microbiome would be influencing tumor growth but not development. To better determine if WT1 and WT2 microbiotas differentially affect tumor development in *CDX2-Cre Apc*$^{fl/fl}$ mice, we plan to repeat this experiment but begin antibiotics and antifungal treatment around four weeks old.

Here, our two WT colonies show that microbiome differences can significantly alter disease severity. These findings further show that microbiome-dependent phenotypes can occur independent of host genetics, emphasizing the importance of proper controls in animal experiments. As shown in **Figure 2.4A**, wildtype littermates do not have significantly different microbiomes compared to knockout littermates and are ideal controls for disease studies where the microbiome is known to play a role. With littermates, the microbiome is largely normalized across pups despite genetic differences and therefore different phenotypes can be directly attributed to host genetic differences. However, littermate controls are not always possible, but microbiome transfer methods can be used to help equilibrate microbiomes before experiments. In this chapter, we confirm that GF mice colonized with a gavage of bacteria had microbiome compositions highly similar to the composition of donor microbiome. In Chapter 3, we explore different microbiome transfer methods to determine which results in best microbiome, and therefore tumor burden phenotype, transfer. Determining the best microbiome transfer method could help normalize microbiomes of experimental and control mice when littermates aren't possible.

CHAPTER 3: Microbiome Transfer Experiments Reveal Novel Candidate Bacteria That May Promote or Prevent Colon Tumorigenesis

3.1 Introduction

In Chapter 2, we showed that the different microbiomes of two WT colonies promote different tumor burdens after AOM/DSS treatment. In this chapter, we wanted to determine if the tumor burden phenotype difference between WT1 and WT2 mice could be transferred via microbiome transfer. As the gut microbiome is comprised mostly of obligate anaerobic microbes and are difficult to culture, the field has explored culture-independent methods of transfer to study the microbiome. Mice are coprophagic, and therefore eat stool, where microbiota may be transferred from one group to another through the ingestion of each other's stool. Cohousing is a commonly used method to transmit microbiome-dependent phenotypes where mice of different microbiome compositions are placed in a cage for a certain amount of time (180, 182). In addition to cohousing, cross-fostering is another method to transfer the microbiome. With cross-fostering, pups are switched to another nursing mother within 48 hours of their birth. It has been shown that cross-fostered pups have microbiomes that more closely resemble the nursing mother than the birth mother (183-185).

In this chapter, we determine whether cohousing or cross-fostering, or gavage into GF mice as described in Chapter 2, more successfully transfers the microbiome and therefore tumor burden phenotype. We also use the microbiome data generated from these microbiome transfer experiments to determine if specific bacteria are significantly associated with low or high tumor burdens.

3.2 Materials and Methods

3.2.1 Mice

SPF WT1 mice were originally purchased from Jackson Laboratory and bred in-house at the University of Michigan (UM). SPF WT2 mice were generated from WT littermates (*Nod1*$^{+/+}$) of backcrosses between Jackson Laboratory B6 mice and transgenic *Nod1*$^{-/-}$ mice (>F8) and subsequently established as a separate wildtype colony on a different rack from WT1 mice to minimize cross-contamination of WT1 and WT2 microbiomes. Animal studies were conducted under protocols approved by the University of Michigan Committee on the Use and Care of Animals.

3.2.2 Inflammation-induced colon tumorigenesis

6-10 week-old mice were injected intraperitoneally with 10mg azoxymethane (Sigma) per kg mouse weight. After five days, mice were treated with three cycles of 2% dextran sulfate sodium (MP Bio, m.w.=36,000-50,000) given for five days in the drinking water followed by 16 days of regular drinking water. Mice were sacrificed between days 60-70 after AOM injection (**Figure 2.1)**. This time range does not significantly affect tumor numbers between mice of the same group (**Figure 2.2**). For tumor counting, colons were flushed of stool with PBS, longitudinally cut open and grossly counted using a magnifier and measured with calipers.

3.2.3 Microbiome transfer

3.2.3.1 Cohousing

6-10 week-old female WT1 and WT2 mice were cohoused for four or six weeks in mostly a 2:2: or 1:1 ratio, respectively. Mice were then treated with AOM and three rounds of 2% DSS. Stool was collected before and during cohousing and on the day of AOM injection for microbiome composition analysis. Tumor were counted between days 66-70 of the AOM/DSS model.

3.2.3.2 Cross-fostering

Several new WT1 and WT2 breeding cages were set up at the same time. All WT1 or WT2 dams were siblings from the same cage to minimize microbiome differences and cage effects. Within 48 hours of birth, pups were switched to a nursing mother of the opposite colony. Pups that were not born within 48 hours of the opposite colony were used as non-cross-fostered controls. Pups were weaned around three weeks of age. Once they reached six weeks of age, pups were

treated with AOM and three rounds of 2% DSS. Stool was collected on the day of AOM for microbiome composition analysis. Tumors were counted on days 60 or 61 of AOM/DSS treatment.

3.2.4 Microbiome culturing

Whole SPF stool and cecal contents were isolated from SPF WT1 and WT2 mice. Stool and cecal contents were collected under strictly anaerobic conditions (85% N_2, 10% H_2, 5% CO_2) in a Coy anaerobic chamber immediately after euthanasia and homogenized in 9ml anaerobic PBS at roughly a 1:10 dilution. Homogenates were plated onto either brain-heart infusion (BHI, BD) agar supplemented with 10% horse blood (Quad Five), chopped-meat carbohydrate broth (CMCB) agar (163), or YCFA agar (164). Plates were cultured at 37°C anaerobically for 48 hours. Cultivable bacteria were resuspended from plates in anaerobic PBS and either frozen directly or mixed in a 1:1 ratio with 500µl of 25% glycerol in CMCB media. Frozen stocks were thawed and plated on the same media from which they were collected from. 48 hours later, bacteria were scraped off into anaerobic PBS and frozen directly. Stocks of both the initial cultivable bacteria and bacteria that grew after thawing were sequenced to determine the bacteria composition.

3.2.5 Bacteria preparation for oral gavage

Whole SPF stool and cecal contents were isolated from young adult SPF WT1 and WT2 mice. Specifically, stool and cecal contents were collected under strictly anaerobic conditions (85% N_2, 10% H_2, 5% CO_2) in a Coy anaerobic chamber immediately after euthanasia and homogenized in anaerobic PBS. Mice received 200µl of homogenate. Homogenates were aliquoted into Eppendorf tubes (one tube/recipient) to ensure homogenates remained anaerobic before gavage. One tube was frozen for later 16S rRNA sequencing.

3.2.6 Isolation of bacterial DNA and 16S rRNA sequence analyses

16S rRNA analysis was performed with fecal samples that had been collected from 6-14 week old mice on the day of AOM injection and were frozen at -20 or -80° C. Bacterial DNA was isolated using the PowerSoil-htp 96 Well Soil DNA isolation kit (Qiagen) with the epMotion 5075 manually with the DNeasy PowerSoil Kit (Qiagen). The V4 region of the 16S rRNA gene was amplified using custom barcoded primers, sequenced with the Illumina MiSeq Personal Sequencing platform, and processed using the mothur software package to reduce sequencing errors and remove chimeras as previously described (Kozich et al., 2013; Schloss et al., 2009). Sequences were aligned to the SILVA 16S rRNA sequence database (Pruesse et al., 2007).

Sequences were grouped based on their taxonomic classification or clustered into operational taxonomic units (OTUs) using a 97% similarity cutoff. Parallel sequencing and processing of a mock community allowed us to determine a sequencing error rate of 1.38%. Dissimilarity in community structure between samples was calculated using the θ_{YC} (thetaYC) distance metric. ThetaYC distances between the samples were used for two-dimensional ordination analysis by non-metric dimensional scaling (NMDS). Analysis of MOlecular VAriance (AMOVA) was used to determine significance between community structure differences of different groups of samples. LEfSe and Metastats in mothur were used to determine statistically differential OTUs between group (166, 167).

In addition, a random forest regression model was used to identify OTUs that are associated with the number of tumors on the day of AOM injection (Zackular et al., 2016). Linear and Poisson regression analyses were used to correlate OTUs to tumor burdens. OTUs identified to be predictive of tumor outcomes based on random forest (see Statistical Analysis) and regression models were cross-referenced with LEfSe and Metastats methods, which were used to identify OTUs associated with low (0-5 tumors) or high tumor burdens (>15 tumors) based on abundance, using an LDA score cutoff of 3 and an abundance difference cutoff of 0.003, respectively. OTUs that were significant in all five statistical models were chosen as candidates. A phylogenetic tree of the candidates was generated based on the V4 region sequence of the 16S rRNA gene using the Clustal Omega program by the EMBL-EBI (Madeira et al., 2019). All FASTQ sequences can be obtained from the Sequence Read Archive at NCBI (BioProject number PRJNA557261).

3.2.7 Statistical analyses

Continuous data are shown as mean ± SEM. Sample sizes can be found in the Figure Legends. Statistical analyses were performed using GraphPad Prism7, R and mothur software. Statistically significant differences were determined by Mann-Whitney when only two groups are compared (e.g., tumor numbers, etc.). Differences in bacterial community structure were analyzed using AMOVA in mothur (168). P-values below 0.05 were considered statistically significant and are represented as follows: *$p<0.05$. A random forest (RF) regression model was used to identify OTUs that are associated with the number of tumors that developed. RF is a decision tree-based approach that allows for nonlinear relationship between the OTU and tumor count data and interactions between OTUs. The RF model included all 521 OTUs with a total normalized count over all mice > 0.005. It was fit using the randomForest package in R with *default*

parameters except that we increased the number of trees in RF to 1,000 trees (186). Finally, OTUs were ranked by importance in the RF model as determined by the percent reduction in the mean square error (MSE) when an OTU was removed from the model. As an alternative to the machine learning method, we also used parametric regression models to study the effect of each OTU on the tumor count data. Specifically, we considered the simple linear regression (lm function in R) and Poisson regression (glm function in R). The resulting p-values were adjusted to control the false discovery rate (187).

3.3 Results

3.3.1 Cohousing and one-to-one cohousing did not transfer the tumor burden phenotype

We first began with the cohousing method of microbiome transfer. Age-matched female WT1 and WT2 mice were cohoused mostly in a 2:2 ratio for four weeks before AOM/DSS treatment (**Figure 3.1A**). Cohoused WT1 and cohoused WT2 mice exhibited significant tumor burden differences similar to non-cohoused control mice (**Figure 3.1B**).

Although the microbiota of cohoused WT1 and cohoused WT2 mice were not significantly different from each other after four weeks of cohousing based on thetaYC distances, cohoused WT1 microbiome compositions remained significantly different from non-cohoused WT2 microbiomes (**Figure 3.1C**). Cohoused WT2 microbiomes also remained distinct from control WT1 microbiomes based on thetaYC measurements, suggesting incomplete microbiome transfer (**Figure 3.1C**). Additionally, by NMDS ordination, cohoused WT1 and cohoused WT2 mice continued to cluster separately, similar to that of non-cohoused SPF WT1 and WT2 controls (**Figure 3.1D**).

While cohousing did not result in complete transmission of tumor phenotype from either WT1 or WT2 mice to the other, there were two cohoused mice that developed tumors similar in number to mice from the other colony (**Figure 3.1B**, black boxes). These mice were cohoused in a 1:1 ratio (one WT1 and one WT2 mouse), which may have resulted in more efficient microbiome transfer by coprophagy.

We therefore performed one-to-one (oto) cohousing experiments and also extended the cohousing time to six weeks to improve microbiome transfer and phenotype transmission (**Figure**

3.2A). However, significant tumor burden differences were observed between oto cohoused WT1 and WT2 mice (**Figure 3.2B**). Furthermore, oto cohoused WT2 mice developed an intermediate tumor burden phenotype, and no differences in tumor numbers between oto cohoused WT1 and non-cohoused WT1 mice were measured (**Figure 3.2B**). Regarding microbiome composition, WT1 control mice were significantly different from oto cohoused WT2 mice, again suggesting incomplete microbiome transfer despite oto cohousing (**Figure 3.2C**). By NMDS ordination, microbiome compositions of oto cohoused WT1 and WT2 mice clustered between control WT1 and WT2 mice, suggesting that cohoused mice have a hybrid microbiome, which may explain the intermediate tumor phenotype (**Figure 3.2D**). However, while no overall microbiome composition differences between cohoused WT1 and WT2 mice were measured by thetaYC distances, LEfSe analysis detected specific OTUs which were still significantly differentially abundant between the two groups (**Figure 3.2E**).

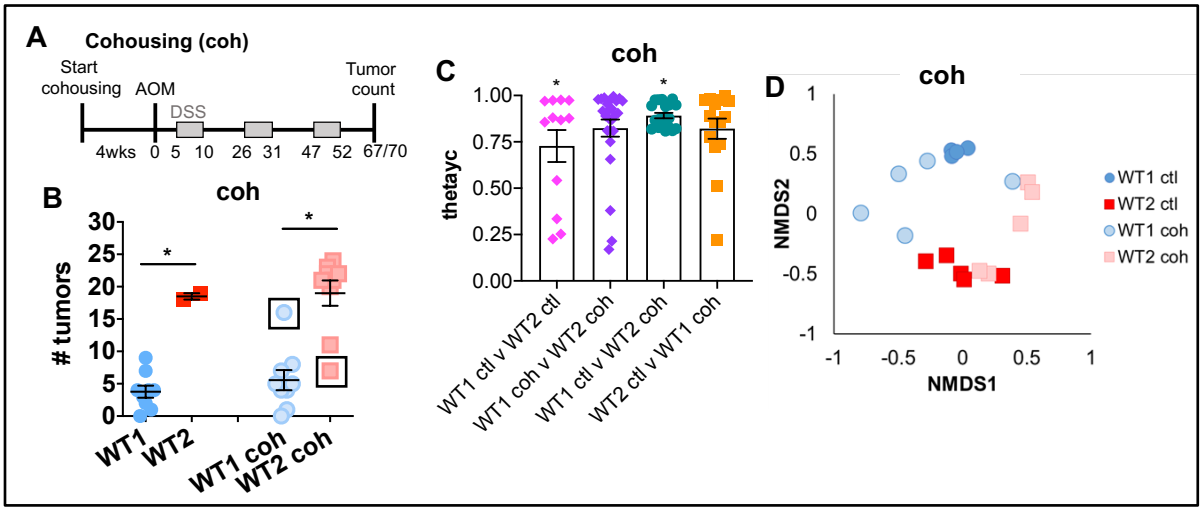

Figure 3.1 Cohousing did not promote microbiome or tumor phenotype transmission
A) WT1 and WT2 mice were cohoused in a 2:2 ratio (coh) for four week. Mice were treated with AOM/DSS and sacrificed for tumor counting on days 67 or 70.
B) Number of tumors after cohousing and AOM/DSS treatment. Data are mean ± SEM. *p<0.05 by Mann-Whitney
C and D) Stool was collected after four weeks of 2:2 cohousing for microbiome analysis. (**C**) Microbiome composition dissimilarity was analyzed by ThetaYC distance. (**D**) Beta diversity is shown as a non-metric dimensional scaling plot (NMDS). *p<0.05 by AMOVA
Data are pooled from at least two independent experiments. Controls: WT1 n=9, WT2=2; coh: n=9/group.

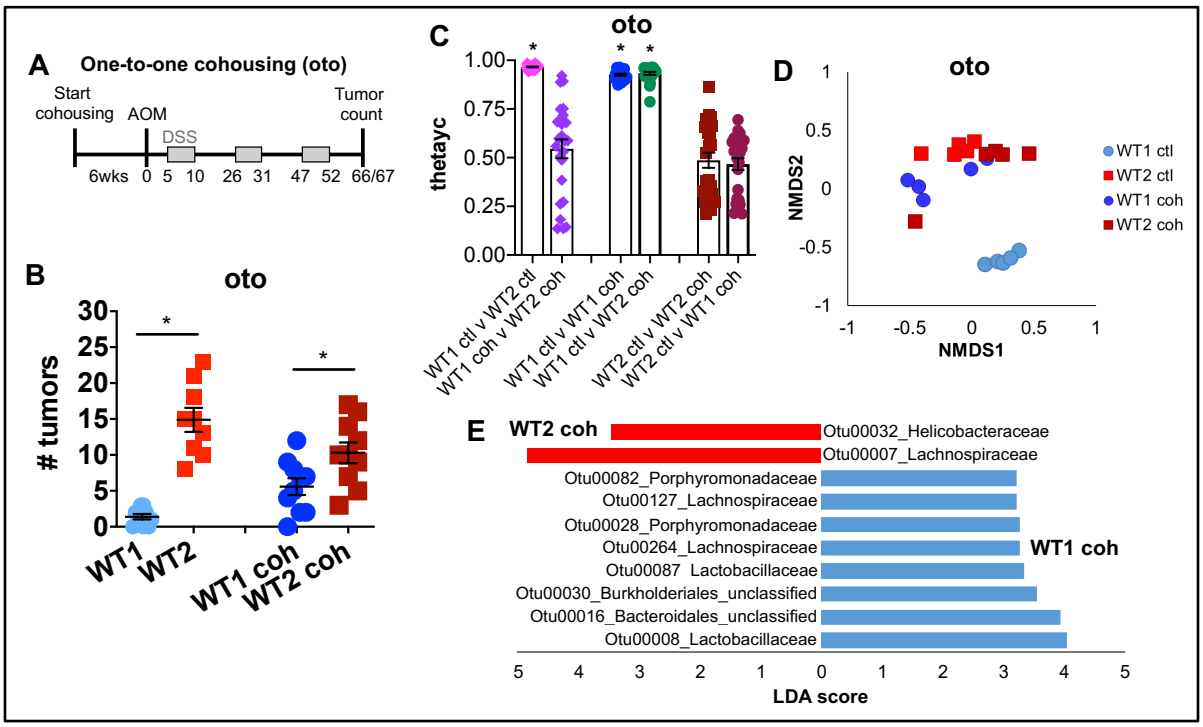

Figure 3.2 One-to-one cohousing did not promote tumor phenotype transmission
A) WT1 and WT2 mice were cohoused in a 1:1 ratio (oto) for six week. Mice were treated with AOM/DSS and sacrificed for tumor counting on days 66 or 67.
B) Number of tumors after oto cohousing and AOM/DSS treatment. Data are mean ± SEM. *p<0.05 by Mann-Whitney
C and D) Stool was collected after six weeks of 1:1 cohousing for microbiome analysis. Microbiome composition dissimilarity was analyzed by ThetaYC distance (**C**) and shown as an NMDS plot (**D**). *p<0.05 by AMOVA
E) Microbiomes of cohoused WT1 (WT1 coh, blue) and WT2 (WT2 coh, red) were compared by LEfSe analysis and several OTUs were found to be associated with one group of mice. OTUs with LDA scores above 3.2 are shown.
Data are pooled from at least two independent experiments. Controls: WT1 n=9, WT2=10; oto groups: n=10/group.

3.3.2 Cross-fostering resulted in an intermediate tumor burden phenotype

As the gut microbiome of an adult mouse is typically determined by maternal transmission, cross-fostering is another microbiome transfer method and may be more effective than cohousing (183, 188). We performed cross-fostering experiments where WT1 or WT2 pups were switched within 48 hours of birth to a WT2 or WT1 nursing mother, respectively. After reaching 6 weeks of age, cross-fostered mice were treated with AOM/DSS to induce tumors (**Figure 3.3A**). Unlike with cohousing, cross-fostered WT1 and WT2 mice no longer developed significantly different tumor burdens; however, average tumor numbers were again intermediate between control WT1 and WT2 mice (**Figure 3.3B**).When we examined gut microbiome compositions of cross-fostered mice, we determined that the microbial community of WT1 mice cross-fostered by WT2 nursing mothers (WT1(WT2)) and WT2 mice cross-fostered by WT1 nursing mothers (WT2(WT1)) were

distinct (**Figures 3.3C and 3.3D**). Although microbiomes of WT2(WT1) and non-cross-fostered WT1 mice were overall similar, the microbiome compositions of WT1(WT2) and non-cross-fostered WT2 mice were still significantly different despite improved microbiome transfer compared to cohousing based on thetaYC distances and NMDS ordination (**Figure 3.3C**). Significant differences in OTUs between WT1(WT2) or WT2(WT1) mice and control WT2 or WT1 mice, respectively, remained as determined by LEfSe, which may explain why the tumor phenotype was not completely transmissible (**Figures 3.3E and 3.3F**).

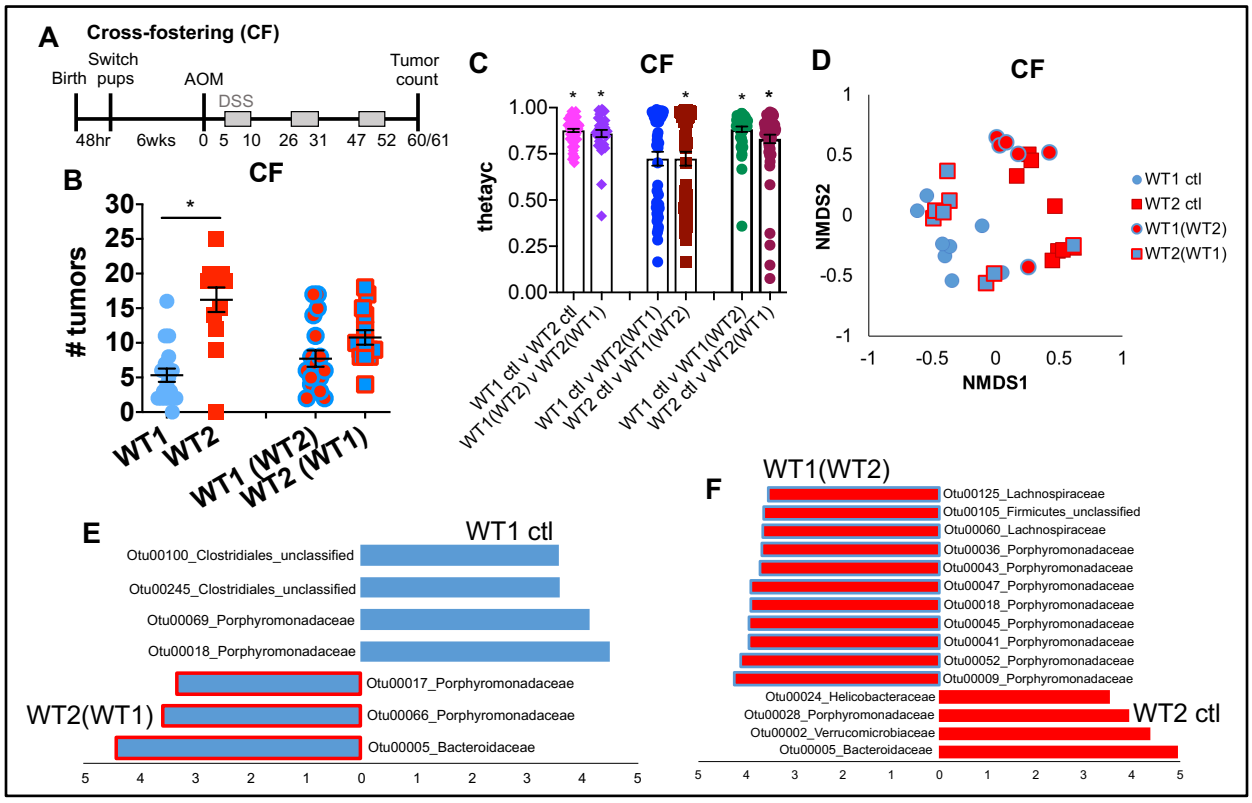

Figure 3.3 Cross-fostering promoted better microbiome transfer but cross-fostered mice developed intermediate tumor burdens between SPF WT1 and WT2 controls

A) WT1 and WT2 mice were cross-fostered (CF) and 6 week-old mice were treated with AOM/DSS and sacrificed for tumor counting on days 60 or 61.

B) Number of tumors after AOM/DSS treatment. Data are mean ± SEM. *p<0.05 by Mann-Whitney

C and D) Stool was collected on the day of AOM for microbiome analysis. Microbiome composition dissimilarity was analyzed by ThetaYC distance (**C**) and shown as an NMDS plot (**D**). *p<0.05 by AMOVA

E and F) OTU differences between cross-fostered and non-cross-fostered control mice were measured by LEfSe analysis. OTUs with LDA scores above 3.5 are shown.

Data are pooled from or representative of at least two independent experiments. Controls: WT1 n=18, WT2 n=13, CF: WT1(WT2) n=18, WT2(WT1) n=14.

3.3.3 Specific bacteria are associated with high or low tumor burdens

As we observed multiple tumor phenotypes associated with various microbial communities that were generated from different microbiome transfer methods, we reasoned that certain bacterial populations may consistently be associated with either low or high tumor burdens regardless of the WT colony. We therefore examined 16S rRNA sequences from the stool of cohoused and cross-fostered WT1 and WT2, control WT1 and WT2 mice, and GF WT mice conventionalized with WT1 or WT2 microbiota that was collected right before AOM/DSS treatment to identify OTUs that directly correlated with tumor outcomes after AOM/DSS treatment. Based on relative abundances, we observed, for example, increased abundance of *Prevotellaceae* on the day of AOM injection in mice that eventually developed high tumor numbers after AOM/DSS treatment and increased abundance of *Anaeroplasmataceae* in mice that eventually developed low tumor burdens (**Figure 3.4A**). OTUs that were significantly associated with low or high tumor numbers were determined by the combination of the following analyses: Metastats (167), LEfSe (166), random forest (189), and linear and Poisson regression. In particular, we identified nine OTUs belonging to at least five different bacterial families that were significantly associated with either high or low tumors (**Figure 3.4B**). Many of these bacteria have not been previously classified, but phylogenetic tree analysis based on based on 16S sequence similarity suggests that some of the bacteria within a specific family may be closely related (**Figure 3.4B**) (190, 191).

More specifically, two OTUs from the *Lachnospiraceae* family are significantly associated with and predictive of low tumor burdens. These OTUs are also more abundant in mice that eventually developed low tumor numbers (**Figure 3.4C**), and interestingly, *Lachnospiraceae* species have also been found to be decreased in CRC patients (26). On the other hand, seven OTUs, including bacteria from the *Prevotellaceae* family, which has been shown to be enriched in CRC patients (26, 72), are predictive of high tumor burdens (i.e., 15+ tumors) and are more abundant in mice that develop high tumor numbers (**Figures 2.5E and 3.4D**). Of note, although *Helicobacteraceae* appeared to be more abundant in WT2 mice (**Figure 2.5E)**, it was not significantly associated with tumor numbers by linear regression or Metastats analyses. Altogether, these data reveal nine bacterial populations that may have tumor-suppressive or tumor-promoting activities.

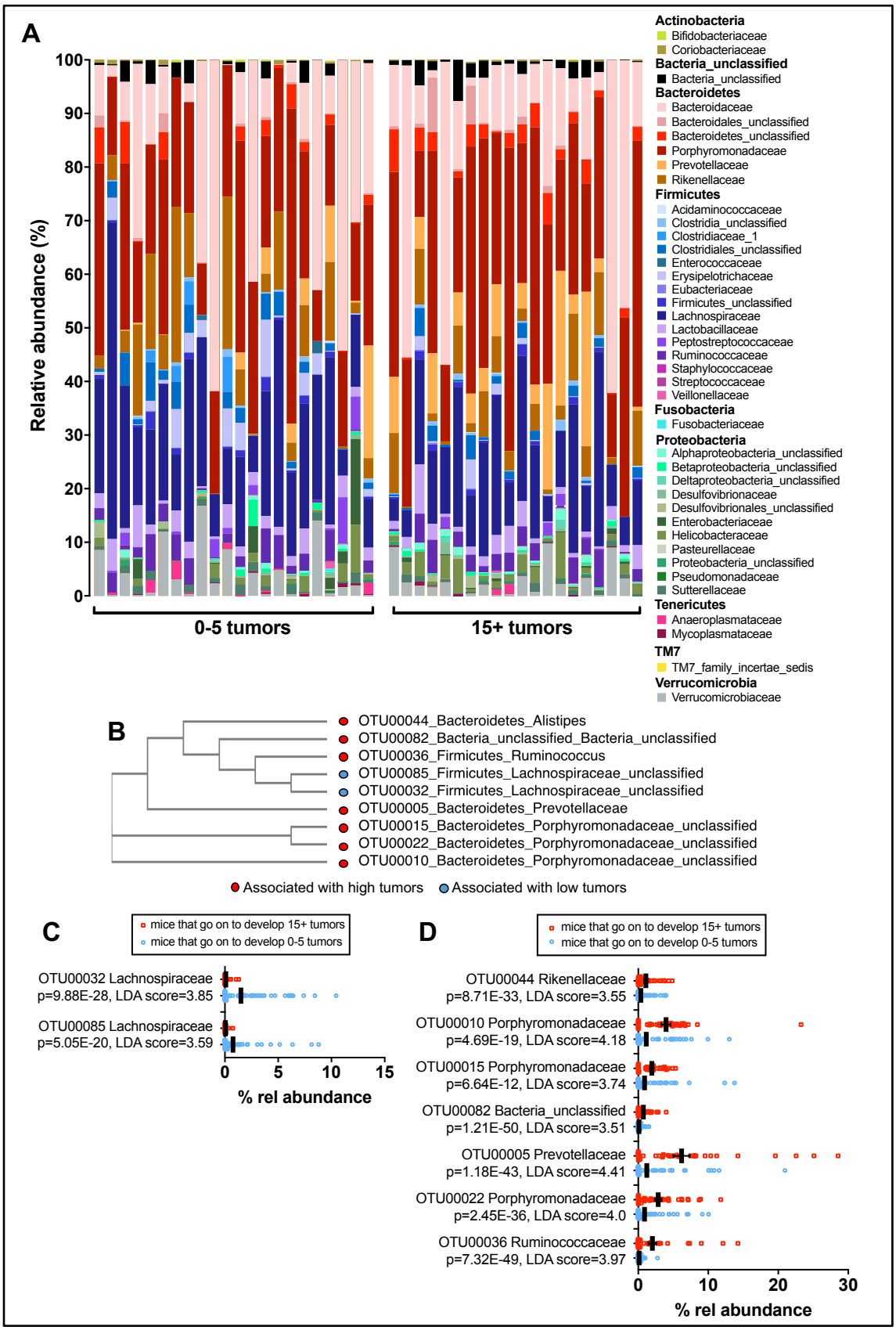
A
Relative abundance (%)
100
90
80
70
60
50
40
30
20
10
0
0-5 tumors
15+ tumors
Actinobacteria
Bifidobacteriaceae
Coriobacteriaceae
Bacteria_unclassified
Bacteria_unclassified
Bacteroidetes
Bacteroidaceae
Bacteroidales_unclassified
Bacteroidetes_unclassified
Porphyromonadaceae
Prevotellaceae
Rikenellaceae
Firmicutes
Acidaminococcaceae
Clostridia_unclassified
Clostridiaceae_1
Clostridiales_unclassified
Enterococcaceae
Erysipelotrichaceae
Eubacteriaceae
Firmicutes_unclassified
Lachnospiraceae
Lactobacillaceae
Peptostreptococcaceae
Ruminococcaceae
Staphylococcaceae
Streptococcaceae
Veillonellaceae
Fusobacteria
Fusobacteriaceae
Proteobacteria
Alphaproteobacteria_unclassified
Betaproteobacteria_unclassified
Deltaproteobacteria_unclassified
Desulfovibrionaceae
Desulfovibrionales_unclassified
Enterobacteriaceae
Helicobacteraceae
Pasteurellaceae
Proteobacteria_unclassified
Pseudomonadaceae
Sutterellaceae
Tenericutes
Anaeroplasmataceae
Mycoplasmataceae
TM7
TM7_family_incertae_sedis
Verrucomicrobia
Verrucomicrobiaceae
B
OTU00044_Bacteroidetes_Alistipes
OTU00082_Bacteria_unclassified_Bacteria_unclassified
OTU00036_Firmicutes_Ruminococcus
OTU00085_Firmicutes_Lachnospiraceae_unclassified
OTU00032_Firmicutes_Lachnospiraceae_unclassified
OTU00005_Bacteroidetes_Prevotellaceae
OTU00015_Bacteroidetes_Porphyromonadaceae_unclassified
OTU00022_Bacteroidetes_Porphyromonadaceae_unclassified
OTU00010_Bacteroidetes_Porphyromonadaceae_unclassified
Associated with high tumors
Associated with low tumors
C
mice that go on to develop 15+ tumors
mice that go on to develop 0-5 tumors
OTU00032 Lachnospiraceae
p=9.88E-28, LDA score=3.85
OTU00085 Lachnospiraceae
p=5.05E-20, LDA score=3.59
0
5
10
15
% rel abundance
D
mice that go on to develop 15+ tumors
mice that go on to develop 0-5 tumors
OTU00044 Rikenellaceae
p=8.71E-33, LDA score=3.55
OTU00010 Porphyromonadaceae
p=4.69E-19, LDA score=4.18
OTU00015 Porphyromonadaceae
p=6.64E-12, LDA score=3.74
OTU00082 Bacteria_unclassified
p=1.21E-50, LDA score=3.51
OTU00005 Prevotellaceae
p=1.18E-43, LDA score=4.41
OTU00022 Porphyromonadaceae
p=2.45E-36, LDA score=4.0
OTU00036 Ruminococcaceae
p=7.32E-49, LDA score=3.97
0
10
20
30
% rel abundance

Figure 3.4 Microbiome transfer experiments reveal bacteria that are associated with low of high tumor burdens
A) Stool was collected on day 0 of AOM/DSS which is the day of AOM injection. Relative abundances of family-level bacteria of naive mice that eventually developed low (0-5) or high (15+) tumors after AOM/DSS treatment are shown. Low tumor n=22, high tumor n=20, *p<0.05 by AMOVA
B) A phylogenetic tree of nine bacterial candidates associated with low (blue) or high (red) tumor burdens was generated based on the sequence similarity of the V4 region of the 16S rRNA gene.
C and D) Relative bacterial abundances in mice at the time of AOM injection that were associated with low (**C**) or high (**D**) tumor burdens. Black lines denote mean relative abundances. Poisson regression p-values are shown. LDA scores were determined by LEfSe analyses and scores above 3.5 are shown. Low n=85, high n=38.
Data are pooled from at least six independent experiments.

3.3.4 Culturing candidate bacteria

We next wanted to determine if these candidate bacteria correlating with tumor burdens directly contribute to the observed tumor phenotypes in WT1 and WT2 mice. We did a BLAST search of the 16S rRNA gene V4 region sequence of these candidate bacteria, and none of the bacteria were a 100% match to a known bacteria, suggesting that our candidates have not been previously isolated.

To determine which type of media the nine candidate bacteria grew best on, we plate anaerobically prepared stool and cecal contents from SPF WT1 and WT2 mice and plated homogenates onto horse blood (BL), chopped meat (CM), and yeast extract-casein hydrolysate-fatty acids (YCFA) agar plates. The cultivable bacteria were frozen and thawed to see which candidates could survive the freezing and thawing process. After 16S rRNA sequencing, despite all nine candidates being detected in the input stool, only four high tumor-associated bacteria and one low tumor-associated bacteria were initially cultivable (**Figure 3.5**). After freeze/thaw, only one high tumor-associated bacteria was detected (**Figure 3.5**). Due to low abundances of these bacteria after plating and freezing/thawing, we would have to pick thousands of colonies to find the exact candidate. However, we were able to determine which type of media some of these candidate bacteria grow best on.

Candidate bacteria Otu#_Family	WT1 microbiome							WT2 microbiome						
	stool input	*cultivable on plates*			*abundance after freeze/thaw*			*stool input*	*cultivable on plates*			*abundance after freeze/thaw*		
		BL	CM	YCFA	BL	CM	YCFA		BL	CM	YCFA	BL	CM	YCFA
Otu00005_Prevotellaceae	0	0	0	0	0	0	0	3.30%	0.10%	0.05%	0	0	0	0
Otu00010_Porphyromonadaceae	0	0	0	0	0	0	0	6.35%	0	0	0	0	0	0
Otu00015_Porphyromonadaceae	0	0	0	0	0	0	0	3.70%	0	0.75%	0.50%	0	0	0.15%
Otu00022_Porphyromonadaceae	0	0	0	0	0	0	0	3%	0.10%	0	0.20%	0	0	0
Otu00036_Ruminococcaceae	1.20%	0.05%	0	0	0	0	0	0.45%	0	0	0	0	0	0
Otu00044_Rikenellaceae	0	0	0	0	0	0	0	1%	0	0	0.10%	0	0	0
Otu00082_Bacteria_uncflassified	0	0	0	0	0	0	0	0.10%	0	0	0	0	0	0
Otu00032_Lachnospiraceae	0.55%	0	0	0	0	0	0	0	0	0	0	0	0	0
Otu00085_Lachnospiraceae	0.25%	0	0	0.10%	0	0	0	0	0	0	0	0	0	0

Figure 3.5 Low abundance of candidate bacteria produces challenges in cultivation and isolation
Percentages indicate relative abundance of the nine candidate bacteria in stool, media plates at 1:10 dilution, and in freeze/thawed glycerol stocks of bacterial suspensions obtained from the indicated media plates. BL=horse's blood agar, CM=chopped media broth agar, and YCFA= yeast extract-casein hydrolysate-fatty acids agar.

As the relative abundances of these candidate bacteria are low, we wanted to determine if gavaging SPF intestinal contents into a GF mouse host could promote the expansion of these nine candidate OTUs from which we could get better cultivation success and freeze/thaw survival. For low tumor-associated bacteria, we gavaged SPF WT1 intestinal contents into GF WT mice, which is the genetic equivalent of SPF WT1 mice. We gavaged SPF WT2 intestinal contents into GF Nod1 KO mice as SPF WT2 microbiomes are similar to that of SPF Nod1 KO mice, where the absence of Nod1 may have altered the microbiome in SPF Nod1 KO mice. We collected stool on day 21 after colonization and compared the candidate bacteria abundances to the donor stool abundances.

Of the two low tumor-associated candidates, OTU32 increased in abundance by day 21 of colonization in the GF WT host (**Figure 3.6A**). This OTU was previously undetected in our initial cultivation efforts (**Figure 3.5**). However, the other low tumor-associated OTU, OTU85 did not have increased abundance in the GF WT host (**Figure 3.6A**). For high tumor-associated candidates, OTU5, OTU36, OTU44, and OTU82 increased in abundance in the GF Nod1 KO host (**Figure 3.6B**) where both OTU36 and OTU82 were previously uncultivable (**Figure 3.5**). OTU10, OTU15, and OTU22 had decreased abundances (**Figure 3.6B**). Altogether, this suggests that this method of increasing candidate bacteria abundances could help us improve cultivation of some candidates but not all, and that we have to explore other methods of promoting candidate bacteria abundances before or during cultivation and isolation.

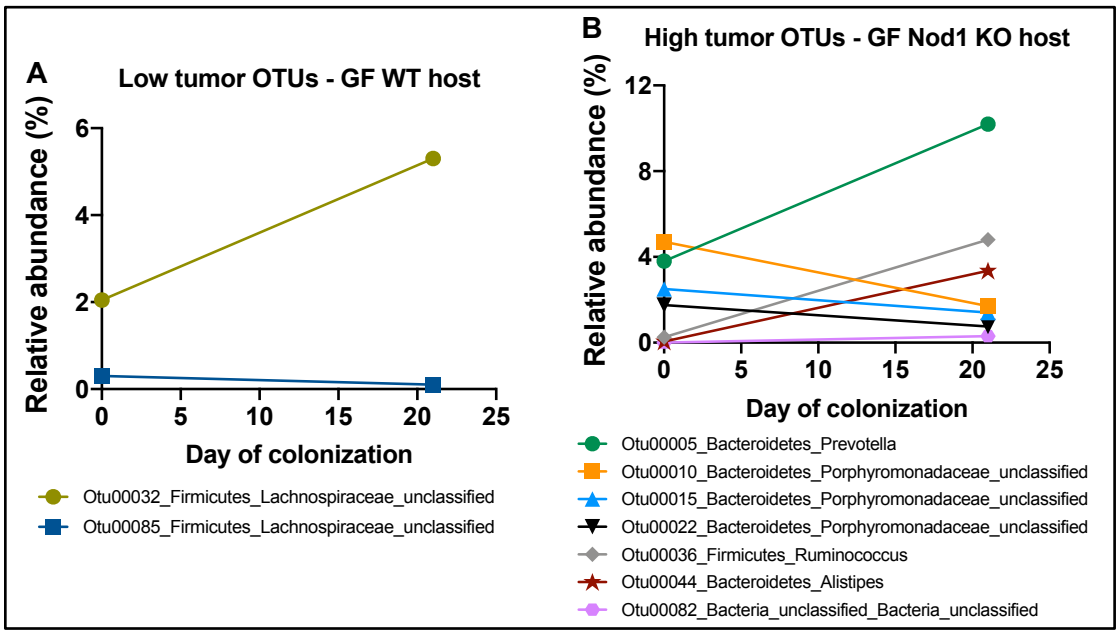

Figure 3.6 Gavaging SPF intestinal contents into a GF host promotes expansion of some candidate OTUs
Percentages indicate relative abundance of the candidate bacteria in the colonized GF mouse stool at day 21 of colonization. Day 0 values represent the abundance of the candidate bacteria in the SPF donor mouse stool.

3.4 Discussion and Future Directions

In this chapter, we performed microbiome transfer methods to determine if the tumor burden phenotype could be transmissible by the respective microbiomes associated with the two colonies. While neither cohousing nor cross-fostering methods promoted better microbiome transfer than direct gavage of intestinal contents into GF mice as described in Chapter 2, we were able to identify novel bacteria species statistically associated with low or high tumor burdens.

There has been significant interest in optimizing microbiome transfer to control for or determine microbiome-specific effects on phenotype. The gold standard is fecal transplantation of donor microbiota into recipient GF mice. As we demonstrated in the previous chapter, the transfer of WT1 or WT2 microbiomes and their corresponding tumor phenotype was optimal using this system. Cohousing is a widely used method of microbiome transfer between mice of dissimilar microbiome compositions in host-microbiome association studies, but the optimal length of time of cohousing and ratio of mice harboring two different communities in a cage remain unclear. Here, we show that four weeks of 2:2 cohousing resulted in poor microbiome and phenotype transfer. Transfer was significantly improved with six weeks of 1:1 cohousing; however, microbiome analyses demonstrated that the transfer was still incomplete with significant

differences in OTU membership between cohoused mice by LEfSe analysis (**Figure 3.2E**), likely explaining the intermediate tumor phenotype. Generation of hybrid microbiomes and incomplete transfer by cohousing has also been observed by others (180, 192, 193).

In this chapter, we show that cross-fostering provided better microbiome transfer from WT1 and WT2 mothers to WT2 and WT1 pups, respectively, than cohousing, demonstrating the strong influence of maternal transmission of the microbiome to offspring although as with 1:1 cohousing, significant differences in microbiome composition remained (**Figures 3.3E and 3.3F**). Despite the improvement in microbiome transfer, the tumor phenotype of cross-fostered mice remained intermediate between that of control WT1 and WT2 mice. It is possible that the transfer of WT1 and WT2 microbiomes was incomplete with these methods given the difficulty of transferring mucosa-associated adherent bacteria (192). Alternatively, the lack of complete phenotype transmissibility with either cohousing or cross-fostering may also reflect the poor survivability of obligate anaerobes outside the colon

Additionally, we identified several OTUs that were predictive of tumor susceptibility by analyzing the gut microbiomes of WT1 and WT2 mice as well as of mice from multiple fecal transfer experiments with hybrid microbiomes. We and others have used similar approaches and statistical tools to identify differential OTU(s) between groups that correlate with disease outcomes (180, 189, 193, 194). Here, the low or high tumor burdens of AOM/DSS-treated mice cannot be attributed to a single bacteria species or family. For example, the bacteria family *Prevotellaceae* is increased in naïve WT2 mice and strongly predictive of high tumor burdens, while *Lachnospiraceae* is significantly associated with decreased inflammation-associated tumorigenesis. Decreased *Lachnospiraceae* have been found in IBD and CRC patients (26, 195), where they may have anti-inflammatory function via butyrate production (26). In contrast, *Prevotellaceae* are enriched in IBD and CRC patients and are also associated with increased susceptibility to DSS-induced colitis in mice, suggesting they may be pro-inflammatory (26, 30, 72, 126). Similarly, a member of the *Ruminococcaceae* was associated with high tumor burdens, where *Ruminococcaceae* have also been found to be enriched in IBD and CRC patients (26, 196). A phylogenetic tree based on 16S rRNA sequence similarity suggests that the OTU candidates associated with different tumor burdens but from the same family are evolutionarily distinct from each other (**Figure 3.4B**) (191, 197). Regardless, as we have only identified a correlation between

the identified OTUs and tumor outcomes, it still remains to be determined whether these bacteria regulate tumor susceptibility alone or via interactions with other bacterial populations.

To determine if these specific bacteria have anti- or pro-tumorigenic effects, we started preliminary culturing efforts. Unfortunately, cultivating these bacteria from WT1 and WT2 mice has been a significant challenge given their generally low abundance. Based on relative bacteria abundances from 16S rRNA sequencing analyses in **Figure 3.5**, fewer than 1% of the colonies were the OTUs of interest on various select media plates, and the only OTU that survived freeze/thaw was 0.15% of total bacteria that survived freeze/thaw. Moving forward, we will try several methods to promote the expansion of certain bacterial populations including treating animals with antibiotics before harvesting intestinal contents or plating intestinal contents on different antibiotic-containing media to increase gram positive or negative bacteria numbers. Furthermore, we can try to bulk culture as many bacteria as possible in liquid media in plates; we can dilute homogenates so that only one bacterium is added per well. We can sequence each well and if candidate bacteria are detected, we can expand the liquid stock to test optimal freezing and thawing conditions including testing different freezing media at different concentrations. Similarly, we can try to directly culture single-species suspensions which would require more people and time. As our candidate bacteria may not immediately grow well in liquid cultures, we would pick colonies from the initial plate to re-streak and dilute on a second plate to ensure each colony is a single species. Afterward, single colonies are picked and grown in liquid media for expansion. Lastly, these liquid stocks are sequenced and frozen down. With this process, we are picking and expanding the abundance of bacteria into a single species stock before freezing, likely ensuring more successful survival after thawing. The downside to this process is the high number of initial colonies that have to be picked because the odds of picking one of the nine candidate bacteria is low.

After cultivating and isolating as many candidates as possible, we plan to gavage low tumor-associated bacteria and high tumor-associated bacteria into two groups of GF WT mice. After colonization, these mice will undergo AOM/DSS to determine if these bacteria are not only associated with, but are sufficient in, mitigating or promoting colon tumorigenesis.

These data show that success of cohousing or cross-fostering for microbiome transfer and normalization can depend on the microbiota involved. Despite not achieving complete microbiome transfer from one colony to the other, we were able to use these data to identify nine novel bacteria

species that are associated with low or high tumor burdens. Our next steps are to cultivate and isolate these nine candidate bacteria and determine if they are sufficient to promote tumor burden differences, and if they do, we plan to explore possible mechanisms of how these bacteria cause differential tumorigenesis.

CHAPTER 4: Two WT Mouse Colonies with Microbiome Differences Have Host Immune Differences

4.1 Introduction

In Chapter 2, we revealed that the microbiome compositions of two WT colonies of mice were significantly different and contributed to tumor burden differences. It has been shown that the gut microbiota can modulate host immune responses (79, 198-200). For instance, GF mice have underdeveloped mucosal immunity and lymphoid organs, where immune development can be induced upon bacteria colonization (201). Furthermore, specific bacteria can modulate certain immune cell subsets. Clostridia-produced butyrate, a short chain fatty acid metabolite, promotes Treg cell differention and inhibits macrophage and neutrophil activation (80, 81, 123). Segmented filamentous bacteria attaches to small intestinal epithelial cells and induces Th17 cell differentiation (182, 202), and *Bacteroides fragilis* makes polysaccharide A which promotes inducible Treg cell differentiation in a TLR2-dependent manner (203, 204).

In this chapter, we explore whether host immune differences occur due to the different microbiomes and how host immune differences may contribute to the contrasting tumor burden phenotypes of the two WT mouse colonies.

4.2 Materials and Methods

4.2.1 Mice

SPF WT1, *Rag1*$^{-/-}$ (*Rag1*^{tm1Mom}) and *Cd8*$^{-/-}$ (B6.129S2-*Cd8a*^{tm1Mak}) mice (all in the C57BL/6 background) were originally purchased from Jackson Laboratory (JL) and bred in-house at the University of Michigan (UM). WT2 mice were generated from WT littermates (*Nod1*$^{+/+}$) of backcrosses between JL B6 mice with transgenic *Nod1*$^{-/-}$ mice (>F8) and subsequently established as a separate wildtype colony. WT1 and WT2 were kept on different racks to minimize cross-

contamination of their microbiomes. Adult male or female 6-10 week-old mice were used except where noted. 7-8 week old *CDX2-Cre Apc*$^{fl/fl}$ mice were used and were bred in house.

11-15 week old GF WT (**Figure 4.10**) and 7-8 week old GF *Rag1*$^{-/-}$ mice (**Figures 4.3 and 4.15**), both in the C57BL/6 background, and derived from JL mice, were bred and housed at the UM Germ-free mouse facility. Sterility was regularly verified by aerobic and anaerobic cultures, Gram stains, and qPCR. GF mice were conventionalized via oral gavage of cecal and stool contents from young adult (6+ weeks) SPF WT1 or WT2 mice.

Animal studies were conducted under protocols approved by the University of Michigan Committee on the Use and Care of Animals.

4.2.2 Inflammation-induced colon tumorigenesis

6-10 week-old mice were injected intraperitoneally with 10mg azoxymethane (Sigma) per kg mouse weight. After five days, mice were treated with three cycles of 2% dextran sulfate sodium (MP Bio, m.w.=36,000-50,000) given for five days in the drinking water followed by 16 days of regular drinking water. Depending on the particular experiment, mice were sacrificed between days 60-70 after AOM injection as specified in the Figure. For tumor counting, colons were flushed of stool with PBS, longitudinally cut open and grossly counted using a magnifier and measured with calipers. For experiments involving conventionalized GF mice, all groups received three rounds of 1.5% DSS water (**Figure 4.3**) or one round of 1.5% DSS followed by two rounds of 1% DSS to maximize survival (**Figure 4.15**).

4.2.3 Microarray

RNA was extracted from distal colon tissue of SPF WT1 and WT2 mice on day 0 and 10 of AOM/DSS treatment with the NucleoSpin RNA Kit (Macherey-Nagel). Equal amounts of RNA from several samples were pooled into for a single microarray sample per genotype and timepoint. RNA samples were submitted to the University of Michigan DNA Sequencing Core for transcriptome analysis using the Affymetrix GeneChip™ Mouse Gene 2.1 ST Array Strip. WT1 and WT2 samples were compared within a timepoint. Probesets where expression values of one of the two samples was 2^4 or greater and with a 2 fold or greater in change are shown.

4.2.4 Bacteria preparation for oral gavage

Whole SPF stool and cecal contents were isolated from young adult SPF WT1 and WT2 mice. Specifically, stool and cecal contents were collected under strictly anaerobic conditions

(85% N_2, 10% H_2, 5% CO_2) in a Coy anaerobic chamber immediately after euthanasia and homogenized in anaerobic PBS. Mice received 200µl of homogenate. Homogenates were aliquoted into Eppendorf tubes (one tube/recipient) to ensure homogenates remained anaerobic before gavage.

4.2.5 Microbiome depletion by antibiotic and antifungal water

8 week-old CD8 KO (**Figure 4.8**), 4-5 week-old WT1 and WT2 mice (**Figure 4.9**), or 7-8 week-old *CDX2-Cre Apc*$^{fl/fl}$ mice (**Figure 4.17**), were treated with antibiotic and antifungal water for one week to target Gram-positive, Gram-negative and anaerobic bacteria and to prevent fungal blooms (205). Mice were treated with an antibiotic cocktail consisting of 0.5g/L vancomycin (Pfizer), 2g/L streptomycin (Sigma), 0.75g/L metronidazole (Sigma), and 0.5g/L fluconazole (Sigma) that was sterile-filtered prior to administration. 2% sucralose (Apriva, Kroger®) was added to increase the antibiotic solution palatability (206). Mice then received regular water for 24 hours, were gavaged with WT1 or WT2 stool and cecal homogenates from donor mice that were at least 6 weeks of age for three consecutive days, and then treated with AOM/DSS four weeks later.

4.2.6 Immune cell isolation

Spleens and mesenteric lymph nodes (MLNs) were isolated from naïve age-matched 6-12 week old WT1 and WT2 mice or from mice on day 60 of AOM/DSS treatment and smashed through 70um cell strainers in complete RPMI (=RPMI (Gibco) + 10% FBS (Sigma Aldrich) + 1% penicillin/streptomycin + 1% L-glutamine). MLN cells were washed once with PBS before downstream flow cytometry analysis. Splenocytes were treated with red blood cell lysis buffer for 3-5 minutes and washed once with PBS before downstream flow cytometry analysis.

Colon LP cells were isolated as previously described (165, 169). Whole colons were isolated from naïve 6-10 week old WT1 and WT2 mice and cut into small pieces and washed with HBSS+ (=HBSS (Gibco) supplemented + 2.5% heat-inactivated FBS (Sigma Aldrich) + 1% penicillin/streptomycin). After two washes with magnetic stirring, colon pieces were incubated in HBSS+ with 1mM DTT (Invitrogen) at 37°C. Colon pieces were washed once and incubated twice in HBSS+ with 1mM EDTA (Lonza) at 37°C with magnetic stirring for 30 minutes. After washing twice, colon tissue was digested in HBSS+ with 400 I.U./mL type III collagenase (Worthington) and 10 µg/mL DNase I (Worthington) at 37°C with magnetic stirring. The single cell suspension

was filtered through a 70-micron filter. Colon LP immune cells were collected at the interface of a 40%/75% Percoll gradient after centrifugation. For tumor endpoint analyses, tumor or adjacent tissue were cut from the colons and processed as described above but with a single EDTA step.

For MC38 subcutaneous tumors, part of the tumor was minced into ~1mm pieces using a scalpel and digested with RPMI + 1% L-glutamine with 400 I.U./mL type III collagenase (Worthington) and 10 µg/mL DNase I (Worthington) at 37°C with magnetic stirring. The single cell suspension was filtered through a 70-micron filter and pelleted. Cells were resuspended in 30ml RPMI + 1% L-glutamine, and 10ml of Ficoll-Paque PLUS (GE Healthcare) was layered underneath. Intratumoral immune cells were collected at the interface after centrifugation and washed once with complete RPMI before downstream flow cytometry analysis.

4.2.7 Flow cytometry and staining

MLN or colon LP immune cells were isolated from mice at day 0, day 12 of AOM/DSS or at the tumor endpoint (typically day 60) and surface stained. For intracellular staining, cells were incubated for 4 hours at 37°C with either 1) GolgiStop (monensin, BD) + 100 ng/ml PMA (Sigma) + 1000 ng/ml ionomycin ("PMA/Iono") or 2) with GolgiStop alone ("no stim"). Cells were surface stained, fixed and permeabilized using the Foxp3/Transcription Factor Staining Buffer Set (eBioscience), and then incubated with fluorochrome-conjugated antibodies against IFNγ, IL-17 and Foxp3 (see below). For adgpk tetramer staining, intratumoral MC38 immune cells were incubated for 30 minutes with PE-Adpgk tetramer (NIH, gift from the James Moon lab) before surface staining. Samples were analyzed by a BD LSRFortessa, FACSCanto II, or FACSAria II flow cytometer. Flow cytometry staining antibodies used:

Antibody and clone	**Source**	**Catalog number**
CD3 APC-Cy7 clone 145-2C11	BioLegend	Cat#100330
CD3 PE-Cy7 clone 17A2	BioLegend	Cat#100220
CD3 FITC clone 145-2C11	BioLegend	Cat#100204
CD45.2 BV421 clone 104	BioLegend	Cat#109832
CD4 APC clone GK1.5	eBioscience	Cat#17-004-82
CD8 PerCP-Cy5.5 clone 53-6.7	BioLegend	Cat#100732
CD8 APC-Cy7 clone 53-6.7	BioLegend	Cat#100714
CD69 APC clone H1.2F3	BioLegend	Cat#104514
CD44 PE clone IM7	BioLegend	Cat#103007

CD62L APC-Cy7 clone MEL-14	BioLegend	Cat#104427
Tim-3 PerCP-Cy5.5 clone B8.2C12	BioLegend	Cat#134011
PD-1 PE-Cy7 clone RMP1-30	BioLegend	Cat#109109
Lag-3 PE clone C9B7W	BioLegend	Cat#125207
IFNγ PE-Cy7 clone XMG1.2	BioLegend	Cat#505826
IL-17 FITC clone TC11-18H10.1	BioLegend	Cat#506907
Foxp3 PE clone FJK-16s	eBioscience	Cat#12-5773-80
NK1.1 PerCP-Cy5.5 clone PK136	BD Pharmingen	Cat#561111
Ly6C FITC clone HK1.4	BioLegend	Cat#128005
Ly6G PE-Cy7 clone 1A8	BioLegend	Cat#127617
CD11b PE clone M1/70	BD Pharmingen	Cat#561689
CD11c APC clone N418	BioLegend	Cat#117310
B220 Pacific Blue clone RA3-6B2	BioLegend	Cat#103227
CD103 PE clone 2E7	BioLegend	Cat#121405

4.2.8 RNA isolation and qPCR

Intraepithelial cells were isolated from naïve WT1 and WT2 mice from the EDTA steps of LP immune cell isolation. Total RNA was isolated using the Nucleospin RNA kit (Macherey-Nagel). cDNA synthesis was performed using the iScript cDNA synthesis kit (BioRad) and used for quantitative PCR using SYBR Green on the ABI 7900HT. Gene transcript levels were normalized to actin. Primer sequences used:

qPCR primer: IL-1β F	5'-GATCCACACTCTCCAGCTGCA-3'
qPCR primer: IL-1β R	5'-CAACCAACAAGTGATATTCTCCATG-3'
qPCR primer: CXCL9 F	5'-GGAACCCTAGTGATAAGGAATGCA-3'
qPCR primer: CXCL9 R	3'-TGAGGTCTTTGAGGGATTTGTAGTG-5'
qPCR primer: CXCL10 F	5'-GACGGTCCGCTGCAACTG-3'
qPCR primer: CXCL10 R	3'-CTTCCCTATGGCCCTCATTCT-5'
qPCR primer: IL-6 F	5'-CACATGTTCTCTGGGAAATCG-3'
qPCR primer: IL-6 R	5'-TTTCTGCAAGTGCATCATCG-3'
qPCR primer: occludin F	5′-GGGAATGTCCAGAACGAGAAGA-3'
qPCR primer: occludin R	5'-CGTGGCAATGAACACCATGA-3'
qPCR primer: *β*-defensin2 F	5′-AAGTATTGGATACGAAGCAG-3′
qPCR primer: *β*-defensin2 R	5′-TGGCAGAAGGAGGACAAATG-3′

qPCR primer: Reg3γ F	5'-TCAGGTGCAAGGTGAAGTTG-3'
qPCR primer: Reg3γ R	5'-GGCCACTGTTACCACTGCTT-3'
qPCR primer: actin F	5'-CAACTTGATGTATGAAGGCTTTGGT-3'
qPCR primer: actin R	5'-ACTTTTATTGGTCTCAAGTCAGTGTACAG-3'

4.2.9 Preparation of heat-killed bacteria

Stool pellets from SPF WT1 and WT2 mice were homogenized in PBS, strained through a 40um cell strainer, and centrifuged at 1000rpm for 10 seconds to pellet debris. The supernatant was centrifuged at 5000rpm for 10 minutes. The white bacteria layer of the pellet was diluted in PBS and incubated at 95°C for one hour. Heat-killed bacteria suspensions were stored at -20°C until use.

4.2.10 Bone marrow-derived dendritic cell (BMDC) preparation and stimulation

BMDCs were prepared from WT1 and WT2 mice as previously described (207). Briefly, bone marrow cells were cultured for seven days in BMDC-media (=RPMI (Gibco) + 10% FBS (Sigma Aldrich) + 1% penicillin/streptomycin + 1% L-glutamine + 20 ng/ml GM-CSF (Peprotech)). BMDCs were isolated using the CD11c Microbeads Ultrapure (Miltenyi Biotec) kit. $4x10^5$ BMDCs were cultured with $4x10^6$ heat-killed bacteria for four hours, washed once in PBS, and then resuspended in fresh BMDC-media and collected after 20 hours.

4.2.11 ELISA

IL-12p70 was measured in 24 hour supernatants of heat-killed bacteria-stimulated BMDCs using the IL-12p70 ELISA kit (R&D Systems).

Stool of naïve WT1 and WT2 mice were homogenized in PBS to 100mg stool/1mL PBS. Supernatants were diluted 1:10 in PBS + 3% FBS + 0.05% Tween-20. IgA was captured using an anti-mouse IgA antibody (Bethyl A90-103A) and measured by detecting the reaction signal of goat anti-mouse IgA HRP conjugate antibody (Bethyl A90-103P) with TMB one-component HRP substrate. Plate signals were read at 450 nm using a microplate reader (Model 3550; Bio-Rad Labs).

4.2.12 CD8 depletion

300µg of anti-CD8 (Bio X Cell, clone YTS 169.4) or isotype control (Bio X Cell, clone LTF-2) antibodies diluted in PBS were intraperitoneally injected into 9 or 12-13 week-old WT1

mice or 7-10 or 12-13 week-old WT2 mice. Specific timings of injections are described in the Figure Legends.

4.2.13 CD8 T cell adoptive transfer

8 week-old GF *Rag1*$^{-/-}$ mice were colonized with SPF WT1 or WT2 intestinal homogenates. WT2 splenic CD8 T cells were bead-isolated using the mouse CD8a+ T Cell Isolation Kit (Miltenyi-Biotec). $3x10^6$ CD8 T cells were intravenously injected into colonized GF *Rag1*$^{-/-}$ mice. Adoptive transfers were done by Hideaki Fujiwara. Four weeks after CD8 T cell colonization, mice were treated with AOM and one round of 1.5% DSS followed by two rounds of 1% DSS to ensure survival. Weights were measured throughout AOM/DSS. Mice were sacrificed on day 60 of AOM/DSS for tumor counting.

4.2.14 MC38 subcutaneous tumor model

$1x10^6$ MC38 cells were injected into the flank of 8-10 week-old SPF WT1 or WT2 mice. All mice were sacrificed on day 23. Endpoint subcutaneous tumors were cut out from the flank and weighed before immune cell isolation processing.

4.2.15 Isolation of bacterial DNA and 16S rRNA sequence analyses

16S rRNA analysis was performed with fecal samples that had been collected from mice on the day of AOM injection and were frozen at -20 or -80° C. Bacterial DNA was isolated using the PowerSoil-htp 96 Well Soil DNA isolation kit (Qiagen) with the epMotion 5075 manually with the DNeasy PowerSoil Kit (Qiagen). The V4 region of the 16S rRNA gene was amplified using custom barcoded primers, sequenced with the Illumina MiSeq Personal Sequencing platform, and processed using the mothur software package to reduce sequencing errors and remove chimeras as previously described (Kozich et al., 2013; Schloss et al., 2009). Sequences were aligned to the SILVA 16S rRNA sequence database (Pruesse et al., 2007). Sequences were grouped based on their taxonomic classification or clustered into operational taxonomic units (OTUs) using a 97% similarity cutoff. Parallel sequencing and processing of a mock community allowed us to determine a sequencing error rate of 1.38%. Dissimilarity in community structure between samples was calculated using the θ_{YC} (thetaYC) distance metric. ThetaYC distances between the samples were used for two-dimensional ordination analysis by non-metric dimensional scaling (NMDS). Microbial alpha diversity was calculated using the inverse Simpson index and the observed number of OTUs (richness) (37). Analysis of MOlecular VAriance (AMOVA) was used to determine

significance between community structure differences of different groups of samples. LEfSe and Metatstats in mothur were used to determine statistically differential OTUs between group (166, 167). All FASTQ sequences can be obtained from the Sequence Read Archive at NCBI (BioProject number PRJNA557261).

4.2.16 Statistical analyses

Continuous data are shown as mean ± SEM. Sample sizes can be found in the Figure Legends. Statistical analyses were performed using GraphPad Prism7, R and mothur software. Statistically significant differences were determined by Mann-Whitney when only two groups are compared (e.g., cell number, etc.). Differences in bacterial community structure were analyzed using AMOVA in mothur (168). P-values below 0.05 were considered statistically significant and are represented as follows: *$p<0.05$.

4.3 Results

4.3.1 Host immune differences are measured between WT1 and WT2 mouse colons

To initially determine if differential gene expression occurred between SPF WT1 and WT2 mice, we performed a microarray using RNA isolated from untreated and early inflammation (day 10 of AOM/DSS) SPF WT1 and WT2 colon tissue. We measured the relative expression of significantly differentially expressed genes and grouped the genes based on function. A large number of immunoglobulin (Ig) and Ig receptor genes were more highly expressed in naïve WT1 colons but were more highly expressed WT2 colons after inflammation (**Figure 4.1**). Additionally, several interferon induced genes including *Oas2*, *Ifit1*, *Ifi44*, and more, were also more highly expressed in WT2 colons after inflammation (**Figure 4.1**), which may be consistent with higher inflammation and increased histologic scores (which includes epithelial loss) in WT2 mice at day 12 of AOM/DSS (**Figures 2.1E and 2.1F**). Additional inflammatory and immune cell-related genes that are increasingly upregulated in inflamed WT2 colons include but are not limited to *Saa3*, *Tarm1*, *Slfn4*, *Duox2*, and *Cd274*. Interestingly, major urinary proteins show a striking difference; they are increased in naïve WT2 colons but after inflammation, increased in WT1 colons (**Figure 4.1**). However, the significance of these proteins in inflammation or host immunity

is unknown. Altogether, this microarray data suggests there may be differential host immune and inflammatory gene expression between WT1 and WT2 mice before and during inflammation.

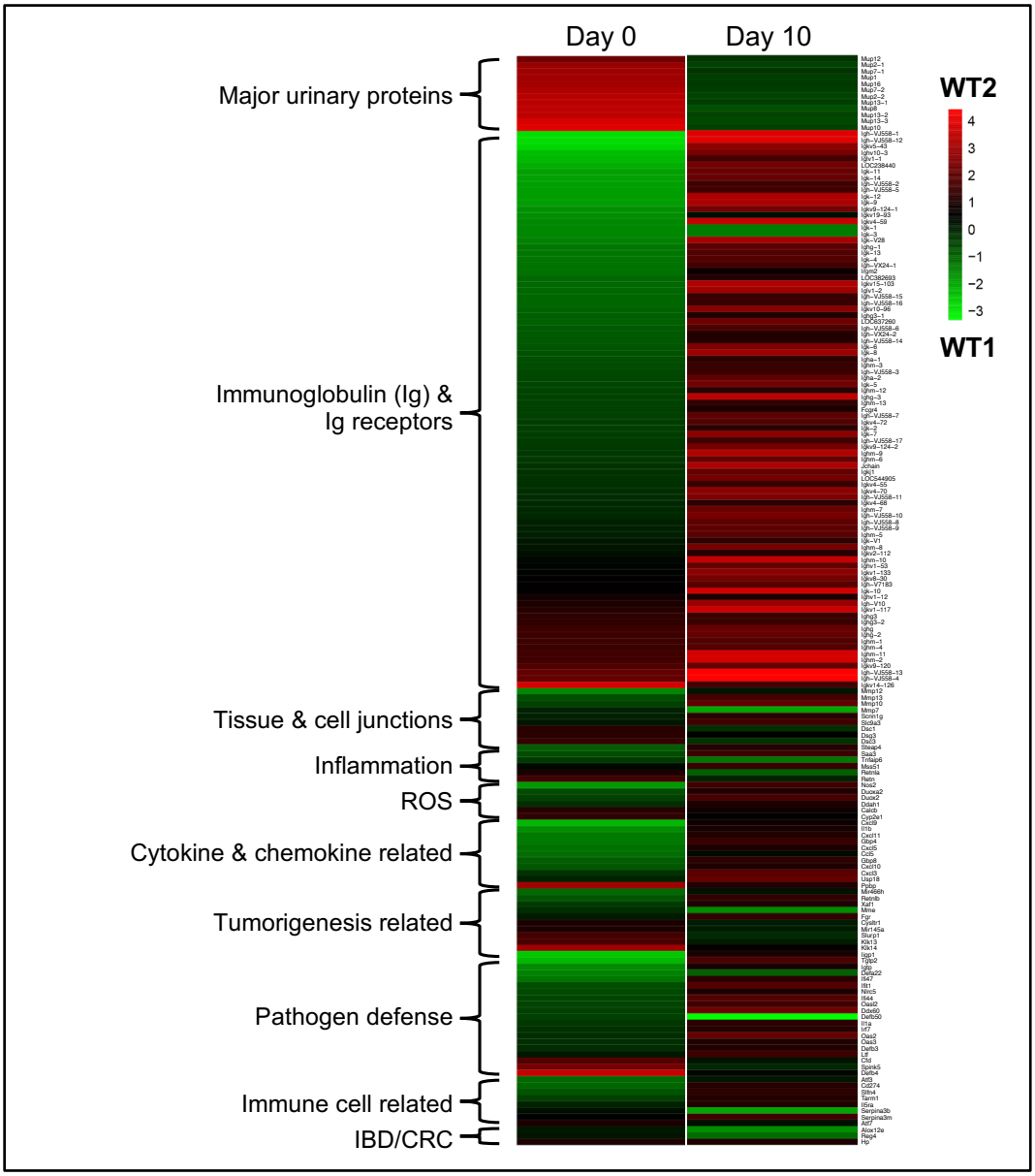

Figure 4.1 Microarray of relative RNA expression from distal colon tissue of WT1 and WT2 mice on day 0 and 10 of AOM/DSS treatment

Red represents genes that are more highly expressed in WT2 mice and green represents genes that are more highly expressed in WT1 mice. WT1: d0 n=4, d10 n=5; WT2: d0 n=3, d10 n=6.

4.3.2 Dysbiotic microbiome of WT2 mice promotes inflammation-associated tumorigenesis via adaptive immune cells

To determine whether the difference in tumor susceptibilities between WT1 and WT2 mice were associated with altered baseline immune responses, immune cell compositions were analyzed from spleen, bone marrow, and entire colon of untreated WT1 and WT2 mice by flow cytometry. No differences in colon LP monocytes, neutrophils, dendritic cells (DCs) or NK cells were observed, but WT2 mice had increased B and T cell populations compared to WT1 mice (**Figure 4.2A**). No differences in immune cell composition were measured in the spleen and mesenteric lymph nodes (MLNs) (**Figures 4.2B and 4.2C**). This suggests that the WT2 microbiome may exert its tumor-promoting effect via colon LP adaptive immune cells.

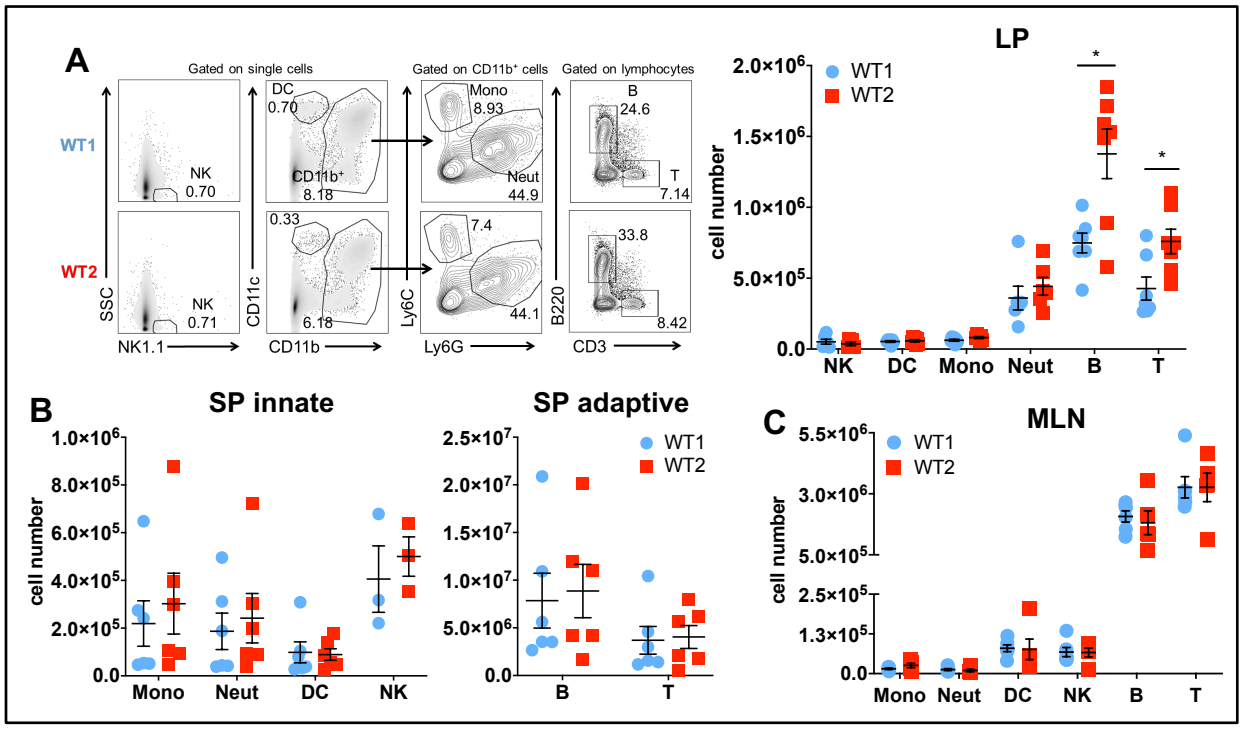

Figure 4.2 WT2 mice have increased colon LP B and T cells
Immune cell subsets were measured by flow cytometry in the colon LP (**A**), spleen (**B**), and MLNs (**C**). Immune subsets measured include: DCs ($CD11c^+$ $CD11b^{int}$), NK cells ($NK1.1^+$), monocytes ($CD11b^+$ $Ly6C^{hi}$ $Ly6G^{int}$), neutrophils ($CD11b^+$ $Ly6C^{int}$ $Ly6G^+$), T cells ($CD3^+$ $B220^-$), and B cells ($B220^+$ $CD3^-$). Data are mean ± SEM and are representative of or pooled from at least two independent experiments. LP: n=5-7/group; SP: n=3-6/group; MLN: n=5-6/group. *p<0.05 by Mann-Whitney

To examine this possibility, GF *Rag1*$^{-/-}$ mice were gavaged with anaerobically prepared SPF WT1 or WT2 stool and cecal homogenates (**Figure 4.3A**). After four weeks, successful colonization of WT1 and WT2 microbiomes were detected as shown by relative family

abundances, as measured by thetaYC distances, and as visualized by NMDS plots (**Figures 4.3B-D**). Following four weeks of colonization, mice were then treated with AOM/DSS to induce tumors.

GF *Rag1*$^{-/-}$ mice with WT2 microbiota developed fewer and smaller tumors compared to SPF WT2 controls (**Figures 4.3E and 4.3F**), suggesting that the dysbiotic WT2 microbiome promotes tumor susceptibility by acting on adaptive immune cells. GF *Rag1*$^{-/-}$ mice with WT1 microbiota developed slightly increased tumor numbers compared to SPF WT1 control mice (**Figure 4.3E**), which may indicate a protective role for adaptive immune cells in the context of the WT1 microbiome. Of note, GF *Rag1*$^{-/-}$ mice had significantly more tumor numbers compared to SPF *Rag1*$^{-/-}$ mice suggesting that the absence of any microbiota can be lead to increased tumorigenesis susceptibility, which is consistent with previous reports which suggest that GF mice are more susceptible to both DSS-induced injury and AOM/DSS-induced tumorigenesis (123, 160).

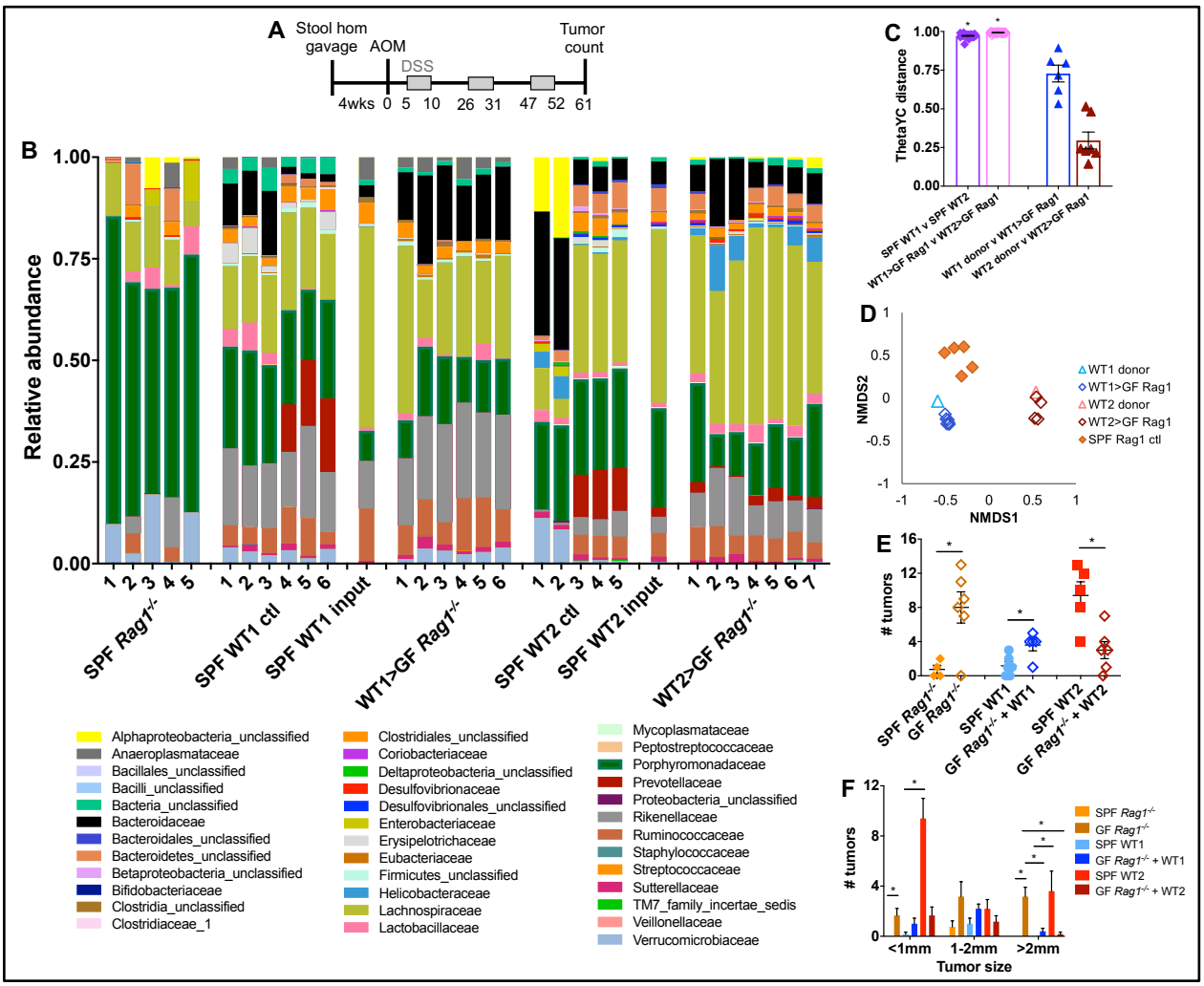

Figure 4.3 The WT2 microbiome promotes increased AOM/DSS-induced colon tumor burdens via adaptive immune cells

A) GF *Rag1*$^{-/-}$ mice were gavaged with SPF WT1 or WT2 stool and cecal contents followed by AOM injection and three rounds of 1.5% DSS after four weeks of colonization. Mice were sacrificed on day 61 for tumor counting.

B) Relative bacterial family abundances of colonized GF *Rag1*$^{-/-}$ mice four weeks after gavage of SPF WT1 or WT2 intestinal contents.

C and D) Microbiome similarity between donors and colonized mice are measured by thetaYC distances (**C**) and shown by an NMDS plot (**D**). *p<0.05 by AMOVA

E and F) Tumor numbers (**E**) and sizes (**F**) are shown. Data are mean ± SEM. *p<0.05 by Mann-Whitney n=4-6/group.

4.3.3 WT2 mice have increased colon LP CD8^{+} IFNγ^{+} T cells

We and others have previously shown a role of T cells in affecting tumor susceptibility in the AOM/DSS model (169, 208). Here, we further examined potential T cell subset differences in the colon LP. By flow cytometry, WT2 mice have increased colon LP CD8 T cells compared to WT1 mice (**Figure 4.4A**). To determine if T cell activity was altered between WT1 and WT2 mice,

we examined LP T cell cytokine production after four hours of *ex vivo*-stimulation by phorbol myristate acetate (PMA) and ionomycin. Specifically, colon LP $CD8^+$, but not $CD4^+$, $IFN\gamma^+$ T cells are increased in naïve WT2 mice (**Figure 4.4B**). In contrast, there were no differences in colon LP $CD4^+$ $IL\text{-}17^+$ or $CD4^+$ $Foxp3^+$ cells (**Figure 4.4B**), suggesting that Th17 and Treg cells do not contribute to the increased inflammation and tumor susceptibility of WT2 mice. To further define the nature of the CD8 T cell differences between WT1 and WT2 mice in the colon LP, we examined levels of activated $CD8^+$ $CD69^+$ cells, resident memory $CD8^+$ $CD69^+$ $CD103^+$ cells, and effector memory $CD8^+$ $CD44^+$ $CD62L^-$ cells and observed increased levels in the WT2 colon LP whereas there were no differences in activated, resident memory, or effector memory CD4 T cells in the colon LP between WT1 and WT mice (**Figures 4.4C-E**). Furthermore, no differences in CD3, CD4 or CD8 T cells were measured in mesenteric lymph nodes (MLNs) of naïve mice (**Figures 4.5A and 4.5B**), and no differences in IFNγ-producing CD8 or CD4 T cells were measured (**Figure 4.5C**). Altogether, this shows that $CD3^+$, and specifically $CD8^+$ $IFN\gamma^+$, T cell differences are specific to the colon LP.

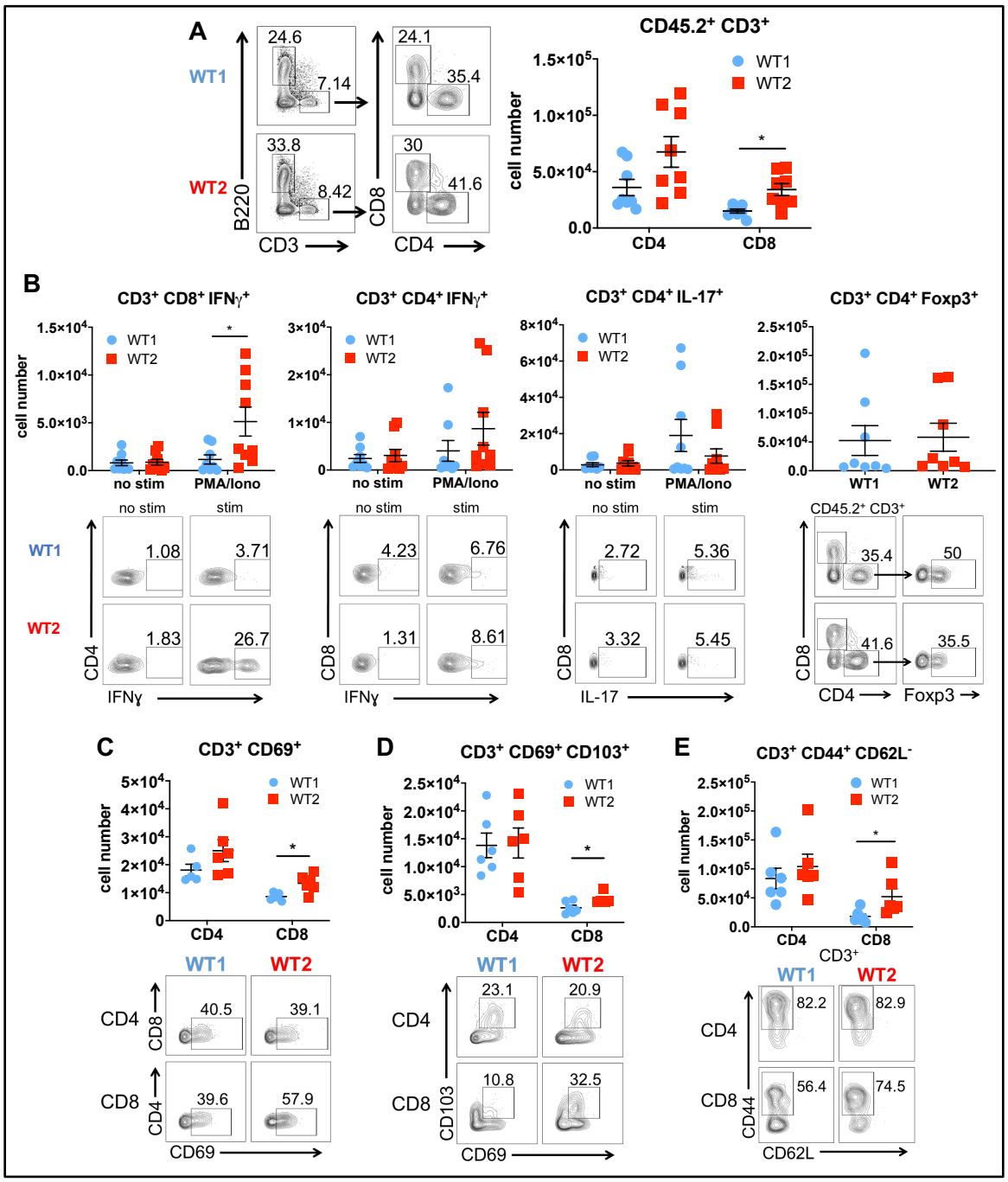

Figure 4.4 Naive WT2 mice have increased IFNγ-producing, activated, resident memory, and effector memory colon LP CD8 T cells

A) Number of CD4 and CD8 T cells in colon LP T cells of WT1 and WT2 mice as determined by flow cytometry. n=8/group.

B) Intracellular cytokine production (IFNγ and IL-17) was measured after four hours of PMA + ionomycin + monensin stimulation. Intracellular Foxp3 staining was performed after four hours of monensin incubation. Representative flow plots are shown. n=8-9/group.

C-E) Naïve colon LP CD4 and CD8 cells were further characterized for activation ($CD69^+$) (**C**), resident memory ($CD69^+$ $CD103^+$) (**D**), or effector memory ($CD8^+$ $CD44^+$ $CD62L^-$) (**E**). Cells are gated on $CD45.2^+$ $CD3^+$ or $CD3^+$, n=5-6/group.

Data are mean ± SEM and are pooled from at least two independent experiments. *p<0.05 by Mann-Whitney

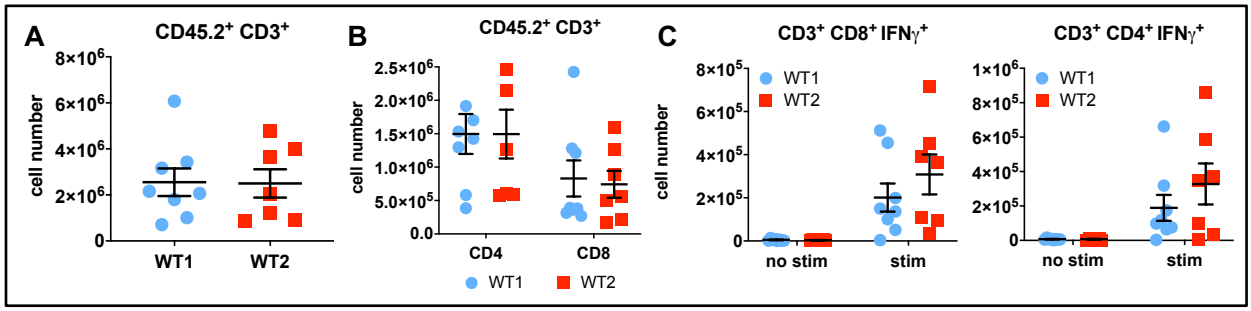

Figure 4.5 No T cell differences are present in mesenteric lymph nodes
A-B) MLN CD3 T cells (**A**) were measured and further characterized into CD4 and CD8 T cells (**B**) by flow cytometry. **C-D**) Intracellular IFNγ production by CD8 (**C**) and CD4 (**D**) T cells was measured after four hours of PMA + ionomycin + monensin stimulation.
Data are mean ± SEM and are pooled from at least two independent experiments. n=5-9/group, *p<0.05 by Mann-Whitney

We next analyzed the colon LP immune cell composition during the acute inflammatory response to DSS, specifically on day 12 of AOM/DSS which is when colon inflammatory immune cell infiltration peaked as measured in WT2 mice (**Figure 4.6**). As in naïve mice, there were significantly increased CD3 and CD8, but not CD4, T cells, in WT2 mice compared to WT1 mice (**Figures 4.7A and 4.7B**). Additionally, colon LP $CD8^+$ $IFN\gamma^+$ T cells were increased in WT2 mice, but no differences in $CD4^+$ $IFN\gamma^+$, $CD4^+$ IL-17^+ or $CD4^+$ $Foxp3^+$ subsets were measured (**Figure 4.7C**). Colon LP monocytes and neutrophils in WT2 mice were also elevated to a greater extent than WT1 mice (**Figure 4.7A**), likely reflecting greater levels of inflammation that occur in WT2 mice due to DSS treatment (**Figure 2.3E**).

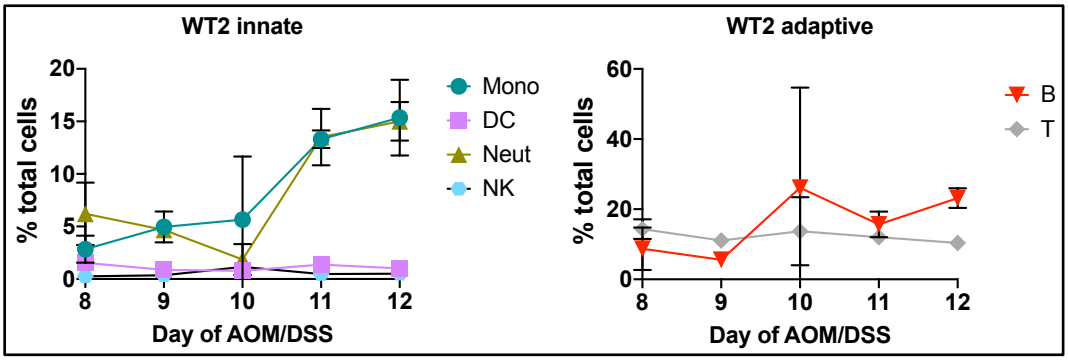

Figure 4.6 WT2 mice have increased colon inflammatory cell infiltration on day 12 of AOM/DSS

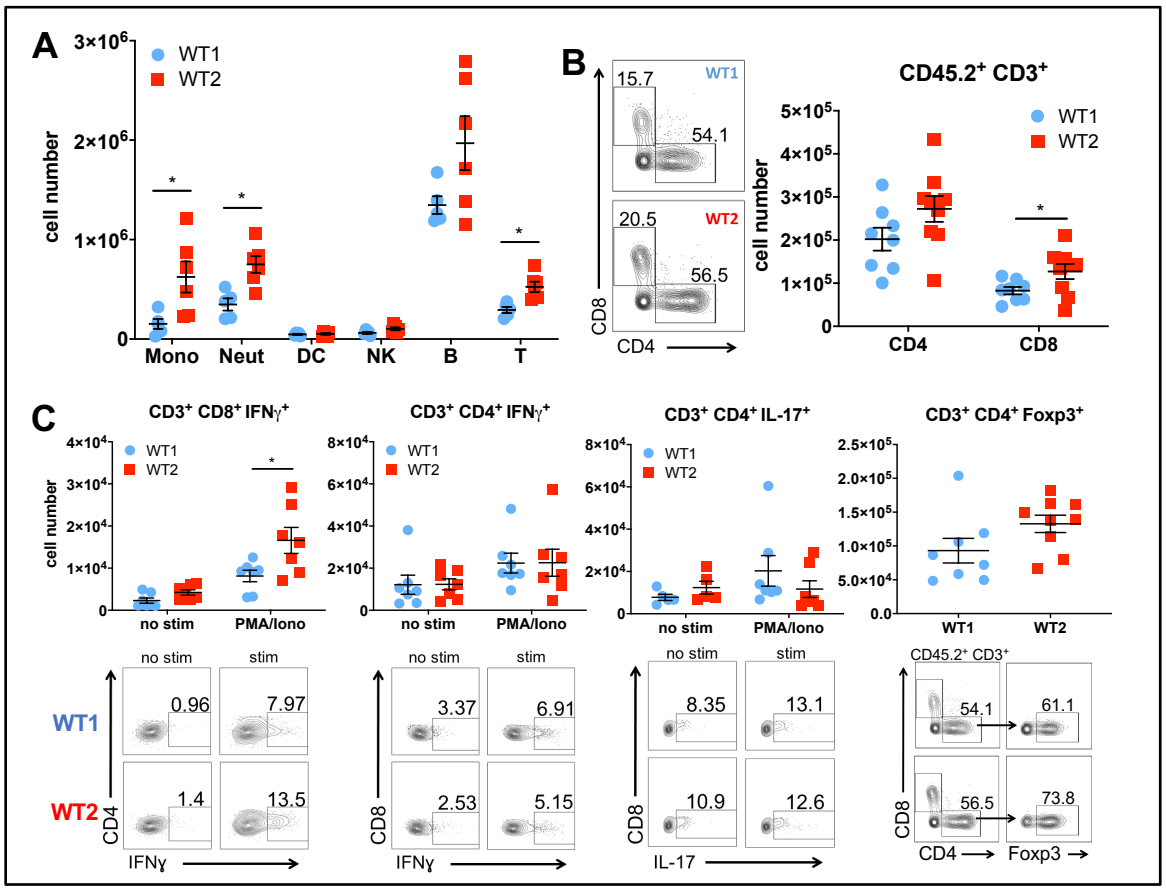

Figure 4.7 WT2 mice have increased colon LP CD8$^+$ IFNγ$^+$ T cells on day 12 of AOM/DSS
Mice were injected with AOM and five days later, treated with 2% DSS for five days. Two days after DSS treatment completion, mice were sacrificed for colon LP flow cytometry analysis.
A and B) Colon LP immune cells (**A**) and T cell subsets (**B**) were analyzed by flow cytometry. Immune subsets measured include: DCs (CD11c$^+$ CD11b^{int}), NK cells (NK1.1$^+$), monocytes (CD11b$^+$ Ly6C^{hi} Ly6G^{int}), neutrophils (CD11b$^+$ Ly6C^{int} Ly6G$^+$), T cells (CD3$^+$ B220$^-$), and B cells (B220$^+$ CD3$^-$).
C) Intracellular cytokine production (IFNγ and IL-17) by colon LP immune cells was measured after four hours of PMA + ionomycin + monensin *ex vivo*-stimulation. Intracellular Foxp3 staining was performed after four hours of monensin incubation. Representative flow plots are shown.
Data are mean ± SEM and are pooled from at least two independent experiments. n=5-9/group, *p<0.05 by Mann-Whitney

4.3.4 Colon LP CD8 T cells partly mediate increased tumor susceptibility in WT2 mice

To determine whether CD8 T cells specifically contributed to increased tumorigenesis in WT2 mice, SPF *Cd8*$^{-/-}$ mice were treated with an antibiotic cocktail and antifungal water before gavage of SPF WT1 or WT2 stool and cecal contents for three consecutive days. This method of microbiome transfer has been successful in stably implanting donor microbiomes (209). Four weeks after the last gavage, mice were treated with AOM/DSS to induce tumors (**Figure 4.8A**).

When we analyzed the microbiome collected on the day of AOM injection after four weeks of colonization, the microbiomes of recolonized *Cd8*$^{-/-}$ mice resembled that of the SPF WT1 or WT2 microbiome donors (**Figure 4.8B**). Namely, *Cd8*$^{-/-}$ mice colonized with WT2 microbiota (WT2>CD8 KO) have increased *Prevotellaceae* and compared to *Cd8*$^{-/-}$ mice colonized with WT1 microbiota (WT1>CD8 KO) (**Figure 4.8B**). Furthermore, WT1>CD8 KO mice were measured to have significantly distinct microbiome compositions as WT2>CD8 KO mice similar to the difference measured between control SPF WT1 and WT2 mice as measured by thetaYC distances and AMOVA (**Figure 4.8C**). While the microbiomes of WT1>CD8 KO mice were similar to WT1 control mice by thetaYC distances, the compositions were still significantly different, possibly due to significant differences in a few specific bacteria (**Figure 4.8C**). Furthermore, by NMDS ordination, WT1>CD8 KO mice clustered closely with WT1 control mice, and WT2>CD8 KO clustered with WT2 control mice suggesting near-complete microbiome transfer (**Figure 4.8D**). Importantly, WT1>CD8 KO mice developed similar tumor numbers as SPF WT1 control mice whereas WT2>CD8 KO mice developed significantly fewer and smaller tumors compared to SPF WT2 control mice (**Figures 4.8E and 4.8F**), strongly suggesting that the dysbiotic microbiome in WT2 mice mediates its tumor-promoting effects in part via pro-inflammatory CD8 T cells.

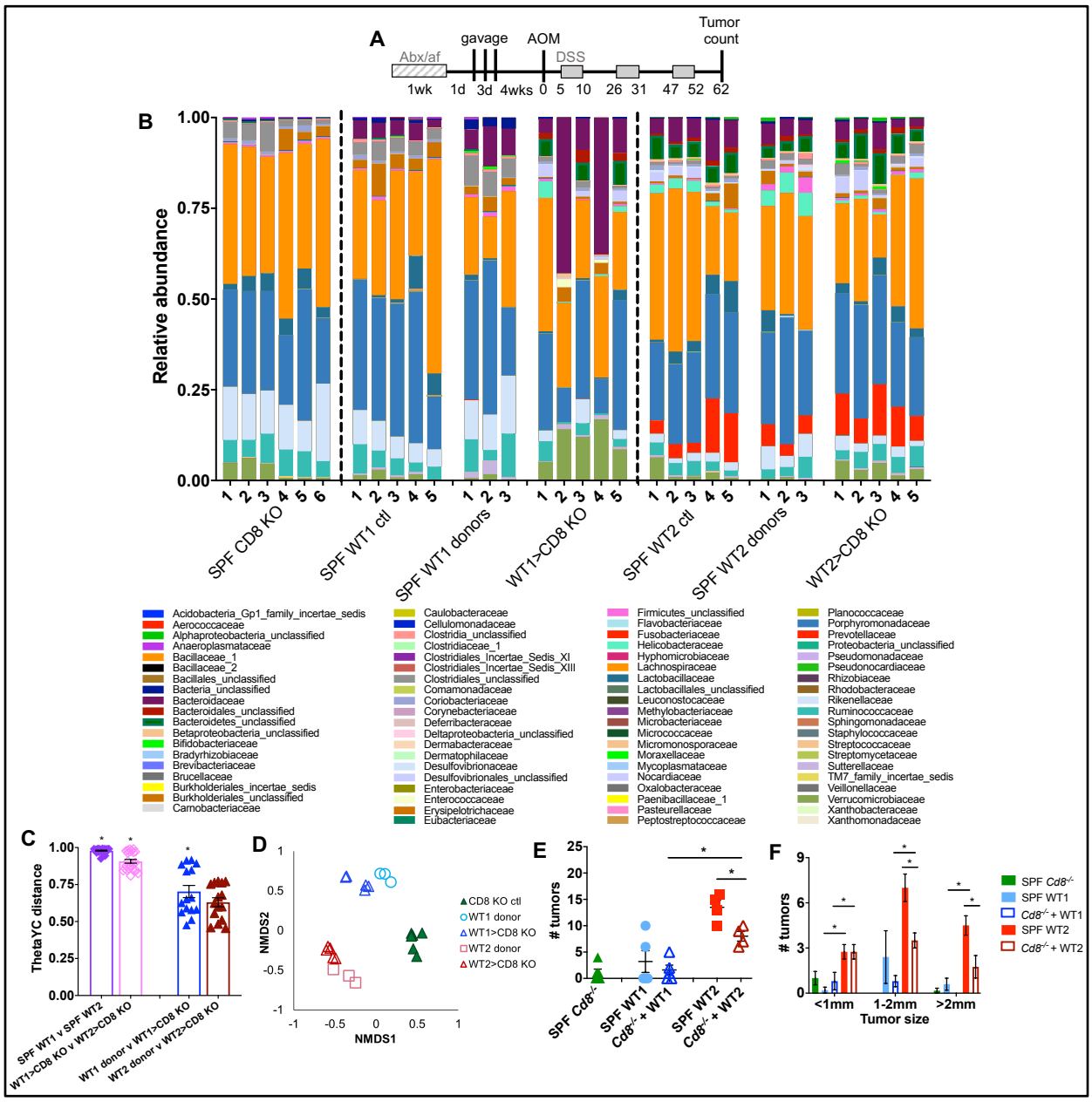

Figure 4.8 Colon LP CD8 T cells partly mediate increased tumor susceptibility in WT2 mice

A) SPF *Cd8*$^{-/-}$ mice were treated with antibiotic and antifungal water for one week prior to three consecutive gavages of SPF WT1 or WT2 microbiota. Four weeks of bacteria colonization, mice were injected with AOM and treated with three rounds of 2% DSS. Mice were sacrifice on day 62 of AOM/DSS for tumor counting.

B) Relative family abundances of *Cd8*$^{-/-}$ mice after four weeks of recolonization. Stool was collected on the day of AOM injection for 16S rRNA sequencing and analysis.

C and D) 16S rRNA sequencing was performed on fecal microbiota from SPF *Cd8*$^{-/-}$ mice recolonized with SPF WT1 or WT2 stool homogenates after antibiotic and antifungal treatment. Microbiome composition dissimilarity was analyzed by ThetaYC distance (**C**) and shown as an NMDS plot (**D**). *p<0.05 by AMOVA

E and F) Tumor numbers (**E**) and sizes (**F**) were measured on day 62 of AOM/DSS. Data are mean ± SEM. *p<0.05 by Mann-Whitney

n=4-6/group.

4.3.5 WT2 microbiota directly promote increased colon LP $CD8^+$ $IFN\gamma^+$ T cells

To determine if WT2 microbiota directly contribute to increased colon LP $CD8^+$ $IFN\gamma^+$ T cells in naïve WT2 mice, we gavaged WT2 mice stool and cecal homogenates into SPF WT1 mice after antibiotic and antifungal water treatment. After nine weeks of recolonization, WT1 mice reconstituted with WT2 microbiota (WT1+WT2bac) had microbiomes closely resembling WT2 donor inputs as well as antibiotic-treated WT2 mice reconstituted with WT2 microbiota (WT2+WT2bac) by NMDS ordination although there were still significant differences between groups based on thetaYC distances (**Figures 4.9A and 4.9B**). Importantly, WT1+WT2bac mice had increased colon LP CD3 and CD8, but not CD4, T cells, as well as increased $CD8^+$ $IFN\gamma^+$ T cells compared to the control WT1 mice that were recolonized with WT1 bacteria (WT1+WT1bac) (**Figures 4.9C and 4.9D**). WT1+WT2bac mice also had increased $CD4^+$ $IFN\gamma^+$ T cells compared to WT1+WT1bac mice, but no differences in $CD4^+$ IL-17^+ or $CD4^+$ $Foxp3^+$ subsets (**Figure 4.9D**).

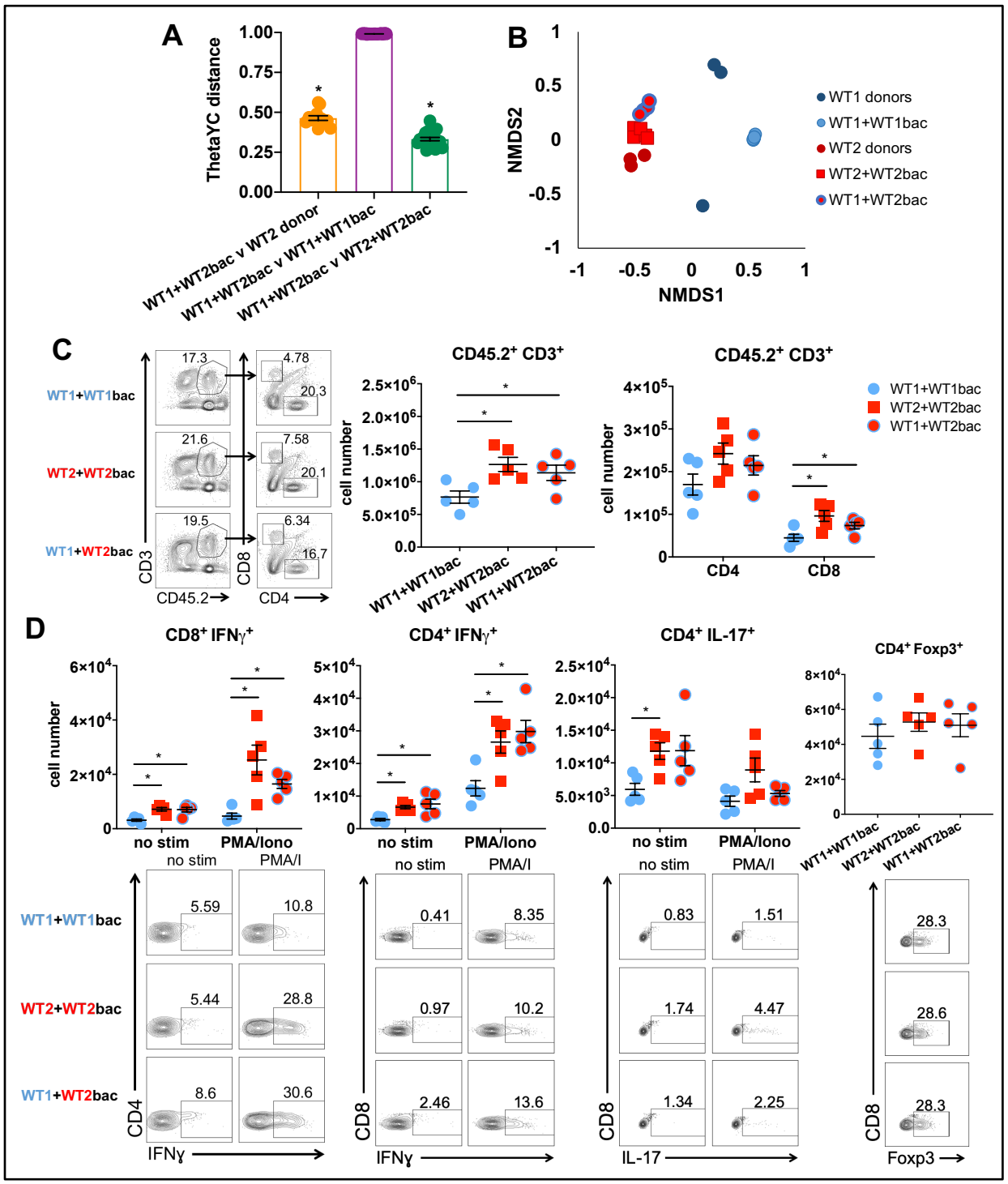

Figure 4.9 SPF WT1 mice colonized with WT2 microbiota have increased colon LP CD8$^+$ IFNγ$^+$ T cells
SPF WT1 and WT2 mice were treated with antibiotics and antifungal water for one week prior to three consecutive gavages of SPF WT1 or WT2 microbiota. Nine weeks after colonization, the colon LP was analyzed by flow cytometry.
A and B) Microbiome composition dissimilarity was analyzed by ThetaYC distance (**A**) and shown as an NMDS plot (**B**). *p<0.05 by AMOVA
C) CD3 T cell and T cell subsets were analyzed by flow cytometry.

D) Colon lamina propria immune cells were *ex vivo*-stimulated with PMA and ionomycin and monensin for four hours before flow cytometry analysis. Non-stimulated cells were incubated with monensin for four hours before and flow cytometry analysis.
Data are mean ± SEM and are representative of two independent experiments. n=5/group, *p<0.05 by Mann-Whitney unless otherwise noted.

We also gavaged GF WT mice with WT1 or WT2 microbiota prepared from stool and cecal contents. After eight weeks of colonization to allow microbial and immune cell reconstitution, the colon LP immune cell populations were analyzed by flow cytometry. While no differences in CD3, CD8, or CD4 T cells were observed (**Figure 4.10A**), GF WT mice colonized with WT2 microbiota had increased colon LP $CD8^+$ $IFN\gamma^+$ T cells, but no differences in $CD4^+$ $IFN\gamma^+$, $CD4^+$ $IL\text{-}17^+$, or $CD4^+$ $Foxp3^+$ subsets, similar to what is observed in naïve SPF WT2 mice (**Figure 4.10B**).

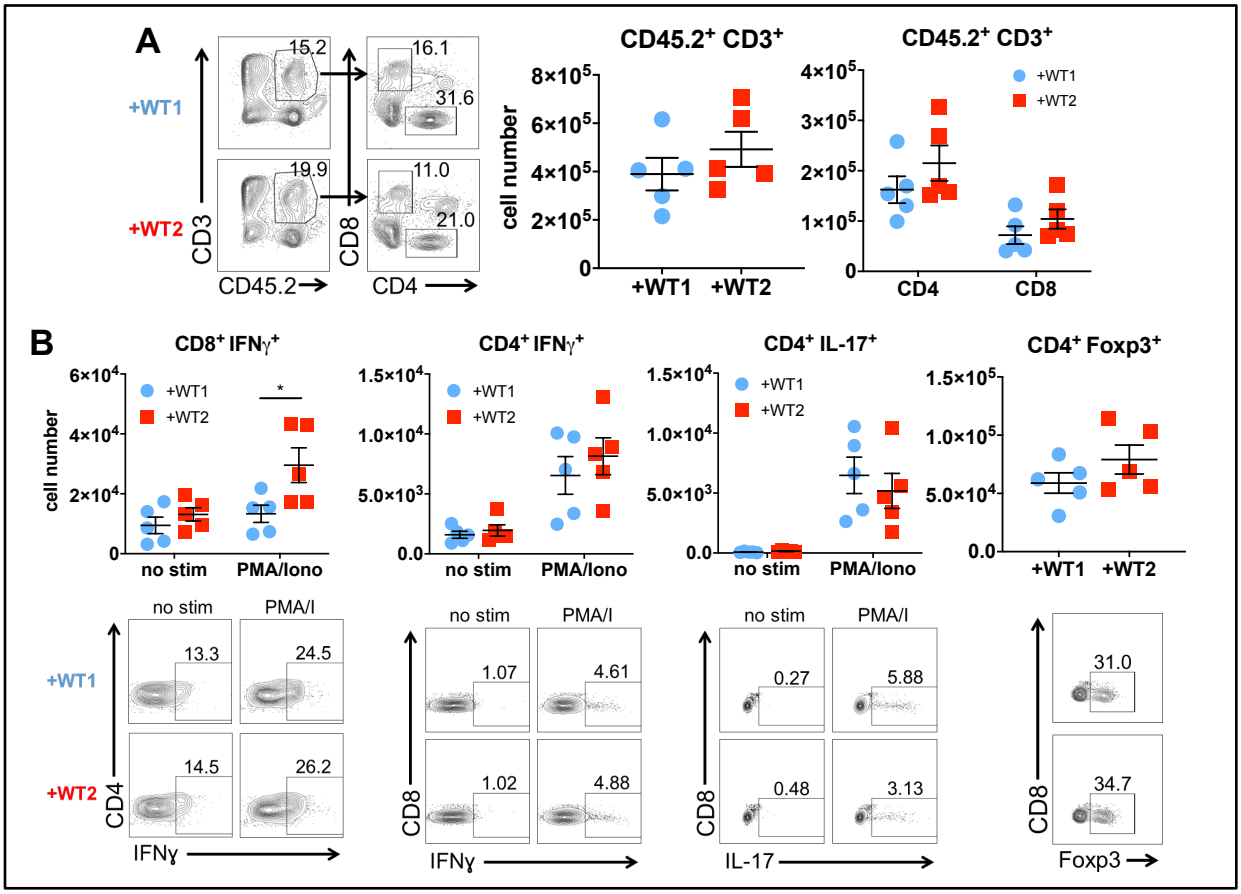

Figure 4.10 GF WT mice colonized with WT2 microbiota have increased colon LP $CD8^+$ $IFN\gamma^+$ T cells
GF WT mice were gavaged with SPF WT1 or WT2 microbiota. Eight weeks after colonization, the colon LP was analyzed by flow cytometry.
A) CD3 T cell and T cell subsets were analyzed by flow cytometry.
B) Colon lamina propria immune cells were ex vivo-stimulated with PMA and ionomycin and monensin for four hours before flow cytometry analysis. Non-stimulated cells were incubated with monensin for four hours before and flow cytometry analysis.
Data are mean ± SEM and representative of two independent experiments. n=5/group, *p<0.05 by Mann-Whitney

4.3.6 WT2 microbiota may promote increased colon LP CD8$^+$ IFNγ$^+$ T cells through IL-12 production by DCs

We explored potential mechanisms of how the WT2 microbiome may alter CD8 T cell responses in the colons of WT2 mice. First, we examined the expression of the T cell chemoattractants CXCL9 and CXCL10 in the colon epithelium of naïve WT1 and WT2 mice by qPCR, and observed no differences, suggesting that the increase in CD8 T cells in the colon LP WT2 is not necessarily due to increased recruitment via epithelial chemokine production (**Figure 4.11A**). To determine if WT2 mice were predisposed to inflammation, we measured expression of IL-6 and the antimicrobial peptides, Reg3γ or β–defensin2, but no differences were detected (**Figure 4.11A**). Interestingly, there was increased expression of IL-1β in WT2 epithelium, which has been shown to promote effector T cell responses including the production of IFNγ (210) as well as occludin, although the significance of this is unclear (**Figure 4.11A**).

Production of IL-12 by dendritic cells (DCs) can promote CD8 T cell activation and IFNγ production (211-213). To determine if WT2 bacteria promotes increased IL-12 production by DCs, we cultured WT1 and WT2 bone marrow-derived dendritic cells (BMDCs) with heat-killed (HK) stool from either SPF WT1 or WT2 mice and measured IL-12 in the supernatant. HK WT2 bacteria promoted increased IL-12 production by both WT1 and WT2 BMDCs compared to HK WT1 bacteria (**Figure 4.11B**). Altogether, these data strongly support a role for the WT2 microbiota in upregulating colon LP IFNγ$^+$ CD8$^+$ T cell responses.

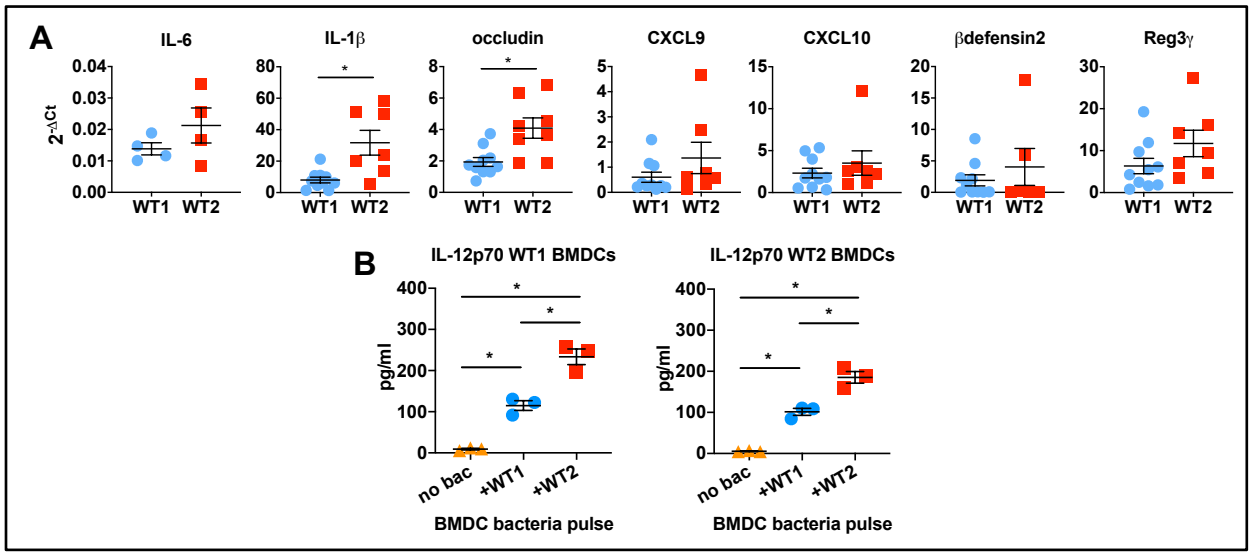

Figure 4.11 WT2 microbiota promotes increased IL-12 production by BMDCs
A) mRNA expression of several epithelial cell-related genes relative to actin by untreated WT1 and WT2 epithelial cells. IL-6: n=4/group; rest: WT1 n=10, WT2 n=6 (βdef2), 7 (CXCL9, Reg3γ, and IL-1β), or 8 (CXCL10 and occludin).
B) IL-12p70 levels were measured by ELISA in 24-hour supernatants of bone marrow-derived dendritic cells exposed to heat-killed SPF WT1 or WT2 bacteria cultures. n=3 mice/colony. WT1 data are representative of three independent experiments. WT2 data are representative of two independent experiments.
*p<0.05 by Mann-Whitney

4.3.7 CD8 T cell depletion does not promote increased tumorigenesis in WT1 mice

To complement our study of the impact of WT1 and WT2 microbiota in *Cd8*$^{-/-}$ mice, we carried out CD8 depletion experiments. We determined that five days after an injection of 300ug anti-CD8 antibody/mouse, mice were specifically depleted in CD8, but not CD4, T cells in the colon LP and spleen (**Figures 4.12A and 4.12B**). Thus, we depleted CD8 T cells in WT1 mice beginning one day prior to the start of AOM/DSS treatment and then every five days until day 12 of the model. However, we observed that WT1 mice became visibly sick with increased weight loss compared to isotype-treated WT1 mice during and immediately after the first cycle of DSS (**Figure 4.13A**), suggesting that the presence of CD8 T cells early on may be important for limiting colitis-susceptibility, which, in turn, can affect tumor susceptibility via a mechanism not related to anti-tumor immunity.

We subsequently conducted a second experiment in which CD8 T cells were depleted starting at day 10 of AOM/DSS, which is at the end of the first round of DSS during acute inflammation, and every five days afterward until the tumor endpoint. With this timing, no difference in weights were measured between CD8-depleted and isotype control-treated WT1 mice (**Figure 4.13B**). However, this resulted in a trend towards increased tumors in CD8 T cell-depleted WT1 mice compared to that of isotype control-treated mice that did not reach significance (**Figure 4.13C**). We believe these CD8 antibody depletion experiments may be difficult to interpret as the timing and length of depletion may separately alter both colitis and tumor susceptibility. Regardless, as shown in **Figure 4.8**, microbiome-depleted CD8 KO mice that were recolonized with WT2 microbiota were partly protected from increased tumorigenesis, which was not observed with CD8 KO mice reconstituted with WT1 microbiota, suggesting CD8 T cells do play a role in mediating increased tumorigenesis, at least in the context of the WT2 microbiome.

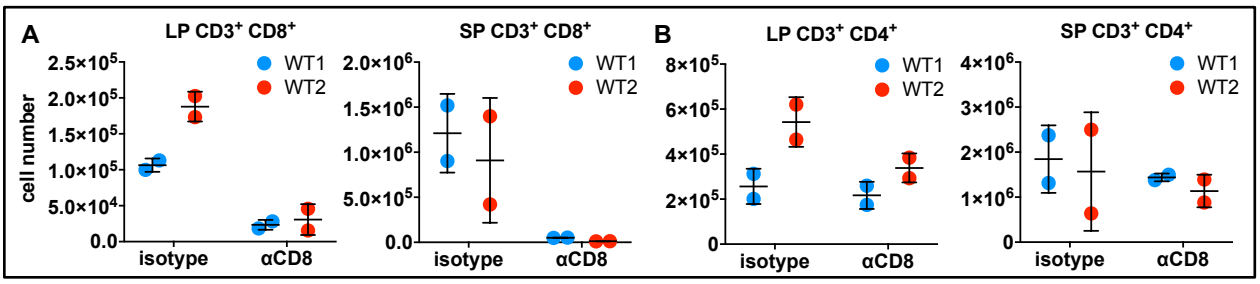

Figure 4.12 Mice remain CD8-depleted five days after antibody-mediated depletion
Mice were treated with anti-CD8 or isotype control antibodies and sacrificed after five days for depletion efficacy by flow cytometry. CD8 (**A**) and CD4 (**B**) T cells in the colon LP and spleen were analyzed.
Data are mean ± SEM. n=2/group, *p<0.05 by Mann-Whitney

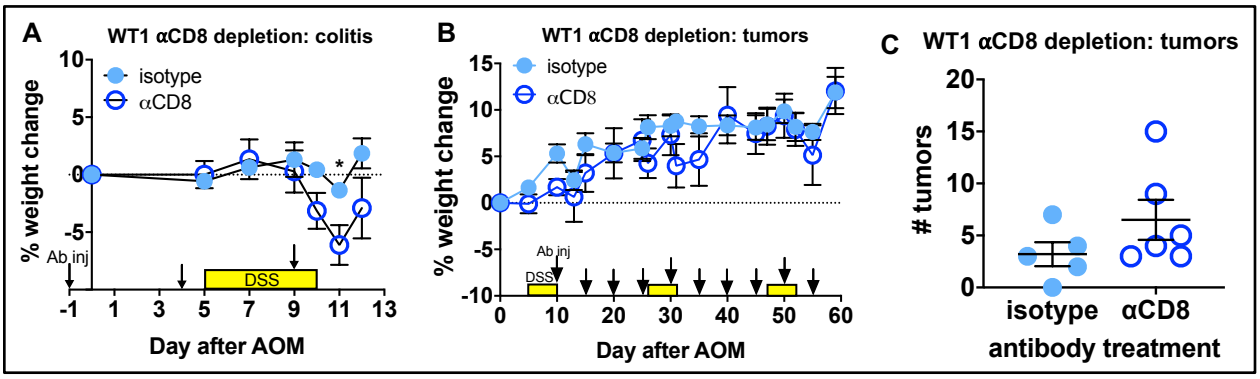

Figure 4.13 Antibody-mediated CD8 depletion in WT1 mice can exacerbate DSS-induced colitis and may promote tumorigenesis
A) 12-13 week-old SPF WT1 mice were treated with anti-CD8 or isotype control antibody on days -1, 4, and 9 of AOM/DSS. Mice were sacrificed on day 12. Percent weight loss is shown.
B and C) 9 week-old SPF WT1 mice were treated with anti-CD8 or isotype control antibody every five days starting on day 10 of AOM/DSS until the tumor endpoint. Weight change (**B**) and tumor numbers (**C**) are shown.
Data are mean ± SEM. n=5-6/group, *p<0.05 by Mann-Whitney

4.3.8 CD8 T cells may promote increased tumorigenesis in the context of the WT2 microbiome

To determine if CD8 T cells promote increased tumorigenesis in the context of the WT2 microbiome, we performed CD8 depletion and T cell adoptive transfer experiments. Similar to WT1 mice (**Figure 4.13A**), WT2 mice treated with anti-CD8 depleting antibody developed more severe weight loss than WT2 mice that received the isotype control (**Figure 4.14A**) suggesting CD8 T cells play a protecting role in early colitis and tumorigenesis. Furthermore, we depleted CD8 T cells during early AOM/DSS and examined that effect on tumorigenesis. While no differences in weight loss was measured (**Figure 4.14B**), there was a trend of decreased tumors in

WT2 mice that were depleted of CD8 T cells in early AOM/DSS compared to WT2 mice that received the isotype control (**Figure 4.14C**).

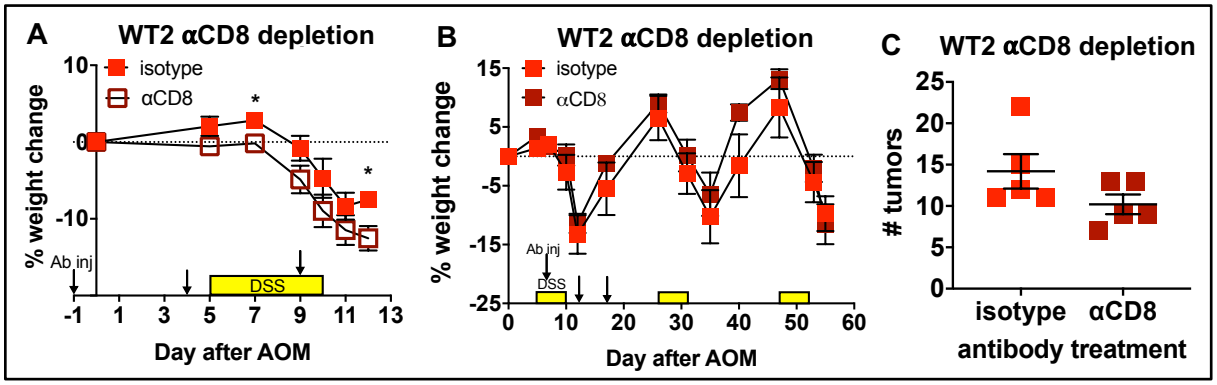

Figure 4.14 Antibody-mediated CD8 depletion in WT2 mice can exacerbate DSS-induced colitis but may reduce tumorigenesis
A) 12-13 week-old SPF WT2 mice were treated with anti-CD8 or isotype control antibody on days -1, 4, and 9 of AOM/DSS. Mice were sacrificed on day 12. Percent weight loss is shown.
B and C) 7-10 week-old SPF WT2 mice were treated with anti-CD8 or isotype control on days 7, 12, and 17 of AOM/DSS treatment. Weights (**B**) and tumor numbers (**C**) are shown.

As we have found CD8 depletion experiments to be dependent on the length of antibody depletion and the timing of treatment, we adoptively transferred T cells into GF *Rag1*$^{-/-}$ mice colonized with WT1 or WT2 microbiomes as this would allow us to directly assess the effect of T cells on tumorigenesis in the context of two different microbiomes. GF *Rag1*$^{-/-}$ mice were gavaged with SPF WT1 or WT2 intestinal contents and after four weeks, were intravenously injected with donor splenic CD8 T cells. Four weeks after immune cell colonization, mice were treated with AOM/DSS to induce tumorigenesis. Unfortunately, we did not transfer Treg cells and this experiment resembled the T cell colitis model where mice in both microbiome groups had increased weight loss. However, GF *Rag1*$^{-/-}$ mice that received WT2 microbiota (WT2>GF Rag) had more weight loss than GF *Rag1*$^{-/-}$ mice that received WT1 microbiota (WT1>GF Rag) (**Figure 4.15A**). Additionally, significantly more WT2>GF Rag mice died during AOM/DSS treatment (**Figure 4.15B**). On day 60 of AOM/DSS, tumor counts revealed WT1>GF Rag mice developed few to no tumors where the single WT2>GF Rag mouse that survived developed 30 tumors (**Figure 4.15C**). Altogether, this preliminary experiment suggests CD8 T cells may directly promote increased tumorigenesis in WT2 mice but must be repeated.

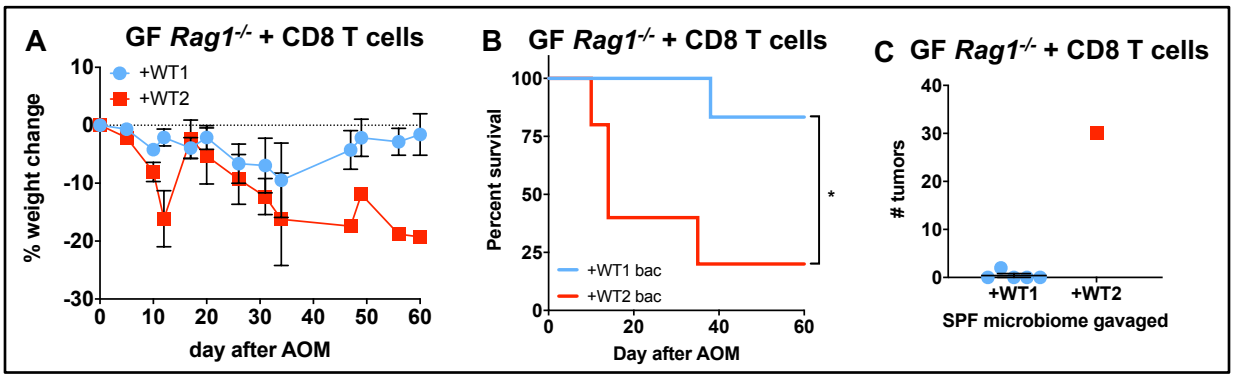

Figure 4.15 CD8 T cells promote increased tumorigenesis in the context of a WT2 microbiome
GF *Rag1*$^{-/-}$ mice were colonized with WT1 or WT2 microbiota for four weeks before receiving 3x10^6 splenic CD8 T cells. Four weeks after CD8 T cell adoptive transfer, mice were treated with AOM and one round of 1.5% DSS followed by two rounds of 1% DSS. Mice were sacrificed for tumor counting on day 60 of AOM/DSS. Weight loss (**A**), survival (**B**), and tumor numbers (**C**) are shown.
Intravenous adoptive transfer injections were done by Hideaki Fujiwara.
Data are mean ± SEM. n=5/group, *p<0.05 by Mann-Whitney

4.3.9 Intratumoral T cells in WT2 mice exhibit an exhausted phenotype

CD8 T cells and IFNγ production are important for anti-tumor immunity (102, 103, 214, 215); consistently, increased CD8 T cells and a Th1 gene signature within the tumor microenvironment correlates with improved CRC patient outcomes (102). Yet, our data suggests that increased homeostatic levels of CD8$^+$ IFNγ$^+$ T cells, associated with dysbiosis, can promote inflammation and tumorigenesis. To determine the activity of CD8 T cells within tumors of WT1 and WT2 mice, we analyzed the immune composition of tumor tissue ("tum") and non-tumor tissue adjacent to tumors ("adj") by flow cytometry. No differences in total T cells or CD4 T cells were measured between WT1 and WT2 mice in both tumor and adjacent tissues (**Figures 4.16A and 4.16B**). However, contrary to naïve and acute inflammatory conditions, WT2 CD8 T cells are decreased in both tumor and adjacent tissue compared to WT1 tissues (**Figure 4.16B**). Furthermore, both intratumoral WT2 CD8 and CD4 T cells have reduced IFNγ responses compared to WT1 CD8 and CD4 T cells upon *ex vivo*-stimulation (**Figures 4.16C and 4.16D**) while no differences in intratumoral CD4$^+$ IL-17$^+$ or CD4$^+$ Foxp3$^+$ cells were observed (**Figures 4.16E and 4.16F**).

Based on the pattern of increased CD8$^+$ IFNγ$^+$ T cells at baseline and during chronic inflammation followed by reduced CD8$^+$ IFNγ$^+$ T cells within the tumor microenvironment and adjacent normal tissue in WT2 mice, we hypothesized that the dysbiotic microbiome of WT2 mice

promotes T cell exhaustion. T cell exhaustion can occur as a result of prolonged antigen exposure and chronic inflammation (216, 217) and is also observed with tumor infiltrating lymphocytes, which can promote tumor progression (218-223). To determine if intratumoral WT2 T cells exhibit an exhausted phenotype, we measured inhibitory receptors typically expressed by exhausted T cells by flow cytometry. Indeed, there were greater numbers of PD-1^+ Lag-3^+ and PD-1^+ Tim-3^+ CD8 T cells within WT2 tumors compared to WT1 tumors (**Figures 4.16G**). Additionally, tumor-infiltrating WT2 CD4 cells also exhibited increased PD-1 and Lag-3 expression compared to WT1 CD4 T cells (**Figures 4.16H**). Altogether, these data suggest that dysbiosis can lead to T cell exhaustion by chronically inducing IFNγ production in CD8 T cells, which may result in impaired immune surveillance and increased susceptibility to tumorigenesis.

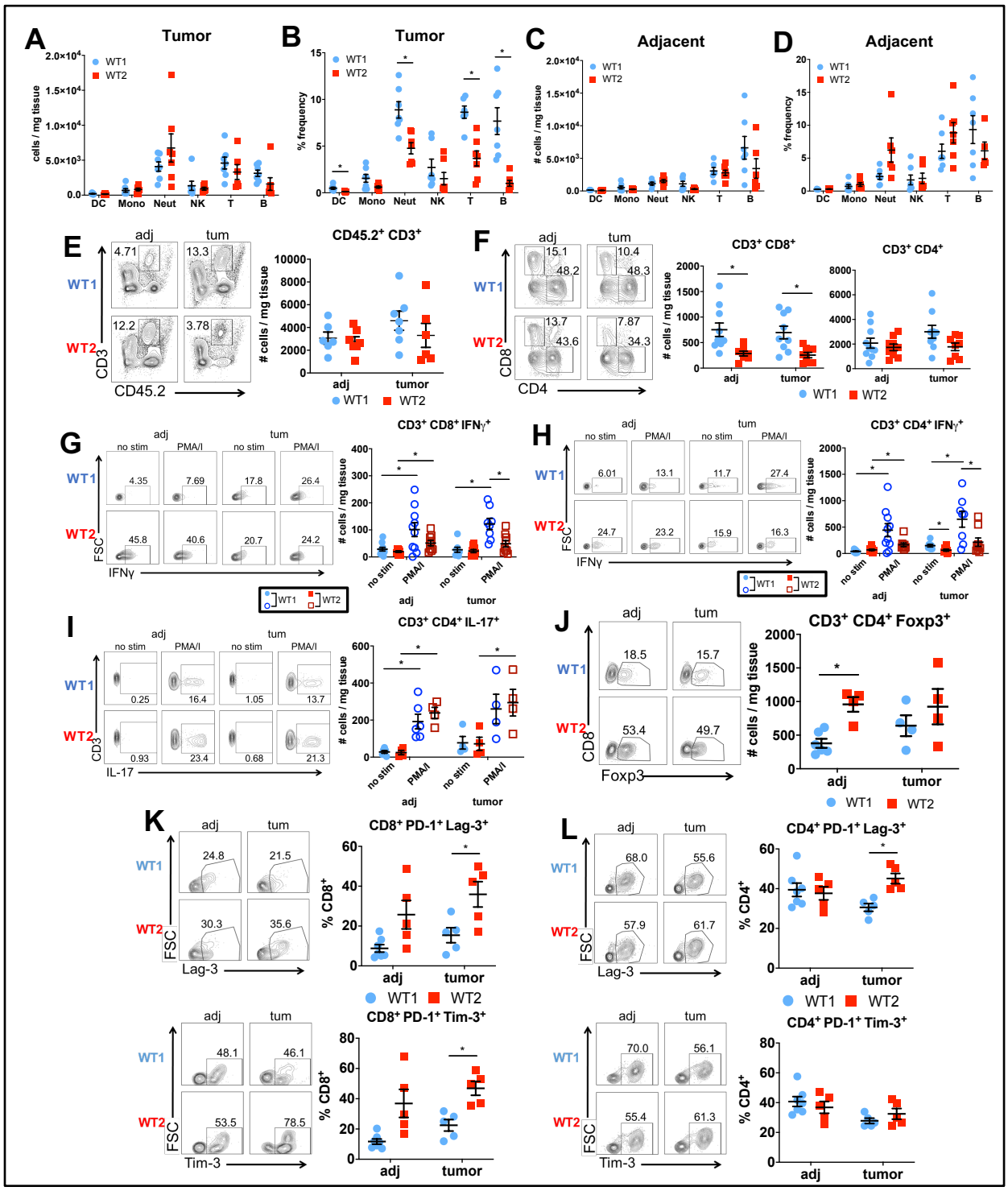

Figure 4.16 Intratumoral WT2 CD8 T cells display decreased IFNγ activity and increased exhaustion

A-D) Immune cell subset differences between SPF WT1 and WT2 mice in tumor (**A and B**) and normal adjacent tissue (**C and D**) in tumor-bearing mice. Immune subsets measured include: DCs ($CD11c^{+}$ $CD11b^{int}$), NK cells ($NK1.1^{+}$), monocytes ($CD11b^{+}$ $Ly6C^{hi}$ $Ly6G^{int}$), neutrophils ($CD11b^{+}$ $Ly6C^{int}$ $Ly6G^{+}$), T cells ($CD3^{+}$ $B220^{-}$), and B cells ($B220^{+}$ $CD3^{-}$). n=5-7/group.

E and F) Number of T cells (**E**), CD4 and CD8 T cells (**F**) in tumor ("tum") and adjacent ("adj") tissue from AOM/DSS-treated WT1 and WT2 mice as analyzed by flow cytometry on day 60. n=6-10/group.

G-J) Representative flow plots after ex vivo-stimulation of cells for four hours and analysis of IFNγ (n=8-10/group), FoxP3 and IL-17 (n=4-6/group).
K and L) Representative flow plots and quantification of PD-1, Tim-3, and Lag-3 on CD8 (**K**) or CD4 T (**L**) cells. n=5-7/group.
Data are mean ± SEM and are pooled from at least two independent experiments. *p<0.05 by Mann-Whitney

4.3.10 Increased intratumoral WT2 exhausted T cells are specific to AOM/DSS tumors

To determine if the increase in WT2 intratumoral exhausted T cells in AOM/DSS-induced tumors is driven by inflammation, we analyzed intratumoral T cells in the *CDX2-Cre Apc$^{fl/fl}$* and MC38 subcutaneous models of CRC. In *CDX2-Cre Apc$^{fl/fl}$* mice gavaged with WT1 or WT2 microbiota, no differences in intratumoral CD3, CD4 or CD8 T cells were measured (**Figures 4.17A and 4.17B**). No differences in intratumoral exhausted CD8 T cells were measured while a small increased in exhausted CD4 PD-1^{+} Tim-3^{+} T cells were measured in *CDX2-Cre Apc$^{fl/fl}$* mice gavaged with WT microbiotas (**Figure 4.17C**). Additionally, in MC38 subcutaneous tumors, no differences in CD3, CD4, CD8 or exhausted T cells were measured between WT1 and WT2 mice (**Figures 4.17D-F**). As exhausted intratumoral T cells are present in these two models which are not expressly driven by inflammation, the intratumoral T cell exhaustion difference between AOM/DSS-treated WT1 and WT2 mice is likely driven by inflammation differences promoted by the microbiome differences.

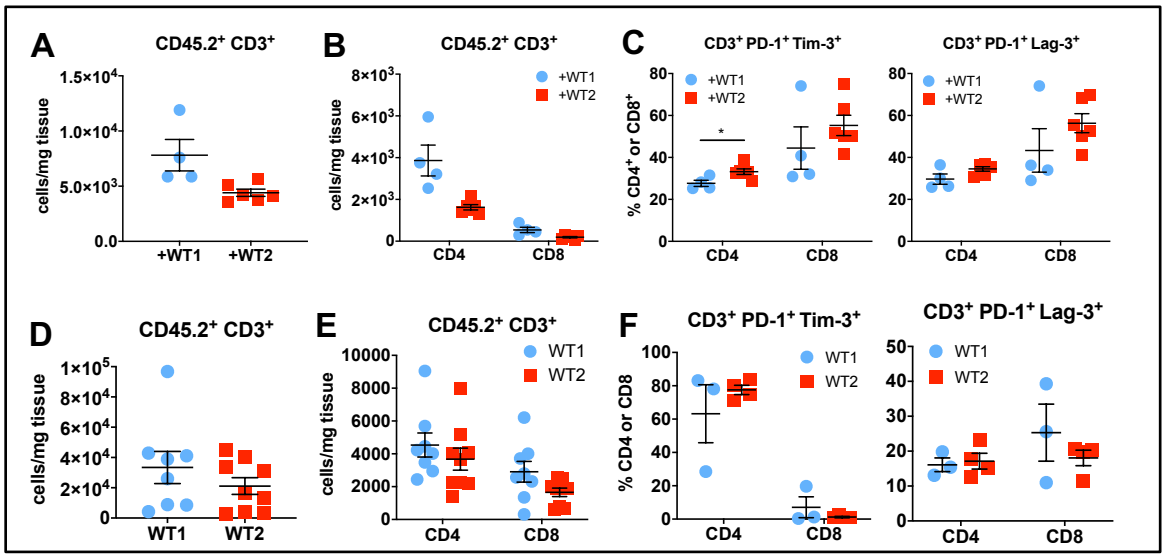

Figure 4.17 No differences in CD8 T cell exhaustion are measured in *CDX2-Cre Apc$^{fl/fl}$* and MC38 tumors
A-C) Microbiome-depleted *CDX2-Cre Apc$^{fl/fl}$* mice were gavaged with WT1 or WT2 microbiomes for three consecutive days. Eleven weeks after the last gavage, intratumoral T cell exhaustion was analyzed by flow cytometry. n=4-6/group, *p<0.05 by Mann-Whitney

D-F) MC38 cells were injected into the flank of WT1 or WT2 mice. Intratumoral T cell exhaustion was analyzed on day 23 by flow cytometry. D and E: n=8-9/group, F: n=3-4/group.

4.3.11 Intratumoral tumor antigen-specific CD8 T cells are not associated with MC38 subcutaneous tumors

We also wanted to assess the effect of the WT2 microbiota on the induction of tumor-specific antigen responses. Since no tumor-specific antigen has been identified in AOM/DSS-induced colon tumors, we used the syngeneic MC38 colorectal cancer cell line. MC38 cells contain the tumor-specific MHC-I presented mutant peptide (ASMTN[R/M]ELM) derived from the gene Adpgk, which can serve as a neo-antigen where adgpk-specific immune cells can be detected by fluorescent tetramers and flow cytometry (Kuai et al., 2017). After subcutaneous injection of $1x10^6$ MC38 cells into the flanks of WT1 and WT2 mice, we isolated tumors on day 23 after injection when tumors reached an average size of $800mm^3$ and $adgpk^+$ $CD8^+$ or $CD4^+$ T cells were measured. There was increased frequency of intratumoral $adgpk^+$ $CD8^+$, but not $CD4^+$, T cells in WT2 mice, suggesting that the presence of WT2 microbiota may result in increased tumor-specific antigen responses (**Figures 4.18A and 4.18B**). However, we did not observe a difference in overall tumor weights (**Figure 4.18C**).

In general, the MC38 subcutaneous tumor model is very different from the AOM/DSS model and therefore, we believe it is difficult to extrapolate definite conclusions drawn from this model to the *in vivo* model of inflammation-associated colon tumorigenesis.

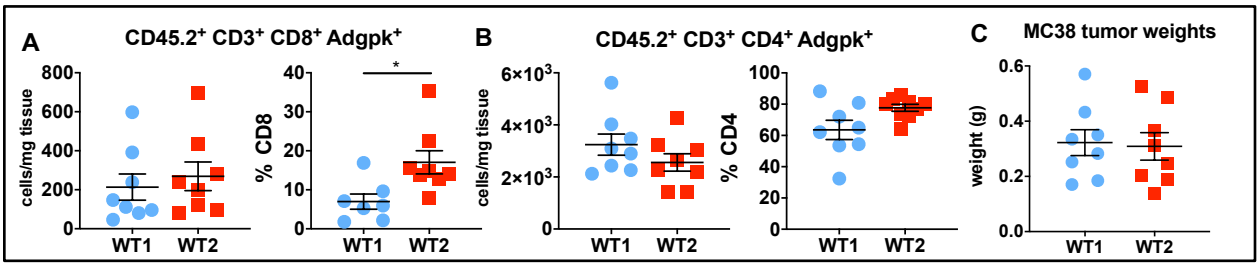

Figure 4.18 Increased intratumoral tumor antigen-specific CD8 T cells in subcutaneous MC38 tumors are not associated with increased tumor size
SPF WT1 and WT2 mice were subcutaneously injected with $1x10^6$ MC38 cells and sacrificed on day 23.
A and B) CD8 (**A**) and CD4 (**B**) T cells were isolated from MC38 tumors and analyzed by flow cytometry for adgpk specificity.
C) Endpoint M38 tumor weights on day 23.
Data are mean ± SEM and are pooled from two independent experiments. n=8/group, *p<0.05 by Mann-Whitney

4.4 Discussion and Future Directions

As microbiota can modulate host immunity, in this chapter, we wanted to determine if the microbiome differences between WT1 and WT2 mice altered immune responses and how that may influence tumorigenesis. Specific to the colon LP, naïve WT2 mice have increased B and T cells; in particular, colon LP $CD8^+$ $IFN\gamma^+$ T cells are increased in naïve WT2 mice where the WT2 microbiome directly promotes increased colon LP $CD8^+$ $IFN\gamma^+$ T cells. We determined that WT2 bacteria can promote increased IL-12 production by DCs where IL-12 can promote T cell IFNγ responses. Interestingly, after AOM/DSS, WT2 mice had decreased intratumoral CD8 T cells and reduced IFNγ responses. This reduction in IFNγ activity after prolonged inflammation is reminiscent of T cell exhaustion. Indeed, intratumoral WT2 CD8 T cells had upregulated exhaustion markers compared to intratumoral WT1 CD8 T cells, specific to AOM/DSS-induced tumors and not in MC38 subcutaneous or *CDX2-Cre* $Apc^{fl/fl}$ WT2 tumors, suggesting rolonged inflammation is necessary for the increased exhaustion phenotype.

In previous chapters, we tested and compared microbiome transfer methods of cohousing and cross-fostering with the gold standard, gavage into GF mice. In this chapter, we used a fourth method: gavage of microbiota into microbiome-depleted SPF mice (**Figures 4.8 and 4.9**). Based on thetaYC dissimilarity, we observed effective microbiome transfer in mice that were gavaged with cecal and fecal contents from donor mice after antibiotic depletion, although not necessarily as complete as in GF mice. Other groups also observed similar transfer results by this method (209, 224, 225). Further studies are needed to determine the antibiotic combination, length of treatment, and number of gavages for optimal transfer of microbiota and phenotype. Nonetheless, this approach may still be a reasonable alternative to GF mice in determining the effects of specific microbial communities on phenotype.

We provide evidence of increased colon LP $CD8^+$ $IFN\gamma^+$ T cells in naïve and acutely inflamed (day 12 of AOM/DSS) WT2 mice but not WT1 mice. How dysbiosis promotes the accumulation of activated $CD8^+$ $IFN\gamma^+$ T cells in naïve WT2 mice is unclear and may be multifactorial in nature. It has been previously shown that *Bifidobacterium* is capable of priming DCs to enhance CD8 T cell proliferation and IFNγ production (226). Similarly, we observed increased IL-12 production by BMDCs stimulated with HK WT2 microbiota (**Figure 4.11B**). Therefore, it is possible that the presence of certain bacterial populations in the gut of WT2 mice

selectively expands and primes the activation of colon LP CD8 T cells via DC activation. Gnotobiotic mouse studies also suggest that the accumulation of $CD8^+$ $IFN\gamma^+$ T cells is a result of chemokine induction by specific bacteria proximal to the intestinal epithelium, (84); however, we did not observe any differences in epithelial production of CXCL9 or CXCL10 in WT1 and WT2 mice. As bacteria-produced metabolites can have immunomodulatory effects (227-229), it is also possible that WT2 microbiota-specific metabolites may contribute to increased colon LP $CD8^+$ $IFN\gamma^+$ T cells. For example, the gut microbiota can modulate levels of all-trans-retinoic acid levels that can promote CD8 T cell responses in CRC (230).

Inconsistencies in antibody-mediated CD8 depletion experiments due to un-optimized dosing and timing suggested to us that CD8 adoptive transfer into immune-deficient mice may be an improved method to examine if CD8 T cells directly mediate tumor differences between WT1 and WT2 mice. We show preliminary results where CD8 T cells may directly promote increased tumorigenesis in GF *Rag1*$^{-/-}$ mice colonized with WT2 microbiota compared to GF *Rag1*$^{-/-}$ mice colonized with WT1 microbiota (**Figure 4.16**). However, the results of this experiment are confounded as these colonized mice experienced CD8 T cell-induced colitis before AOM/DSS-induced inflammation due to the absence of CD4 Treg cells. To clarify the findings of this experiment, we should repeat the experiment but adoptively transfer both CD8 T and Treg cells to ameliorate extraneous colitis, as seen in the T cell transfer colitis model (231), which may affect AOM/DSS tumorigenesis.

By gavaging WT2 microbiota into microbiome-depleted WT1 mice or GF mice, we show in **Figures 4.9 and 4.10** that the WT2 microbiota directly promotes increased colon LP $CD8^+$ $IFN\gamma^+$ T cells. However, it remains unclear if the WT2 microbiome can not only alter host immune responses but lead to increased intratumoral CD8 T cell exhaustion. We can use these two microbiome transfer methods, as we know they promote appropriate immune changes, with the addition of AOM/DSS treatment, to determine if the WT2 microbiota can directly promote increased intratumoral exhausted CD8 T cells.

In this chapter, we focus on examining the role of CD8 T cells in promoting increased tumorigenesis. However, our data also suggest a role of B cells in mediating tumorigenesis. Although there are conflicting results about the role of B cells in cancer due to B cell subset differences, similar to CD8 T cells, increased mature, tumor-infiltrating B cells are associated with better CRC patient prognosis and lower cancer stages (232-234). Furthermore, in one study, tumor-

infiltrating B20^{+} B cells were significantly with associated with intratumoral CD8 T cells (232). Consistently, in this chapter, we show that increased frequency of intratumoral B cells are found in WT1 mice where WT1 mice develop fewer AOM/DSS-induced tumors and rarely have tumor-associated mortality compared to WT2 mice (**Figure 4.16B**). In **Figure 4.1**, microarray data shows significant upregulation of immunoglobulin (Ig) and Ig receptor expression in early inflamed (day 10 of AOM/DSS) WT2 mouse colons compared to WT1 mouse colons. Preliminary Ig measurements also reveal decreased IgA levels in the stool of naïve WT2 mice compared to that of WT1 mice (**Figure 4.19A**). Additionally, in breast cancer, as production of tumor-associated autoantibodies may promote anti-tumor responses (235, 236), it would be worthwhile to determine the expression of Igs and Ig receptors at the tumor endpoint. As IgA has been shown to target colitogenic bacteria (237), it would also be valuable to determine if these Igs are specific for gut microbiota. Interestingly, we show that the absence of adaptive immune cells significantly reduces tumorigenesis in WT2 mice (**Figure 4.3**), where the absence of CD8 T cells only partially reduces tumorigenesis (**Figure 4.8**), further suggesting B cells may play a tumor-promoting role in WT2 microbiota mice. However, no colon LP B cell differences were measured in either WT2-colonized GF WT or microbiome-depleted WT1 mice (**Figures 4.19B and 4.19C**), suggesting the WT2 microbiota might not directly promote increased colon LP B cells as measured in untreated WT2 mice (**Figure 4.2A**). Overall, additional studies are needed to determine the role of B cells in the context of WT1 and WT2 microbiomes.

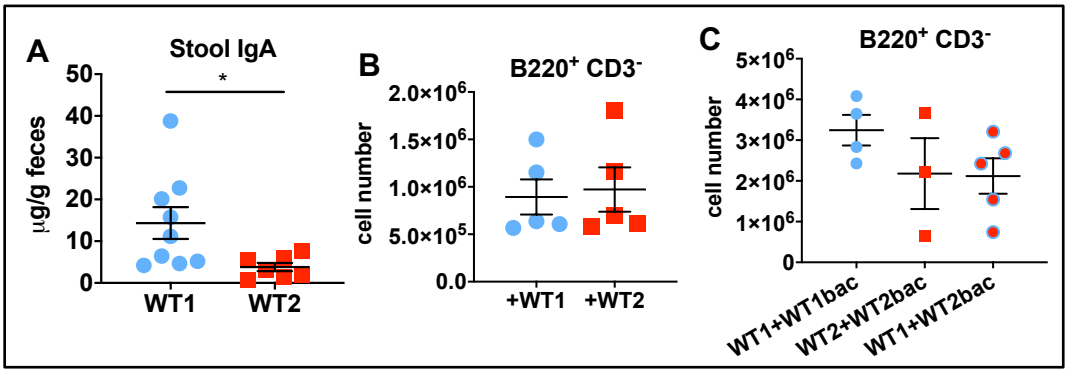

Figure 4.19 Naïve WT2 mice have decreased stool IgA levels and SPF WT2 microbiota do not directly promote colon LP B cell differences

A)Stool of WT1 and WT2 mice were homogenized in PBS, and IgA was measured in the supernatant by ELISA. WT1 n=9, WT2 n=7, *p<0.05 by Mann-Whitney

B) GF WT mice were colonized with SPF WT1 or WT2 microbiota and colon LP immune cell subsets were analyzed after eight weeks of bacteria colonization. B cells were determined as B220^{+} CD3^{-} cells. n=5/group.

C) SPF WT1 mice were microbiome depleted and colonized with SPF WT2 microbiota. Colon LP immune cell subsets were analyzed after nine weeks of bacteria colonization. n=3-5/group.

It is also unclear why WT2 mice have decreased intratumoral CD8 T cells. While no differences in intratumoral Tregs were measured, WT2 mice have increased Tregs in the normal adjacent tissue at the tumor endpoint (**Figure 4.16J**), where Tregs have the ability to kill CD8 T cells and antigen-presenting DCs to dampen inflammation and anti-tumor responses (238, 239). Additionally, intratumoral DCs, which can promote anti-tumor responses by CD8 T cells, are reduced in frequency in WT2 mice, where WT2 intratumoral CD8 T cells may have decreased DC help. Whether adjacent-tissue Tregs in WT2 tumor-bearing mice promote an immunosuppressive environment or kill DCs and CD8 T cells remains unknown.

Lastly, while we've shown that WT2 mice have increased exhausted intratumoral CD8 T cells, it remains to be determined if prevention of CD8 T cell exhaustion and/or reduced tumor numbers or size is possible with checkpoint blockade immunotherapy. To this end, we can treat WT2 mice with anti-PD-1 antibody starting at various timepoints of AOM/DSS and measure tumor outcomes where antibody clone, optimal dose, start day, and length of treatment are factors that have to optimized. These factors are important as anti-PD-1 can promote increased colon inflammation, which is a common side effect, which can be attributed to CD8 T cells and gut microbiota (240, 241), and therefore could alter our inflammation-dependent tumor results. As most patients receive anti-PD-1 blockade after tumors have formed, starting injections around DSS round 3, as WT2 mice develop tumors by the end of DSS round 2 (37), may be a starting point.

Here, we have shown that the WT2 microbiome promotes increased colon LP $CD8^+$ $IFN\gamma^+$ T cells in naïve mice where WT2 intratumoral CD8 T cells become more exhausted at the tumor endpoint, consistent with increased tumor burdens. Future studies are needed to further elucidate the mechanism(s) by which the microbiota activates CD8 T cells and promotes their exhaustion.

CHAPTER 5: Conclusion

5.1 Summary

The overall objective of this dissertation was to explore microbiome-host interactions that underlie susceptibility to inflammation-associated tumorigenesis in two C57BL/6 WT colonies.

In Chapter 2, we present two colonies of WT mice that develop different colitis-associated tumor burdens. WT1 mice develop five tumors on average, and WT2 mice develop 15 tumors on average. Since WT2 mice derive from the WT littermates of *Nod1*$^{-/-}$ mice, where the microbiomes of *Nod1*$^{-/-}$ mice promote increased susceptibility to colitis-associated colon tumorigenesis, we determined that the WT2 microbiome composition is significantly different from that of WT1 mice. Naïve WT2 mice already have microbiome compositions that resemble that of IBD and CRC patients compared to naïve WT1 mice. Additionally, the tumor burden differences between the two colonies can be directly attributed to the microbiome differences. Lastly, some of the bacteria that promote tumor burden differences are cultivable.

In Chapter 3, we delve deeper into examining microbiome differences between the two colonies. We first try several cohousing and cross-fostering microbiome transfer methods to determine if tumor burden phenotype can be transmissible through microbiome transfer. While cross-fostering yielded overall better microbiome transfer than cohousing, cross-fostered mice had an intermediate tumor burden phenotype where significant bacteria differences between cross-fostered and control mice remained. Despite incomplete microbiome transfer, we were able to use the microbiome data from these mice to determine specific bacteria that are statistically associated with low or high tumor burdens. We consolidated a list of nine candidate bacteria: two low tumor-associated bacteria and seven high tumor-associated bacteria. Their low relative abundances in stool proved to be difficult to overcome in preliminary efforts to culture these bacteria.

In Chapter 4, we explored possible host immune differences between WT1 and WT2 mice as specific microbiota can promote host immune cell differences. We found that specific to the colon LP, naïve WT2 mice have increased $CD8^+$ $IFN\gamma^+$ T cells, where this increase can be directly

attributed to the WT2 microbiome. Similarly, WT2 mice also had increased colon LP $CD8^+$ $IFN\gamma^+$ T cells on day 12 of AOM/DSS or during the acute inflammation response. However, at the tumor endpoint, WT2 tumors have decreased CD8 and IFNγ-producing T cells in addition to increased exhausted CD8 T cells compared to WT1 tumors, which is consistent with increased WT2 tumorigenesis. No differences in intratumoral CD8 T cells were measured in non-inflammation-associated colon cancer models. We also show preliminary data that CD8 T cells adoptively transferred into *Rag1*$^{-/-}$ mice promote increased tumorigenesis in the presence of WT2, but not WT1, microbiota.

These findings are broadly summarized in **Figure 5.1**.

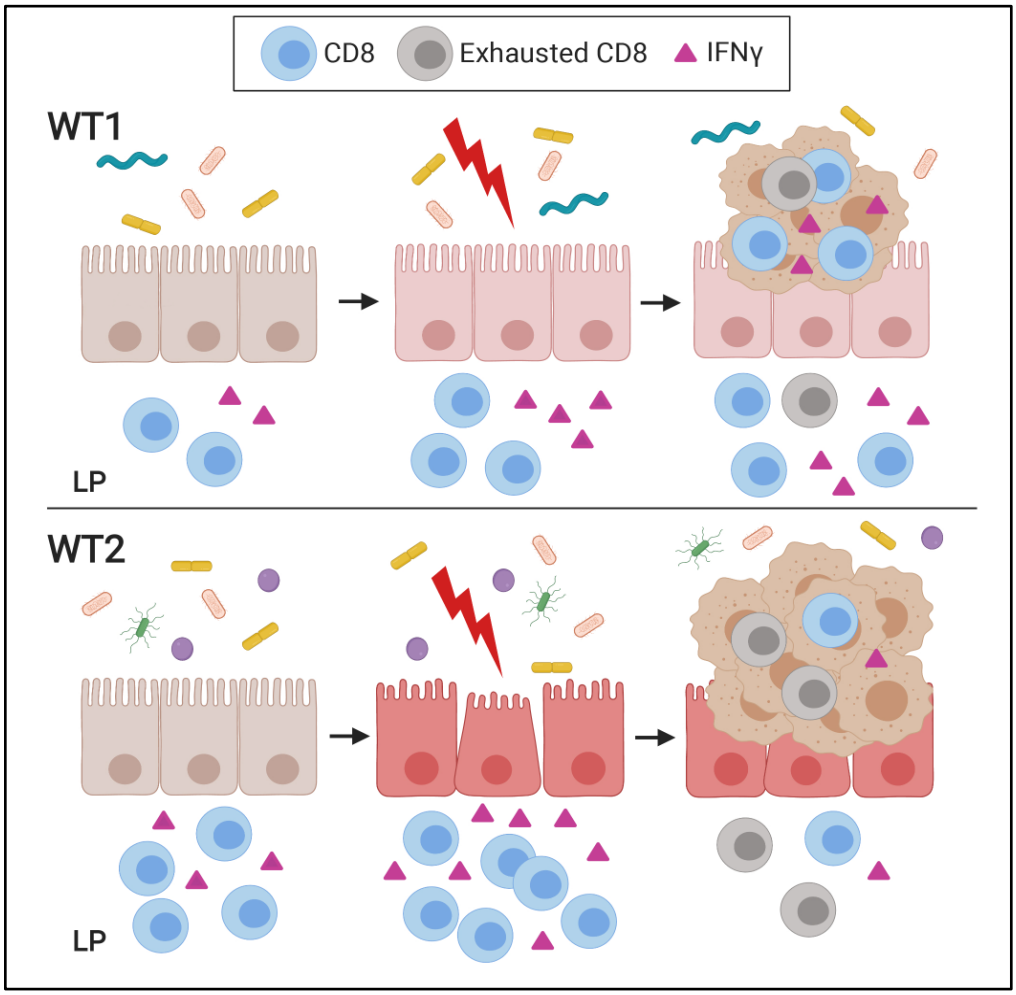

Figure 5.1 Visualization of the microbiota and CD8 T cell activity in WT1 and WT2 mice during AOM/DSS tumorigenesis
WT1 and WT2 mice have significant microbiome differences, where WT2 microbiota promote increased colon LP CD8+ IFNγ+ T cells. During AOM/DSS treatment, WT2 mice develop more colon inflammation and have more colon LP CD8+ IFNγ+ T cells than WT1 mice. At the tumor endpoint, WT2 mice have more colon tumors and increased intratumoral T cell exhaustion than WT1 mice. The figure image was made with BioRender.com.

In summary, the main contributions of this dissertation to the field are as follows:

1. Dysbiosis promotes increased colon LP $CD8^+$ $IFN\gamma^+$ T cells and CRC susceptibility
2. Increased $CD8^+$ $IFN\gamma^+$ T cells are associated with more colon inflammation and tumorigenesis
3. Dysbiosis-associated inflammation and tumorigenesis are associated with greater intratumoral CD8 T cell exhaustion

5.2 Discussion and Future Directions

Notably, our results suggest a novel role of dysbiosis in promoting T cell exhaustion, which, within the tumor microenvironment, can reduce anti-tumor immunity. Specifically, in contrast to increased colon LP $CD8^+$ $IFN\gamma^+$ T cells in naïve and acutely-inflamed WT2 mice, there were significantly decreased tumor-infiltrating $CD8^+$ $IFN\gamma^+$ cells as well as in normal adjacent tissue. A potential explanation for the observed reduction in $CD8^+$ $IFN\gamma^+$ cells is that chronic stimulation and activation of intestinal LP CD8 T cells by WT2 gut microbiota leads to their exhaustion and results in reduced immune surveillance and ultimately increased tumor burden. Conversely, it is also possible that WT1 microbiota limit T cell exhaustion during the development of inflammation and tumors in the colon. Thus, it may be important to identify bacterial populations that not only induce protective $CD8^+$ $IFN\gamma^+$ responses within the tumor microenvironment, but also attenuate T cell exhaustion to maximize anti-tumor immunity.

In Chapter 3, we reveal nine tumor-associated candidate bacteria which have not been previously classified to the species level. We plan to isolate as many of these bacteria as possible, and we hope to show by proof of principle that after AOM/DSS treatment, GF WT mice colonized with low tumor-associated candidates will develop few tumors, and that GF WT mice colonized with high tumor-associated candidates will develop higher tumor burdens. Additionally, while we've shown that WT2 microbiota can directly promote increased colon LP $CD8^+$ $IFN\gamma^+$ T cells in untreated mice, we can also determine if the high tumor-associated candidate bacteria also directly promotes increased colon LP $CD8^+$ $IFN\gamma^+$ T cells.

It is important to note that in this dissertation, we focused on the bacteria component of the microbiome, but enteric viruses (virome), which includes bacteriophages, and fungi (mycobiome) may also contribute to CRC susceptibility in these two mouse colonies, as dysbiotic bacteriophage and fungal compositions have been reported in CRC patients (242-244). It has also been proposed that enteric bacteriophages can directly promote dysbiotic bacterial microbiomes during IBD and

CRC (243, 245, 246). One group further determined that bacteriophages exacerbated colon tumor growth and stimulated host immunity as phage-primed dendritic cells promoted IFNγ responses by CD4 T cells via TLR9 (247). In addition to the virome, the mycobiome has also been implicated in colitis and CRC. One study observed altered mycobiomes after DSS-induced colitis in mice and increased colitis after anti-fungal treatment compared to normal control mice (248). Additionally, another group found that while the mycobiome member *Schizosaccharomyces pombe* was detected in both CRC patients and healthy controls, four *S. pombe*-secreted proteins were specifically associated with late stage CRC, suggesting a possible role of the mycobiome secretome (249). Altogether, further studies are needed to determine how the virome and mycobiome are involved in CRC development. It would be worthwhile to investigate the viral and fungal microbiome components in our unique two-colony system in the context of CRC.

One mechanism to be explored relates to our preliminary PICRUSt data in Chapter 1, is determining differences in microbial metabolites that are produced by low tumor-associated bacteria and high tumor-associated bacteria, where the differential metabolites can influence anti- or pro-tumorigenic activity. It is also possible that these bacteria are not sufficient to induce tumor burden differences. In that case, we would analyze metabolite differences between naïve WT1 and WT2 mice as we know the differing microbiomes promote tumor burden differences, possibly via promoting CD8 T cell differences.

We've shown that the WT2 microbiome promotes increased CD8 T cell differences and plan to determine how WT2 bacteria, and possibly high tumor-associated candidate bacteria, promotes increased CD8 T cells before tumorigenesis. As direct adhesion of segmented filamentous bacteria to intestinal epithelial cells is necessary for its ability to induce Th17 cell differentiation (202), one mechanism we could explore is localization and direct interaction of microbiota with the host. We and others have used fluorescence in situ hybridization (FISH) to visualize spatial localization of gut bacteria with respect to the host (194, 250-252). With FISH, we can also determine not only where certain bacteria are in relation to the mucus layer and epithelium, but also in relation to immune cells, including CD8 T cells at both naïve and tumor endpoint timepoints.

WT2 mice, which develop significantly more tumors after AOM/DSS treatment than WT1 mice, have an altered microbiome that is associated with increased LP $CD8^+$ $IFN\gamma^+$ T cells at baseline and during acute inflammatory responses in the colon. Although CD8 T cells are known

for their cytotoxic, anti-tumor activity, our results suggest that in the presence of dysbiosis, they can also have a pathogenic role by promoting damaging, chronic inflammation, and consequently, tumor development. Consistently, *Rag1*$^{-/-}$ and *Cd8*$^{-/-}$ mice transplanted with microbiomes from WT2 donor mice developed significantly fewer tumors. Furthermore, intratumoral WT2 CD8 T cells display decreased IFNγ activity and increased markers of exhaustion, further suggesting the inflammatory environment promoted by the WT2 microbiome leads to CD8 T cells exhaustion which in turn results in increased tumorigenesis. We have also shown that DCs stimulated with heat-killed WT2 microbiota promotes IL-12 production which can induce IFNγ responses by CD8 T cells. We have begun CD8 T cell and bacteria-primed BMDC cocultures to determine if the IL-12 production by DCs is sufficient to induce CD8 T cell IFNγ responses. However, it remains unclear how the microbiota promotes increased IL-12 production by DCs. Additionally, it is unknown how naïve WT2 mice have increased colon LP CD8 T cells as we've determined that there are no differences in chemokine production between naïve WT1 and WT2 mice. Since recruitment is unlikely, it is possible the increase in WT2 colon LP CD8 T cells is due to cellular expansion, which can be measured by Ki67 staining and flow cytometry. However, the exact mechanisms of how the WT2 microbiota promotes increased inflammation and CD8 T cell activation in naïve mice are unknown.

Although there is significant evidence supporting a role of commensal-specific CD4 T cells in mediating inflammatory Th1 and Th17 responses (253, 254), less is known about the contribution of CD8 T cells in driving colon inflammation. CD8 T cells have been implicated in IBD where increased colon LP activated cytotoxic CD8 T cells are associated with active disease (255). In certain mouse models, host antigen-reactive CD8 T cells have been shown to be major drivers of colitis (256-258). However, whether WT2 microbiota promotes the generation of commensal-specific CD8 T cells to potentiate colitis-associated tumorigenesis remains to be determined. Additionally, the absence of CD8 T cells in the presence of a WT2 microbiome does not completely suppress tumorigenesis suggesting the possibility that WT2 microbiota can also promote tumorigenesis via CD8-independent mechanisms and/or CD8 T cells can also contribute to tumor suppression.

In this study, we focus on the role of CD8 T cells, but our data in Chapter 3 suggest a possible role for B cells. Compared to *Rag1*$^{-/-}$ mice colonized with WT2 mice, *Cd8*$^{-/-}$ mice colonized with WT2 mice didn't develop as few tumors as WT1 mice, suggesting that B cells or

CD4 T cells may play a role in promoting tumorigenesis in WT2 mice. No differences in CD4 subsets were measured between WT1 and WT2 mice, but naive WT2 mice have increased colon LP B cells and decreased intratumoral B cells, strongly suggesting that B cells may play a role in WT2 microbiota-mediated tumorigenesis. While GF WT and microbiome-depleted WT1 mice colonized with WT2 microbiota displayed increased colon LP $CD8^+$ $IFN\gamma^+$ T cells similar to SPF WT2 controls, no differences in B cells were measured (**Figures 4.19B and 4.19C**), demonstrating that the WT2 microbiota aren't sufficient to promote increased colon LP B cells as measured in control untreated SPF WT2 mice (**Figure 4.2A**).

It is possible that B cells are playing a secondary role in promoting WT2 tumorigenesis. (232) show that CRC patients with both increased tumor-infiltrating $CD20^+$ B cells, which includes naive, germinal center B cells, and memory B cells, as well as CD8 T cells, had better outcomes compared to patients with high CD8 T cell tumor infiltration but poor B cell tumor infiltration. Moreover, in patients with low tumor-infiltrating CD8 T cells, the level of B cell infiltration was no longer a strong predictor of patient outcomes, further linking CD8 T cells and B cells (232). Tumor-infiltrating B cells are not as well characterized and may have different roles in different cancers, but some studies suggest anti-tumor activities of intratumoral B cells include producing tumor antigen-specific antibodies, promoting intratumoral CD8 T cell anti-tumor responses, as well as FasL and/or TRAIL-mediated tumor cell killing (236, 259, 260). While B cells can have anti-tumorigenic activity, they can also contribute to autoimmune diseases where they produce autoantibodies that target self-antigens and commensal bacteria and can interact with the complement system, act as antigen-presenting cells to T cells, and influence DC migration (233, 261, 262). Altogether, our data suggests B cells play a role in mediating tumorigenesis, possibly via CD8 T cell interactions. B cell differences, including B cell subsets, Ig production, Ig specificity, localization and interaction with CD8 T cells, and more, between WT1 and WT2 mice at naïve and tumor timepoints remain to be determined.

In addition to CD8 T cells, DCs, and B cells, colon epithelial cells may also contribute to inflammatory and tumorigenic responses as the AOM/DSS model causes epithelial barrier injury and tumors develop due to abnormal epithelial barrier repair and cell division. Furthermore, as discussed in Chapter 1, specific microbiota have been shown to promote increased Wnt cell cycle signaling and epithelial cell proliferation. Our microarray and qPCR data (**Figures 4.1 and 4.11**) propose possible epithelial gene expression and therefore functional differences between WT1 and

WT2 mice, but more experiments are needed to determine if and when they play a role in immune and tumor differences.

One area of study we've only begun to explore in this project is the role of the gut microbiome in checkpoint blockade immunotherapy efficacy which has been shown in multiple other studies (226, 263-265). Both CD8 T cells and gut microbiota can affect immune checkpoint inhibitor success, and certain microbiota are associated with increased CD8 T cell anti-tumor activity via augmented DC responses (84, 226). It would be interesting to determine if the microbiome differences promote immune checkpoint inhibitor therapy response differences and if the microbiome could be manipulated to improve immunotherapy responses. As certain bacteria are being explored as predictors of immunotherapy efficacy (266), it is possible our two colonies could reveal new bacteria that are linked to immunotherapy effectiveness. In the future, patients' microbiota could be screened to determine their responsiveness to certain therapies over others. Additionally, while there are differences in PD-1^+ T cells between WT1 and WT2 tumors, it is unclear if there are differences in PD-L1 expression in the different tumors, where PD-L1 is the ligand for PD-1 and is upregulated by tumors as a means of immune evasion. It would be worthwhile to explore the effects of the different WT1 and WT2 microbiota and metabolites on PD-L1 expression by tumors, as the binding of PD-L1 on tumor cells to PD-1 on T cells results in inhibitory signaling in T cells which leads to exhaustion.

In conclusion, our data demonstrate a role of the gut microbiome in altering CD8 T cell activity in the colon LP to impact tumorigenesis through early CD8 T cell activation, which can have long-term negative consequences by increasing susceptibility to inflammation and exhaustion, which can result in colon tumorigenesis. While more studies are needed to determine mechanisms of action, our findings further our knowledge of host-commensal interactions in CRC and reinforce the idea of the gut microbiome's potential in advancing personalized medicine.

APPENDIX

Chapter 1

Modified from a review chapter titled, "The Gut Microbiome and Colorectal Cancer," which was co-authored with Grace Y. Chen that was accepted for publication in the Springer Physiology in Health and Disease series titled: Inflammation, Infection, and Microbiome in Cancers: Evidence, Mechanisms, and Implications.

Contributions: Amy I. Yu and Grace Y. Chen wrote the final manuscript.

Chapter 2, 3, and 4

Modified from the manuscript published at *Cell Reports* titled, "Gut microbiota modulate CD8 T cell responses to influence colitis-associated tumorigenesis," which was co-authored with Lili Zhao, Kathryn A. Eaton, Sharon Ho, Jiachen Chen, Sara Poe, James Becker, Allison Gonzalez, Delaney McKinstry, Muneer Hasso, Jonny Mendoza-Castrejon, Joel Whitfield, Charles Koumpouras, Patrick D. Schloss, Eric C. Martens, and Grace Y. Chen (267).
Manuscript and supplemental information can be found online at: https://doi.org/10.1016/j.celrep.2020.03.035

Contributions: Amy I. Yu and Grace Y. Chen were responsible for conceptualization and methodology. Formal and statistical analyses were done by Amy I. Yu, Lili Zhao, and Grace Y. Chen. Experimental investigation was carried out by Amy I. Yu, Lili Zhao, Kathryn A. Eaton, Sharon Ho, Jiachen Chen, Sara Poe, James Becker, Allison Gonzalez, Delaney McKinstry, Muneer Hasso, Jonny Mendoza-Castrejon, Joel Whitfield, Charles Koumpouras, Eric C. Martens, and Grace Y. Chen. Histologic interpretation and scoring was completed by board-certified veterinary pathologist Kathryn A. Eaton. Patrick D. Schloss and Eric C. Martens provided resources for the completion of this manuscript. Amy I. Yu and Grace Y. Chen wrote the final manuscript. This work was supported by funding acquired by Amy I. Yu: 1) University of Michigan Rackham Research Grant, 2) NIH grant T32 AI007413, and Grace Y. Chen: 1) NIH grant R01 CA166879,

2) an American Cancer Society Research Scholar Grant, and 3) the Tom Liu Memorial Golf Tournament Fund from the University of Michigan Rogel Cancer Center.

Acknowledgments: We thank Joseph Zackular, Nielsen Baxter, Nicholas Pudlo, Hideaki Fujiwara and Pavan Reddy, Blake Heath and Leo Lei, Kai Han and James Moon, Sho Kitamoto and Nobuhiko Kamada, Naohiro Inohara, Gabriel Nuñez, Asma Nusrat, Yatrik Shah, and Sergey Seregin for their help, advice, and critical manuscript reading. We would also like to thank the University of Michigan Flow Cytometry, Germ-free and Gnotobiotic, Cancer Center Immunology, DNA Sequencing, Histology, and Microscopy Cores for technical support.

REFERENCES

1. Arnold M, Sierra MS, Laversanne M, Soerjomataram I, Jemal A, and Bray F. Global patterns and trends in colorectal cancer incidence and mortality. *Gut.* 2017;66(4):683-91.
2. Keum N, and Giovannucci E. Global burden of colorectal cancer: emerging trends, risk factors and prevention strategies. *Nat Rev Gastroenterol Hepatol.* 2019;16(12):713-32.
3. Stoffel EM, and Murphy CC. Epidemiology and Mechanisms of the Increasing Incidence of Colon and Rectal Cancers in Young Adults. *Gastroenterology.* 2019.
4. Siegel RL, Miller KD, Goding Sauer A, Fedewa SA, Butterly LF, Anderson JC, et al. Colorectal cancer statistics, 2020. *CA Cancer J Clin.* 2020.
5. Aune D, Chan DS, Lau R, Vieira R, Greenwood DC, Kampman E, et al. Dietary fibre, whole grains, and risk of colorectal cancer: systematic review and dose-response meta-analysis of prospective studies. *BMJ.* 2011;343:d6617.
6. Capurso G, and Lahner E. The interaction between smoking, alcohol and the gut microbiome. *Best Pract Res Clin Gastroenterol.* 2017;31(5):579-88.
7. Turnbaugh PJ, Hamady M, Yatsunenko T, Cantarel BL, Duncan A, Ley RE, et al. A core gut microbiome in obese and lean twins. *Nature.* 2009;457(7228):480-4.
8. Turnbaugh PJ, Ley RE, Mahowald MA, Magrini V, Mardis ER, and Gordon JI. An obesity-associated gut microbiome with increased capacity for energy harvest. *Nature.* 2006;444(7122):1027-31.
9. Song M, Chan AT, and Sun J. Influence of the Gut Microbiome, Diet, and Environment on Risk of Colorectal Cancer. *Gastroenterology.* 2019.
10. Makki K, Deehan EC, Walter J, and Backhed F. The Impact of Dietary Fiber on Gut Microbiota in Host Health and Disease. *Cell Host Microbe.* 2018;23(6):705-15.
11. Li KJ, Chen ZL, Huang Y, Zhang R, Luan XQ, Lei TT, et al. Dysbiosis of lower respiratory tract microbiome are associated with inflammation and microbial function variety. *Respir Res.* 2019;20(1):272.
12. Flynn KJ, Ruffin MTt, Turgeon DK, and Schloss PD. Spatial Variation of the Native Colon Microbiota in Healthy Adults. *Cancer Prev Res (Phila).* 2018;11(7):393-402.
13. Missiaglia E, Jacobs B, D'Ario G, Di Narzo AF, Soneson C, Budinska E, et al. Distal and proximal colon cancers differ in terms of molecular, pathological, and clinical features. *Ann Oncol.* 2014;25(10):1995-2001.
14. Kim K, Castro EJT, Shim H, Advincula JVG, and Kim YW. Differences Regarding the Molecular Features and Gut Microbiota Between Right and Left Colon Cancer. *Ann Coloproctol.* 2018;34(6):280-5.
15. O'Hara AM, and Shanahan F. *EMBO Rep*. 2006:688-93.
16. Rajilic-Stojanovic M, and de Vos WM. The first 1000 cultured species of the human gastrointestinal microbiota. *FEMS Microbiol Rev.* 2014;38(5):996-1047.
17. Roy S, and Trinchieri G. Microbiota: a key orchestrator of cancer therapy. *Nat Rev Cancer.* 2017;17(5):271-85.

18. Savage D. Microbial ecology of the gastrointestinal tract. *Annu Rev Microbiol.* 1977;31:107-33.
19. Arumugam M, Raes J, Pelletier E, Le Paslier D, Yamada T, Mende DR, et al. Enterotypes of the human gut microbiome. *Nature.* 2011;473(7346):174-80.
20. Eckburg PB, Bik EM, Bernstein CN, Purdom E, Dethlefsen L, Sargent M, et al. Diversity of the Human Intestinal Microbial Flora. *Science.* 2005;308(5728):1635-8.
21. Costea PI, Hildebrand F, Arumugam M, Backhed F, Blaser MJ, Bushman FD, et al. Enterotypes in the landscape of gut microbial community composition. *Nat Microbiol.* 2018;3(1):8-16.
22. Ding T, and Schloss PD. Dynamics and associations of microbial community types across the human body. *Nature.* 2014;509(7500):357-60.
23. Carding S, Verbeke K, Vipond DT, Corfe BM, and Owen LJ. Dysbiosis of the gut microbiota in disease. *Microb Ecol Health Dis.* 2015;26.
24. Thomas AM, Manghi P, Asnicar F, Pasolli E, Armanini F, Zolfo M, et al. Metagenomic analysis of colorectal cancer datasets identifies cross-cohort microbial diagnostic signatures and a link with choline degradation. *Nat Med.* 2019;25(4):667-78.
25. Wirbel J, Pyl PT, Kartal E, Zych K, Kashani A, Milanese A, et al. Meta-analysis of fecal metagenomes reveals global microbial signatures that are specific for colorectal cancer. *Nat Med.* 2019;25(4):679-89.
26. Wang T, Cai G, Qiu Y, Fei N, Zhang M, Pang X, et al. Structural segregation of gut microbiota between colorectal cancer patients and healthy volunteers. *ISME J.* 2012;6(2):320-9.
27. Ahn J, Sinha R, Pei Z, Dominianni C, Wu J, Shi J, et al. Human gut microbiome and risk for colorectal cancer. *J Natl Cancer Inst.* 2013;105(24):1907-11.
28. Baxter NT, Zackular JP, Chen GY, and Schloss PD. Structure of the gut microbiome following colonization with human feces determines colonic tumor burden. *Microbiome.* 2014;2:20.
29. Zackular JP, Rogers MA, Ruffin MTt, and Schloss PD. The human gut microbiome as a screening tool for colorectal cancer. *Cancer Prev Res (Phila).* 2014;7(11):1112-21.
30. Flemer B, Lynch DB, Brown JMR, Jeffery IB, Ryan FJ, Claesson MJ, et al. Tumour-associated and non-tumour-associated microbiota in colorectal cancer. *Gut.* 2017;66(4):633-43.
31. Flynn KJ, Baxter NT, and Schloss PD. Metabolic and Community Synergy of Oral Bacteria in Colorectal Cancer. *mSphere.* 2016;1(3).
32. Koliarakis I, Messaritakis I, Nikolouzakis TK, Hamilos G, Souglakos J, and Tsiaoussis J. Oral Bacteria and Intestinal Dysbiosis in Colorectal Cancer. *Int J Mol Sci.* 2019;20(17).
33. Mima K, Cao Y, Chan AT, Qian ZR, Nowak JA, Masugi Y, et al. Fusobacterium nucleatum in Colorectal Carcinoma Tissue According to Tumor Location. *Clin Transl Gastroenterol.* 2016;7(11):e200.
34. Baxter NT, Ruffin MTt, Rogers MA, and Schloss PD. Microbiota-based model improves the sensitivity of fecal immunochemical test for detecting colonic lesions. *Genome Med.* 2016;8(1):37.
35. Sze MA, and Schloss PD. Leveraging Existing 16S rRNA Gene Surveys To Identify Reproducible Biomarkers in Individuals with Colorectal Tumors. *MBio.* 2018;9(3).
36. Sze MA, Baxter NT, Ruffin MTt, Rogers MAM, and Schloss PD. Normalization of the microbiota in patients after treatment for colonic lesions. *Microbiome.* 2017;5(1):150.

37. Zackular JP, Baxter NT, Iverson KD, Sadler WD, Petrosino JF, Chen GY, et al. The gut microbiome modulates colon tumorigenesis. *MBio.* 2013;4(6):e00692-13.
38. Tanaka T, Kohno H, Suzuki R, Yamada Y, Sugie S, and Mori H. A novel inflammation-related mouse colon carcinogenesis model induced by azoxymethane and dextran sodium sulfate. *Cancer Sci.* 2003;94(11):965-73.
39. Wong SH, Zhao L, Zhang X, Nakatsu G, Han J, Xu W, et al. Gavage of Fecal Samples From Patients With Colorectal Cancer Promotes Intestinal Carcinogenesis in Germ-Free and Conventional Mice. *Gastroenterology.* 2017;153(6):1621-33 e6.
40. Li L, Li X, Zhong W, Yang M, Xu M, Sun Y, et al. Gut microbiota from colorectal cancer patients enhances the progression of intestinal adenoma in Apc min/+ mice. *EBioMedicine.* 2019.
41. Tomkovich S, Dejea CM, Winglee K, Drewes JL, Chung L, Housseau F, et al. Human colon mucosal biofilms from healthy or colon cancer hosts are carcinogenic. *J Clin Invest.* 2019;130:1699-712.
42. Nguyen TL, Vieira-Silva S, Liston A, and Raes J. How informative is the mouse for human gut microbiota research? *Dis Model Mech.* 2015;8(1):1-16.
43. Chung H, Pamp SJ, Hill JA, Surana NK, Edelman SM, Troy EB, et al. Gut immune maturation depends on colonization with a host-specific microbiota. *Cell.* 2012;149(7):1578-93.
44. Marchesi JR, Dutilh BE, Hall N, Peters WH, Roelofs R, Boleij A, et al. Towards the human colorectal cancer microbiome. *PLoS One.* 2011;6(5):e20447.
45. Kostic AD, Gevers D, Pedamallu CS, Michaud M, Duke F, Earl AM, et al. Genomic analysis identifies association of Fusobacterium with colorectal carcinoma. *Genome Res.* 2012;22(2):292-8.
46. Han YW. Fusobacterium nucleatum: a commensal-turned pathogen. *Curr Opin Microbiol.* 2015;0:141-7.
47. Signat B, Roques C, Poulet P, and Duffaut D. Fusobacterium nucleatum in periodontal health and disease. *Curr Issues Mol Biol.* 2011;13(2):25-36.
48. Castellarin M, Warren RL, Freeman JD, Dreolini L, Krzywinski M, Strauss J, et al. Fusobacterium nucleatum infection is prevalent in human colorectal carcinoma. *Genome Res.* 2012;22(2):299-306.
49. Kostic AD, Chun E, Robertson L, Glickman JN, Gallini CA, Michaud M, et al. Fusobacterium nucleatum potentiates intestinal tumorigenesis and modulates the tumor-immune microenvironment. *Cell Host Microbe.* 2013;14(2):207-15.
50. Lee DW, Han SW, Kang JK, Bae JM, Kim HP, Won JK, et al. Association Between Fusobacterium nucleatum, Pathway Mutation, and Patient Prognosis in Colorectal Cancer. *Ann Surg Oncol.* 2018;25(11):3389-95.
51. Mima K, Nishihara R, Qian ZR, Cao Y, Sukawa Y, Nowak JA, et al. Fusobacterium nucleatum in colorectal carcinoma tissue and patient prognosis. *Gut.* 2016;65(12):1973-80.
52. Yu T, Guo F, Yu Y, Sun T, Ma D, Han J, et al. Fusobacterium nucleatum Promotes Chemoresistance to Colorectal Cancer by Modulating Autophagy. *Cell.* 2017;170(3):548-63 e16.
53. Dejea CM, Wick EC, Hechenbleikner EM, White JR, Mark Welch JL, Rossetti BJ, et al. Microbiota organization is a distinct feature of proximal colorectal cancers. *Proc Natl Acad Sci U S A.* 2014;111(51):18321-6.

54. Rubinstein MR, Baik JE, Lagana SM, Han RP, Raab WJ, Sahoo D, et al. Fusobacterium nucleatum promotes colorectal cancer by inducing Wnt/beta-catenin modulator Annexin A1. *EMBO Rep.* 2019;20(4).
55. Sears CL, Islam S, Saha A, Arjumand M, Alam NH, Faruque AS, et al. Association of enterotoxigenic Bacteroides fragilis infection with inflammatory diarrhea. *Clin Infect Dis.* 2008;47(6):797-803.
56. Wu S, Rhee KJ, Albesiano E, Rabizadeh S, Wu X, Yen HR, et al. A human colonic commensal promotes colon tumorigenesis via activation of T helper type 17 T cell responses. *Nat Med.* 2009;15(9):1016-22.
57. Haghi F, Goli E, Mirzaei B, and Zeighami H. The association between fecal enterotoxigenic B. fragilis with colorectal cancer. *BMC Cancer.* 2019;19(1):879.
58. Toprak N, Yagci A, Gulluoglu B, Akin M, Demirkalem P, Celenk T, et al. A possible role of Bacteroides fragilis enterotoxin in the aetiology of colorectal cancer. *Clin Microbiol Infect.* 2006;12(8):782-6.
59. Dejea CM, Fathi P, Craig JM, Boleij A, Taddese R, Geis AL, et al. Patients with familial adenomatous polyposis harbor colonic biofilms containing tumorigenic bacteria. *Science.* 2018;359(6375):592-7.
60. Drewes JL, White JR, Dejea CM, Fathi P, Iyadorai T, Vadivelu J, et al. High-resolution bacterial 16S rRNA gene profile meta-analysis and biofilm status reveal common colorectal cancer consortia. *NPJ Biofilms Microbiomes.* 2017;3:34.
61. Hale VL, Jeraldo P, Chen J, Mundy M, Yao J, Priya S, et al. Distinct microbes, metabolites, and ecologies define the microbiome in deficient and proficient mismatch repair colorectal cancers. *Genome Med.* 2018;10(1):78.
62. Swidsinski A, Khilkin M, Kerjaschki D, Schreiber S, Ortner M, Weber J, et al. Association between intraepithelial Escherichia coli and colorectal cancer. *Gastroenterology.* 1998;115(2):281-6.
63. Martin HM, Campbell BJ, Hart CA, Mpofu C, Nayar M, Singh R, et al. Enhanced Escherichia coli adherence and invasion in Crohn's disease and colon cancer. *Gastroenterology.* 2004;127(1):80-93.
64. Maddocks ODK, Short AJ, Donnenberg MS, Bader S, and Harrison DJ. Attaching and Effacing Escherichia coli Downregulate DNA Mismatch Repair Protein In Vitro and Are Associated with Colorectal Adenocarcinomas in Humans. *PLoS One.* 2009;4(5):e5517.
65. Nougayrede JP, Homburg S, Taieb F, Boury M, Brzuszkiewicz E, Gottschalk G, et al. Escherichia coli induces DNA double-strand breaks in eukaryotic cells. *Science.* 2006;313(5788):848-51.
66. Arthur JC, Perez-Chanona E, Muhlbauer M, Tomkovich S, Uronis JM, Fan TJ, et al. Intestinal inflammation targets cancer-inducing activity of the microbiota. *Science.* 2012;338(6103):120-3.
67. Kuhn R, Lohler J, Rennick D, Rajewsky K, and Muller W. Interleukin-10-deficient mice develop chronic enterocolitis. *Cell.* 1993;75(2):263-74.
68. Arthur JC, Gharaibeh RZ, Muhlbauer M, Perez-Chanona E, Uronis JM, McCafferty J, et al. Microbial genomic analysis reveals the essential role of inflammation in bacteria-induced colorectal cancer. *Nat Commun.* 2014;5:4724.
69. Bonnet M, Buc E, Sauvanet P, Darcha C, Dubois D, Pereira B, et al. Colonization of the human gut by E. coli and colorectal cancer risk. *Clin Cancer Res.* 2014;20(4):859-67.

70. Cougnoux A, Dalmasso G, Martinez R, Buc E, Delmas J, Gibold L, et al. Bacterial genotoxin colibactin promotes colon tumour growth by inducing a senescence-associated secretory phenotype. *Gut.* 2014;63(12):1932-42.
71. Raisch J, Buc E, Bonnet M, Sauvanet P, Vazeille E, de Vallee A, et al. Colon cancer-associated B2 Escherichia coli colonize gut mucosa and promote cell proliferation. *World J Gastroenterol.* 2014;20(21):6560-72.
72. Sobhani I, Tap J, Roudot-Thoraval F, Roperch JP, Letulle S, Langella P, et al. Microbial Dysbiosis in Colorectal Cancer (CRC) Patients. *PLoS One.* 2011;6(1).
73. Chen W, Liu F, Ling Z, Tong X, and Xiang C. Human Intestinal Lumen and Mucosa-Associated Microbiota in Patients with Colorectal Cancer. *PLoS One.* 2012;7(6).
74. Chen HM, Yu YN, Wang JL, Lin YW, Kong X, Yang CQ, et al. Decreased dietary fiber intake and structural alteration of gut microbiota in patients with advanced colorectal adenoma. *Am J Clin Nutr.* 2013;97(5):1044-52.
75. Weir TL, Manter DK, Sheflin AM, Barnett BA, Heuberger AL, and Ryan EP. Stool microbiome and metabolome differences between colorectal cancer patients and healthy adults. *PLoS One.* 2013;8(8):e70803.
76. Zeller G, Tap J, Voigt AY, Sunagawa S, Kultima JR, Costea PI, et al. Potential of fecal microbiota for early-stage detection of colorectal cancer. *Mol Syst Biol.* 2014;10:766.
77. Feng Q, Liang S, Jia H, Stadlmayr A, Tang L, Lan Z, et al. Gut microbiome development along the colorectal adenoma-carcinoma sequence. *Nat Commun.* 2015;6:6528.
78. Yu J, Feng Q, Wong SH, Zhang D, Liang QY, Qin Y, et al. Metagenomic analysis of faecal microbiome as a tool towards targeted non-invasive biomarkers for colorectal cancer. *Gut.* 2017;66(1):70-8.
79. Geva-Zatorsky N, Sefik E, Kua L, Pasman L, Tan TG, Ortiz-Lopez A, et al. Mining the Human Gut Microbiota for Immunomodulatory Organisms. *Cell.* 2017;168(5):928-43.e11.
80. Furusawa Y, Obata Y, Fukuda S, Endo TA, Nakato G, Takahashi D, et al. Commensal microbe-derived butyrate induces the differentiation of colonic regulatory T cells. *Nature.* 2013;504(7480):446-50.
81. Atarashi K, Tanoue T, Shima T, Imaoka A, Kuwahara T, Momose Y, et al. Induction of Colonic Regulatory T Cells by Indigenous Clostridium Species. *Science.* 2011;331(6015):337-41.
82. Muzes G, Molnar B, and Sipos F. Regulatory T cells in inflammatory bowel diseases and colorectal cancer. *World J Gastroenterol.* 2012;18(40):5688-94.
83. Razi S, Baradaran Noveiry B, Keshavarz-Fathi M, and Rezaei N. IL-17 and colorectal cancer: From carcinogenesis to treatment. *Cytokine.* 2019;116:7-12.
84. Tanoue T, Morita S, Plichta DR, Skelly AN, Suda W, Sugiura Y, et al. A defined commensal consortium elicits CD8 T cells and anti-cancer immunity. *Nature.* 2019;565(7741):600-5.
85. Coussens LM, and Werb Z. Inflammation and cancer. *Nature.* 2002;420(6917):860-7.
86. Johdi NA, Mazlan L, Sagap I, and Jamal R. Profiling of cytokines, chemokines and other soluble proteins as a potential biomarker in colorectal cancer and polyps. *Cytokine.* 2017;99:35-42.
87. Lu CC, Kuo HC, Wang FS, Jou MH, Lee KC, and Chuang JH. Upregulation of TLRs and IL-6 as a marker in human colorectal cancer. *Int J Mol Sci.* 2014;16(1):159-77.

88. Yan G, Liu T, Yin L, Kang Z, and Wang L. Levels of peripheral Th17 cells and serum Th17-related cytokines in patients with colorectal cancer: a meta-analysis. *Cell Mol Biol (Noisy-le-grand).* 2018;64(6):94-102.
89. Grivennikov SI, Wang K, Mucida D, Stewart CA, Schnabl B, Jauch D, et al. Adenoma-linked barrier defects and microbial products drive IL-23/IL-17-mediated tumour growth. *Nature.* 2012;491(7423):254-8.
90. Liu H, Redline RW, and Han YW. Fusobacterium nucleatum induces fetal death in mice via stimulation of TLR4-mediated placental inflammatory response. *J Immunol.* 2007;179(4):2501-8.
91. Lee P, and Tan KS. Fusobacterium nucleatum activates the immune response through retinoic acid-inducible gene I. *J Dent Res.* 2014;93(2):162-8.
92. Chaushu S, Wilensky A, Gur C, Shapira L, Elboim M, Halftek G, et al. Direct Recognition of Fusobacterium nucleatum by the NK Cell Natural Cytotoxicity Receptor NKp46 Aggravates Periodontal Disease. *PLoS Pathog.* 2012;8(3).
93. Rhee KJ, Wu S, Wu X, Huso DL, Karim B, Franco AA, et al. Induction of persistent colitis by a human commensal, enterotoxigenic Bacteroides fragilis, in wild-type C57BL/6 mice. *Infect Immun.* 2009;77(4):1708-18.
94. Chung L, Thiele Orberg E, Geis AL, Chan JL, Fu K, DeStefano Shields CE, et al. Bacteroides fragilis Toxin Coordinates a Pro-carcinogenic Inflammatory Cascade via Targeting of Colonic Epithelial Cells. *Cell Host Microbe.* 2018;23(2):203-14.e5.
95. Thiele Orberg E, Fan H, Tam AJ, Dejea CM, Destefano Shields CE, Wu S, et al. The myeloid immune signature of enterotoxigenic Bacteroides fragilis-induced murine colon tumorigenesis. *Mucosal Immunol.* 2017;10(2):421-33.
96. Sanfilippo L, Li CK, Seth R, Balwin TJ, Menozzi MG, and Mahida YR. Bacteroides fragilis enterotoxin induces the expression of IL-8 and transforming growth factor-beta (TGF-beta) by human colonic epithelial cells. *Clin Exp Immunol.* 2000;119(3):456-63.
97. Hwang S, Gwon SY, Kim MS, Lee S, and Rhee KJ. Bacteroides fragilis Toxin Induces IL-8 Secretion in HT29/C1 Cells through Disruption of E-cadherin Junctions. *Immune Netw.* 2013;13(5):213-7.
98. McCormack G, Moriarty D, O'Donoghue DP, McCormick PA, Sheahan K, and Baird AW. Tissue cytokine and chemokine expression in inflammatory bowel disease. *Inflamm Res.* 2001;50(10):491-5.
99. Kim JM, Oh YK, Kim YJ, Oh HB, and Cho YJ. Polarized secretion of CXC chemokines by human intestinal epithelial cells in response to Bacteroides fragilis enterotoxin: NF-kappa B plays a major role in the regulation of IL-8 expression. *Clin Exp Immunol.* 2001;123(3):421-7.
100. Wu S, Powell J, Mathioudakis N, Kane S, Fernandez E, and Sears CL. Bacteroides fragilis Enterotoxin Induces Intestinal Epithelial Cell Secretion of Interleukin-8 through Mitogen-Activated Protein Kinases and a Tyrosine Kinase-Regulated Nuclear Factor-κB Pathway. *Infect Immun.* 2004;72(10):5832-9.
101. Bui JD, and Schreiber RD. Cancer immunosurveillance, immunoediting and inflammation: independent or interdependent processes? *Curr Opin Immunol.* 2007;19(2):203-8.
102. Galon J, Costes A, Sanchez-Cabo F, Kirilovsky A, Mlecnik B, Lagorce-Pages C, et al. Type, density, and location of immune cells within human colorectal tumors predict clinical outcome. *Science.* 2006;313(5795):1960-4.

103. Pages F, Berger A, Camus M, Sanchez-Cabo F, Costes A, Molidor R, et al. Effector memory T cells, early metastasis, and survival in colorectal cancer. *N Engl J Med.* 2005;353(25):2654-66.
104. Mima K, Sukawa Y, Nishihara R, Qian ZR, Yamauchi M, Inamura K, et al. Fusobacterium nucleatum and T-cells in Colorectal Carcinoma. *JAMA Oncol.* 2015;1(5):653-61.
105. Gur C, Ibrahim Y, Isaacson B, Yamin R, Abed J, Gamliel M, et al. Binding of the Fap2 protein of Fusobacterium nucleatum to human inhibitory receptor TIGIT protects tumors from immune cell attack. *Immunity.* 2015;42(2):344-55.
106. Han YW, Shi W, Huang GT, Kinder Haake S, Park NH, Kuramitsu H, et al. Interactions between periodontal bacteria and human oral epithelial cells: Fusobacterium nucleatum adheres to and invades epithelial cells. *Infect Immun.* 2000;68(6):3140-6.
107. Xu M, Yamada M, Li M, Liu H, Chen SG, and Han YW. FadA from Fusobacterium nucleatum utilizes both secreted and nonsecreted forms for functional oligomerization for attachment and invasion of host cells. *J Biol Chem.* 2007;282(34):25000-9.
108. Rubinstein MR, Wang X, Liu W, Hao Y, Cai G, and Han YW. Fusobacterium nucleatum promotes colorectal carcinogenesis by modulating E-cadherin/beta-catenin signaling via its FadA adhesin. *Cell Host Microbe.* 2013;14(2):195-206.
109. Wu S, Lim KC, Huang J, Saidi RF, and Sears CL. Bacteroides fragilis enterotoxin cleaves the zonula adherens protein, E-cadherin. *Proc Natl Acad Sci U S A.* 1998;95(25):14979-84.
110. Wu S, Morin PJ, Maouyo D, and Sears CL. Bacteroides fragilis enterotoxin induces c-Myc expression and cellular proliferation. *Gastroenterology.* 2003;124(2):392-400.
111. Lu R, Liu X, Wu S, Xia Y, Zhang Y, Petrof EO, et al. Consistent activation of the β-catenin pathway by Salmonella type-three secretion effector protein AvrA in chronically infected intestine. *Am J Physiol Gastrointest Liver Physiol.* 2012;303(10):G1113-25.
112. Ye Z, Petrof EO, Boone D, Claud EC, and Sun J. Salmonella Effector AvrA Regulation of Colonic Epithelial Cell Inflammation by Deubiquitination. *Am J Pathol.* 2007;171(3):882-92.
113. Lu R, Wu S, Zhang Y, Xia Y, Liu X, Zheng Y, et al. Enteric bacterial protein AvrA promotes colonic tumorigenesis and activates colonic beta-catenin signaling pathway. *Oncogenesis.* 2014;3(6):e105.
114. Grivennikov S, Karin E, Terzic J, Mucida D, Yu GY, Vallabhapurapu S, et al. IL-6 and Stat3 are required for survival of intestinal epithelial cells and development of colitis-associated cancer. *Cancer Cell.* 2009;15(2):103-13.
115. Scanu T, Spaapen RM, Bakker JM, Pratap CB, Wu LE, Hofland I, et al. Salmonella Manipulation of Host Signaling Pathways Provokes Cellular Transformation Associated with Gallbladder Carcinoma. *Cell Host Microbe.* 2015;17(6):763-74.
116. Cuevas-Ramos G, Petit CR, Marcq I, Boury M, Oswald E, and Nougayrède JP. Escherichia coli induces DNA damage in vivo and triggers genomic instability in mammalian cells. *Proc Natl Acad Sci U S A.* 2010;107(25):11537-42.
117. Gill SR, Pop M, DeBoy RT, Eckburg PB, Turnbaugh PJ, Samuel BS, et al. Metagenomic Analysis of the Human Distal Gut Microbiome. *Science.* 2006;312(5778):1355-9.
118. Peng L, Li ZR, Green RS, Holzman IR, and Lin J. Butyrate enhances the intestinal barrier by facilitating tight junction assembly via activation of AMP-activated protein kinase in Caco-2 cell monolayers. *J Nutr.* 2009;139(9):1619-25.

119. Candido EP, Reeves R, and Davie JR. Sodium butyrate inhibits histone deacetylation in cultured cells. *Cell.* 1978;14(1):105-13.
120. Davie JR. Inhibition of histone deacetylase activity by butyrate. *J Nutr.* 2003;133(7 Suppl):2485s-93s.
121. Chang P, Hao L, Offermanns S, and Medzhitov R. The microbial metabolite butyrate regulates intestinal macrophage function via histone deacetylase inhibition. - PubMed - NCBI. *Proc Natl Acad Sci U S A.* 2014;111(6):2247-52.
122. Bolden J, Peart M, and Johnstone R. Anticancer activities of histone deacetylase inhibitors. *Nat Rev Drug Discov.* 2006;5(9):769-84.
123. Maslowski KM, Vieira AT, Ng A, Kranich J, Sierro F, Yu D, et al. Regulation of inflammatory responses by gut microbiota and chemoattractant receptor GPR43. *Nature.* 2009;461(7268):1282-6.
124. Chen GY, Liu M, Wang F, Bertin J, and Núñez G. A Functional Role for Nlrp6 in Intestinal Inflammation and Tumorigenesis*. *J Immunol.* 2011;186(12):7187-94.
125. Zaki MH, Vogel P, Body-Malapel M, Lamkanfi M, and Kanneganti TD. IL-18 production downstream of the Nlrp3 inflammasome confers protection against colorectal tumor formation. *J Immunol.* 2010;185(8):4912-20.
126. Elinav E, Strowig T, Kau AL, Henao-Mejia J, Thaiss CA, Booth CJ, et al. NLRP6 inflammasome regulates colonic microbial ecology and risk for colitis. *Cell.* 2011;145(5):745-57.
127. Singh N, Gurav A, Sivaprakasam S, Brady E, Padia R, Shi H, et al. Activation of Gpr109a, receptor for niacin and the commensal metabolite butyrate, suppresses colonic inflammation and carcinogenesis. *Immunity.* 2014;40(1):128-39.
128. Bonnotte B, Favre N, Reveneau S, Micheau O, Droin N, Garrido C, et al. Cancer cell sensitization to Fas-mediated apoptosis by sodium butyrate. *Cell Death & Differentiation.* 1998;5(6):480-7.
129. Owen-Schaub LB, Radinsky R, Kruzel E, Berry K, and Yonehara S. Anti-Fas on nonhematopoietic tumors: levels of Fas/APO-1 and bcl-2 are not predictive of biological responsiveness. *Cancer Res.* 1994;54(6):1580-6.
130. Owen-Schaub LB, Angelo LS, Radinsky R, Ware CF, Gesner TG, and Bartos DP. Soluble Fas/APO-1 in tumor cells: a potential regulator of apoptosis? *Cancer Lett.* 1995;94(1):1-8.
131. Zhang L, and Fang B. Mechanisms of resistance to TRAIL-induced apoptosis in cancer. *Cancer Gene Therapy.* 2004;12(3):228-37.
132. Hernandez A, Wang QD, Schwartz SA, and Evers BM. Sensitization of human colon cancer cells to TRAIL-mediated apoptosis. *J Gastrointest Surg.* 2001;5(1):56-65.
133. Zhang XD, Franco AV, Nguyen T, Gray CP, and Hersey P. Differential localization and regulation of death and decoy receptors for TNF-related apoptosis-inducing ligand (TRAIL) in human melanoma cells. *J Immunol.* 2000;164(8):3961-70.
134. Hernandez A, Thomas R, Smith F, Sandberg J, Kim S, Chung D, et al. Butyrate sensitizes human colon cancer cells to TRAIL-mediated apoptosis. - PubMed - NCBI. *Surgery.* 2001;130(2):265-72.
135. Ohara T, and Mori T. Antiproliferative Effects of Short-chain Fatty Acids on Human Colorectal Cancer Cells via Gene Expression Inhibition. *Anticancer Res.* 2019;39(9):4659-66.

136. Sivaprakasam S, Gurav A, Paschall AV, Coe GL, Chaudhary K, Cai Y, et al. An essential role of Ffar2 (Gpr43) in dietary fibre-mediated promotion of healthy composition of gut microbiota and suppression of intestinal carcinogenesis. *Oncogenesis.* 2016;5(6):e238.
137. Sze MA, Topcuoglu BD, Lesniak NA, Ruffin MTt, and Schloss PD. Fecal Short-Chain Fatty Acids Are Not Predictive of Colonic Tumor Status and Cannot Be Predicted Based on Bacterial Community Structure. *MBio.* 2019;10(4).
138. Begley M, Gahan CG, and Hill C. The interaction between bacteria and bile. *FEMS Microbiol Rev.* 2005;29(4):625-51.
139. Islam K, Fukiya S, Hagio M, Fujii N, Ishizuka S, Ooka T, et al. Bile acid is a host factor that regulates the composition of the cecal microbiota in rats. *Gastroenterology.* 2011;141(5):1773-81.
140. Ridlon J, Kang D, and Hylemon P. Bile salt biotransformations by human intestinal bacteria. *J Lipid Res.* 2006;47(2):241-59.
141. Ou J, DeLany J, Zhang M, Sharma S, and O'Keefe S. Association between low colonic short-chain fatty acids and high bile acids in high colon cancer risk populations. *Nutr Cancer.* 2012;64(1):34-40.
142. Louis P, Hold GL, and Flint HJ. The gut microbiota, bacterial metabolites and colorectal cancer. *Nat Rev Microbiol.* 2014;12(10):661-72.
143. Reddy BS, Hanson D, Mangat S, Mathews L, Sbaschnig M, Sharma C, et al. Effect of high-fat, high-beef diet and of mode of cooking of beef in the diet on fecal bacterial enzymes and fecal bile acids and neutral sterols. *J Nutr.* 1980;110(9):1880-7.
144. Payne CM, Weber C, Crowley-Skillicorn C, Dvorak K, Bernstein H, Bernstein C, et al. Deoxycholate induces mitochondrial oxidative stress and activates NF-kappaB through multiple mechanisms in HCT-116 colon epithelial cells. *Carcinogenesis.* 2007;28(1):215-22.
145. Venturi M, Hambly RJ, Glinghammar B, Rafter JJ, and Rowland IR. Genotoxic activity in human faecal water and the role of bile acids: a study using the alkaline comet assay. *Carcinogenesis.* 1997;18(12):2353-9.
146. Casellas F, Mourelle M, Papo M, Guarner F, Antolin M, Armengol JR, et al. Bile acid induced colonic irritation stimulates intracolonic nitric oxide release in humans. *Gut.* 1996;38(5):719-23.
147. Bernstein H, Bernstein C, Payne CM, and Dvorak K. Bile acids as endogenous etiologic agents in gastrointestinal cancer. *World J Gastroenterol.* 2009;15(27):3329-40.
148. Pool-Zobel BL, and Leucht U. Induction of DNA damage by risk factors of colon cancer in human colon cells derived from biopsies. *Mutat Res.* 1997;375(2):105-15.
149. Reddy BS, Narasawa T, Weisburger JH, and Wynder EL. Promoting effect of sodium deoxycholate on colon adenocarcinomas in germfree rats. *J Natl Cancer Inst.* 1976;56(2):441-2.
150. Magnuson BA, Carr I, and Bird RP. Ability of Aberrant Crypt Foci Characteristics to Predict Colonic Tumor Incidence in Rats Fed Cholic Acid. *Cancer Research.* 1993;53(19):4499-504.
151. Cao H, Xu M, Dong W, Deng B, Wang S, Zhang Y, et al. Secondary bile acid-induced dysbiosis promotes intestinal carcinogenesis. *Int J Cancer.* 2017;140(11):2545-56.
152. Cheng K, and Raufman JP. Bile acid-induced proliferation of a human colon cancer cell line is mediated by transactivation of epidermal growth factor receptors. *Biochem Pharmacol.* 2005;70(7):1035-47.

153. Pai R, Tarnawski AS, and Tran T. Deoxycholic acid activates beta-catenin signaling pathway and increases colon cell cancer growth and invasiveness. *Mol Biol Cell.* 2004;15(5):2156-63.
154. Liu L, Dong W, Wang S, Zhang Y, Liu T, Xie R, et al. Deoxycholic acid disrupts the intestinal mucosal barrier and promotes intestinal tumorigenesis. *Food Funct.* 2018;9(11):5588-97.
155. Dong W, Liu L, Dou Y, Xu M, Liu T, Wang S, et al. Deoxycholic acid activates epidermal growth factor receptor and promotes intestinal carcinogenesis by ADAM17-dependent ligand release. *J Cell Mol Med.* 2018;22(9):4263-73.
156. Cook JW, Kennaway EL, and Kennaway NM. Production of Tumours in Mice by Deoxycholic Acid. *Nature.* 1940;145:627.
157. De Robertis M, Massi E, Poeta ML, Carotti S, Morini S, Cecchetelli L, et al. The AOM/DSS murine model for the study of colon carcinogenesis: From pathways to diagnosis and therapy studies. *J Carcinog.* 2011;10:9.
158. Chassaing B, Aitken JD, Malleshappa M, and Vijay-Kumar M. Dextran Sulfate Sodium (DSS)-Induced Colitis in Mice. *Curr Protoc Immunol.* 2014;104.
159. Neufert C, Becker C, and Neurath MF. An inducible mouse model of colon carcinogenesis for the analysis of sporadic and inflammation-driven tumor progression. *Nat Protoc.* 2007;2(8):1998-2004.
160. Zhan Y, Chen PJ, Sadler WD, Wang F, Poe S, Nunez G, et al. Gut microbiota protects against gastrointestinal tumorigenesis caused by epithelial injury. *Cancer Res.* 2013;73(24):7199-210.
161. Greten FR, Eckmann L, Greten TF, Park JM, Li ZW, Egan LJ, et al. IKKbeta links inflammation and tumorigenesis in a mouse model of colitis-associated cancer. *Cell.* 2004;118(3):285-96.
162. Suzuki R, Kohno H, Sugie S, and Tanaka T. Sequential observations on the occurrence of preneoplastic and neoplastic lesions in mouse colon treated with azoxymethane and dextran sodium sulfate. *Cancer Sci.* 2004;95(9):721-7.
163. Hehemann JH, Kelly AG, Pudlo NA, Martens EC, and Boraston AB. Bacteria of the human gut microbiome catabolize red seaweed glycans with carbohydrate-active enzyme updates from extrinsic microbes. *Proc Natl Acad Sci U S A.* 2012;109(48):19786-91.
164. Ze X, Duncan SH, Louis P, and Flint HJ. Ruminococcus bromii is a keystone species for the degradation of resistant starch in the human colon. *Isme j.* 2012;6(8):1535-43.
165. Chen GY, Shaw MH, Redondo G, and Núñez G. The innate immune receptor Nod1 protects the intestine from inflammation-induced tumorigenesis. *Cancer Res.* 2008;68(24):10060-7.
166. Segata N, Izard J, Waldron L, Gevers D, Miropolsky L, Garrett WS, et al. Metagenomic biomarker discovery and explanation. *Genome Biol.* 2011;12(6):R60.
167. White J, Nagarajan N, and Pop M. Statistical Methods for Detecting Differentially Abundant Features in Clinical Metagenomic Samples. *PLoS Comput Biol.* 2009.
168. Excoffier L, Smouse PE, and Quattro JM. Analysis of molecular variance inferred from metric distances among DNA haplotypes: application to human mitochondrial DNA restriction data. *Genetics.* 1992;131(2):479-91.
169. Zhan Y, Seregin SS, Chen J, and Chen GY. Nod1 Limits Colitis-Associated Tumorigenesis by Regulating IFN-gamma Production. *J Immunol.* 2016;196(12):5121-9.

170. Chassaing B, Srinivasan G, Delgado MA, Young AN, Gewirtz AT, and Vijay-Kumar M. Fecal lipocalin 2, a sensitive and broadly dynamic non-invasive biomarker for intestinal inflammation. *PLoS One.* 2012;7(9):e44328.
171. Yue JC, and Clayton MK. A Similarity Measure Based on Species Proportions. *Communications in Statistics - Theory and Methods.* 2006;34(11):2123-31.
172. Langille MGI, Zaneveld J, Caporaso JG, McDonald D, Knights D, Reyes JA, et al. Predictive functional profiling of microbial communities using 16S rRNA marker gene sequences. *Nat Biotechnol.* 2013;31(9):814-21.
173. Kwong LN, and Dove WF. APC and its modifiers in colon cancer. *Adv Exp Med Biol.* 2009;656:85-106.
174. Hoy YE, Bik EM, Lawley TD, Holmes SP, Monack DM, Theriot JA, et al. Variation in Taxonomic Composition of the Fecal Microbiota in an Inbred Mouse Strain across Individuals and Time. *PLoS One.* 2015;10(11):e0142825.
175. Rogers GB, Kozlowska J, Keeble J, Metcalfe K, Fao M, Dowd SE, et al. Functional divergence in gastrointestinal microbiota in physically-separated genetically identical mice. *Sci Rep.* 2014;4:5437.
176. Keubler LM, Buettner M, Häger C, and Bleich A. A Multihit Model: Colitis Lessons from the Interleukin-10–deficient Mouse. *Inflamm Bowel Dis.* 2015;21(8):1967-75.
177. Yang I, Eibach D, Kops F, Brenneke B, Woltemate S, Schulze J, et al. Intestinal microbiota composition of interleukin-10 deficient C57BL/6J mice and susceptibility to Helicobacter hepaticus-induced colitis. *PLoS One.* 2013;8(8):e70783.
178. Hufeldt MR, Nielsen DS, Vogensen FK, Midtvedt T, and Hansen AK. Variation in the gut microbiota of laboratory mice is related to both genetic and environmental factors. *Comp Med.* 2010;60(5):336-47.
179. Ivanov, II, Frutos Rde L, Manel N, Yoshinaga K, Rifkin DB, Sartor RB, et al. Specific microbiota direct the differentiation of IL-17-producing T-helper cells in the mucosa of the small intestine. *Cell Host Microbe.* 2008;4(4):337-49.
180. Caruso R, Ono M, Bunker ME, Nunez G, and Inohara N. Dynamic and Asymmetric Changes of the Microbial Communities after Cohousing in Laboratory Mice. *Cell Rep.* 2019;27(11):3401-12 e3.
181. Goodman SN, Fanelli D, and Ioannidis JP. What does research reproducibility mean? *Sci Transl Med.* 2016;8(341):341ps12.
182. Ivanov, II, Atarashi K, Manel N, Brodie EL, Shima T, Karaoz U, et al. Induction of intestinal Th17 cells by segmented filamentous bacteria. *Cell.* 2009;139(3):485-98.
183. Daft JG, Ptacek T, Kumar R, Morrow C, and Lorenz RG. Cross-fostering immediately after birth induces a permanent microbiota shift that is shaped by the nursing mother. *Microbiome.* 2015;3(1):17.
184. Ubeda C, Lipuma L, Gobourne A, Viale A, Leiner I, Equinda M, et al. Familial transmission rather than defective innate immunity shapes the distinct intestinal microbiota of TLR-deficient mice. *J Exp Med.* 2012;209(8):1445-56.
185. Ericsson AC, and Franklin CL. Manipulating the Gut Microbiota: Methods and Challenges. *ILAR J.* 2015;56(2):205-17.
186. Breiman L. Random Forests. *Machine Learning.* 2001(1):5-32.
187. Benjamini Y, and Yekutieli D. The control of the false discovery rate in multiple testing under dependency. *The Annals of Statistics.* 2001;29(4):1165-88.
188. Moore RJ, and Stanley D. *Clin Transl Immunology*. 2016:e92-.

189. Zackular JP, Baxter NT, Chen GY, and Schloss PD. Manipulation of the Gut Microbiota Reveals Role in Colon Tumorigenesis. *mSphere.* 2016;1(1).
190. Edgar R. Taxonomy annotation and guide tree errors in 16S rRNA databases. *PeerJ.* 2018;6.
191. Clarridge JE. Impact of 16S rRNA Gene Sequence Analysis for Identification of Bacteria on Clinical Microbiology and Infectious Diseases. *Clin Microbiol Rev.* 2004;17(4):840-62.
192. Robertson SJ, Lemire P, Maughan H, Goethel A, Turpin W, Bedrani L, et al. Comparison of Co-housing and Littermate Methods for Microbiota Standardization in Mouse Models: Cell Reports. *Cell Reports.* 2019;27(6):1910-9.
193. Surana N, and Kasper D. Moving beyond microbiome-wide associations to causal microbe identification. *Nature.* 2017;552(7684):244-7.
194. Seregin SS, Golovchenko N, Schaf B, Chen J, Pudlo NA, Mitchell J, et al. NLRP6 protects IL10−/− mice from colitis by limiting colonization of Akkermansia muciniphila. *Cell Rep.* 2017;19(4):733-45.
195. Morgan XC, Tickle TL, Sokol H, Gevers D, Devaney KL, Ward DV, et al. Dysfunction of the intestinal microbiome in inflammatory bowel disease and treatment. *Genome Biol.* 2012;13(9):R79.
196. Joossens M, Huys G, Cnockaert M, Preter VD, Verbeke K, Rutgeerts P, et al. Dysbiosis of the faecal microbiota in patients with Crohn's disease and their unaffected relatives. 2011.
197. Woese CR. Bacterial evolution. *Microbiol Rev.* 1987;51(2):221-71.
198. Belkaid Y, and Hand TW. Role of the microbiota in immunity and inflammation. *Cell.* 2014;157(1):121-41.
199. Honda K, and Littman DR. The microbiota in adaptive immune homeostasis and disease. *Nature.* 2016;535(7610):75.
200. Thaiss CA, Zmora N, Levy M, and Elinav E. The microbiome and innate immunity. *Nature.* 2016;535(7610):65.
201. Macpherson AJ, and Harris NL. Interactions between commensal intestinal bacteria and the immune system. *Nature Reviews Immunology.* 2004;4(6):478.
202. Atarashi K, Tanoue T, Ando M, Kamada N, Nagano Y, Narushima S, et al. Th17 Cell Induction by Adhesion of Microbes to Intestinal Epithelial Cells. *Cell.* 2015;163(2):367-80.
203. Mazmanian SK, Round JL, and Kasper DL. A microbial symbiosis factor prevents intestinal inflammatory disease. *Nature.* 2008;453(7195):620-5.
204. Round JL, and Mazmanian SK. Inducible Foxp3+ regulatory T-cell development by a commensal bacterium of the intestinal microbiota. *Proc Natl Acad Sci U S A.* 2010;107(27):12204-9.
205. Kennedy EA, King KY, and Baldridge MT. Mouse Microbiota Models: Comparing Germ-Free Mice and Antibiotics Treatment as Tools for Modifying Gut Bacteria. *Front Physiol.* 2018;9.
206. Abt MC, Osborne LC, Monticelli LA, Doering TA, Alenghat T, Sonnenberg GF, et al. Commensal Bacteria Calibrate the Activation Threshold of Innate Antiviral Immunity. *Immunity.* 2012;37(1):158-70.
207. Toubai T, Fujiwara H, Rossi C, Riwes M, Tamaki H, Zajac C, et al. Host NLRP6 exacerbates graft-versus-host disease independent of gut microbial composition. *Nature Microbiology.* 2019;4(5):800-12.

208. Becker C, Fantini MC, Schramm C, Lehr HA, Wirtz S, Nikolaev A, et al. TGF-beta suppresses tumor progression in colon cancer by inhibition of IL-6 trans-signaling. *Immunity.* 2004;21(4):491-501.
209. Staley C, Kaiser T, Beura LK, Hamilton MJ, Weingarden AR, Bobr A, et al. Stable engraftment of human microbiota into mice with a single oral gavage following antibiotic conditioning. *Microbiome.* 2017;5.
210. Ben-Sasson SZ, Wang K, Cohen J, and Paul WE. IL-1beta strikingly enhances antigen-driven CD4 and CD8 T-cell responses. *Cold Spring Harb Symp Quant Biol.* 2013;78:117-24.
211. Brzoza KL, Rockel AB, and Hiltbold EM. Cytoplasmic entry of Listeria monocytogenes enhances dendritic cell maturation and T cell differentiation and function. *J Immunol.* 2004;173(4):2641-51.
212. Curtsinger JM, Schmidt CS, Mondino A, Lins DC, Kedl RM, Jenkins MK, et al. Inflammatory cytokines provide a third signal for activation of naive CD4+ and CD8+ T cells. *J Immunol.* 1999;162(6):3256-62.
213. Trinchieri G. Interleukin-12: a cytokine at the interface of inflammation and immunity. *Adv Immunol.* 1998;70:83-243.
214. Mager LF, Wasmer MH, Rau TT, and Krebs P. Cytokine-Induced Modulation of Colorectal Cancer. *Front Oncol.* 2016;6.
215. Castro F, Cardoso AP, Goncalves RM, Serre K, and Oliveira MJ. Interferon-Gamma at the Crossroads of Tumor Immune Surveillance or Evasion. *Front Immunol.* 2018;9:847.
216. Wherry EJ, Blattman JN, Murali-Krishna K, Most Rvd, and Ahmed R. Viral Persistence Alters CD8 T-Cell Immunodominance and Tissue Distribution and Results in Distinct Stages of Functional Impairment. *J Virol.* 2003;77(8):4911-27.
217. Wherry EJ, and Ahmed R. Memory CD8 T-Cell Differentiation during Viral Infection. *J Virol.* 2004;78(11):5535-45.
218. Baitsch L, Baumgaertner P, Devevre E, Raghav SK, Legat A, Barba L, et al. Exhaustion of tumor-specific CD8(+) T cells in metastases from melanoma patients. *J Clin Invest.* 2011;121(6):2350-60.
219. Lee PP, Yee C, Savage PA, Fong L, Brockstedt D, Weber JS, et al. Characterization of circulating T cells specific for tumor-associated antigens in melanoma patients. *Nature Medicine.* 1999;5(6):677-85.
220. Grosso JF, Goldberg MV, Getnet D, Bruno TC, Yen H-R, Pyle KJ, et al. Functionally Distinct LAG-3 and PD-1 Subsets on Activated and Chronically Stimulated CD8 T Cells. *J Immunol.* 2009;182(11):6659-69.
221. Sakuishi K, Apetoh L, Sullivan JM, Blazar BR, Kuchroo VK, and Anderson AC. Targeting Tim-3 and PD-1 pathways to reverse T cell exhaustion and restore anti-tumor immunity. *J Exp Med.* 2010;207(10):2187-94.
222. Matsuzaki J, Gnjatic S, Mhawech-Fauceglia P, Beck A, Miller A, Tsuji T, et al. Tumor-infiltrating NY-ESO-1-specific CD8+ T cells are negatively regulated by LAG-3 and PD-1 in human ovarian cancer. *Proc Natl Acad Sci U S A.* 2010;107(17):7875-80.
223. Fourcade J, Sun Z, Benallaoua M, Guillaume P, Luescher IF, Sander C, et al. Upregulation of Tim-3 and PD-1 expression is associated with tumor antigen-specific CD8+ T cell dysfunction in melanoma patients. *J Exp Med.* 2010;207(10):2175-86.

224. Le Roy T, Debédat J, Marquet F, Da-Cunha C, Ichou F, Guerre-Millo M, et al. Comparative Evaluation of Microbiota Engraftment Following Fecal Microbiota Transfer in Mice Models: Age, Kinetic and Microbial Status Matter. *Front Microbiol.* 2018;9.
225. Shen TC, Albenberg L, Bittinger K, Chehoud C, Chen YY, Judge CA, et al. Engineering the gut microbiota to treat hyperammonemia. *J Clin Invest.* 2015;125(7):2841-50.
226. Sivan A, Corrales L, Hubert N, Williams JB, Aquino-Michaels K, Earley ZM, et al. Commensal Bifidobacterium promotes antitumor immunity and facilitates anti-PD-L1 efficacy. *Science.* 2015;350(6264):1084-9.
227. Levy M, Thaiss CA, and Elinav E. Metabolites: messengers between the microbiota and the immune system. *Genes Dev.* 2016;30(14):1589-97.
228. Kim CH. Immune regulation by microbiome metabolites. *Immunology.* 2018;154(2):220-9.
229. Smith PM, Howitt MR, Panikov N, Michaud M, Gallini CA, Bohlooly YM, et al. The microbial metabolites, short-chain fatty acids, regulate colonic Treg cell homeostasis. *Science.* 2013;341(6145):569-73.
230. Bhattacharya N, Yuan R, Prestwood TR, Penny HL, DiMaio MA, Reticker-Flynn NE, et al. Normalizing Microbiota-Induced Retinoic Acid Deficiency Stimulates Protective CD8(+) T Cell-Mediated Immunity in Colorectal Cancer. *Immunity.* 2016;45(3):641-55.
231. Powrie F, Leach MW, Mauze S, Menon S, Caddle LB, and Coffman RL. Inhibition of Th1 responses prevents inflammatory bowel disease in scid mice reconstituted with CD45RBhi CD4+ T cells. *Immunity.* 1994;1(7):553-62.
232. Edin S, Kaprio T, Hagstrom J, Larsson P, Mustonen H, Bockelman C, et al. The Prognostic Importance of CD20(+) B lymphocytes in Colorectal Cancer and the Relation to Other Immune Cell subsets. *Sci Rep.* 2019;9(1):19997.
233. Nelson BH. CD20+ B cells: the other tumor-infiltrating lymphocytes. *J Immunol.* 2010;185(9):4977-82.
234. Meshcheryakova A, Tamandl D, Bajna E, Stift J, Mittlboeck M, Svoboda M, et al. B cells and ectopic follicular structures: novel players in anti-tumor programming with prognostic power for patients with metastatic colorectal cancer. *PLoS One.* 2014;9(6):e99008.
235. Garaud S, Buisseret L, Solinas C, Gu-Trantien C, de Wind A, Van den Eynden G, et al. Tumor infiltrating B-cells signal functional humoral immune responses in breast cancer. *JCI Insight.* 2019;5.
236. Nishikawa H, Tanida K, Ikeda H, Sakakura M, Miyahara Y, Aota T, et al. Role of SEREX-defined immunogenic wild-type cellular molecules in the development of tumor-specific immunity. *Proc Natl Acad Sci U S A.* 2001;98(25):14571-6.
237. Palm NW, de Zoete MR, Cullen TW, Barry NA, Stefanowski J, Hao L, et al. Immunoglobulin A coating identifies colitogenic bacteria in inflammatory bowel disease. *Cell.* 2014;158(5):1000-10.
238. Boissonnas A, Scholer-Dahirel A, Simon-Blancal V, Pace L, Valet F, Kissenpfennig A, et al. Foxp3+ T cells induce perforin-dependent dendritic cell death in tumor-draining lymph nodes. *Immunity.* 2010;32(2):266-78.
239. Cao X, Cai SF, Fehniger TA, Song J, Collins LI, Piwnica-Worms DR, et al. Granzyme B and perforin are important for regulatory T cell-mediated suppression of tumor clearance. *Immunity.* 2007;27(4):635-46.

240. Coutzac C, Adam J, Soularue E, Collins M, Racine A, Mussini C, et al. Colon Immune-Related Adverse Events: Anti-CTLA-4 and Anti-PD-1 Blockade Induce Distinct Immunopathological Entities. *J Crohns Colitis.* 2017;11(10):1238-46.
241. Soularue E, Lepage P, Colombel JF, Coutzac C, Faleck D, Marthey L, et al. Enterocolitis due to immune checkpoint inhibitors: a systematic review. *Gut.* 2018;67(11):2056-67.
242. Coker OO, Nakatsu G, Dai RZ, Wu WKK, Wong SH, Ng SC, et al. Enteric Fungal Microbiota Dysbiosis and Ecological Alterations in Colorectal Cancer. *Gut.* 2019;68(4).
243. G N, H Z, WKK W, SH W, OO C, Z D, et al. Alterations in Enteric Virome Are Associated With Colorectal Cancer and Survival Outcomes. *Gastroenterology.* 2018;155(2).
244. C L, L X, X Y, H M, N L, R Z, et al. Dysbiosis of Fungal Microbiota in the Intestinal Mucosa of Patients With Colorectal Adenomas. *Scientific reports.* 2015;5.
245. GD H, MB D, MT R, CC K, and PD S. Diagnostic Potential and Interactive Dynamics of the Colorectal Cancer Virome. *mBio.* 2018;9(6).
246. JM N, SA H, MT B, L D, CY L, BC K, et al. Disease-specific Alterations in the Enteric Virome in Inflammatory Bowel Disease. *Cell.* 2015;160(3).
247. L G, K B, R B, B H, DG B, C H-G, et al. Expansion of Bacteriophages Is Linked to Aggravated Intestinal Inflammation and Colitis. *Cell Host Microbe.* 2019;25(2).
248. Qiu X, Zhang F, Yang X, Wu N, Jiang W, Li X, et al. Changes in the composition of intestinal fungi and their role in mice with dextran sulfate sodium-induced colitis. *Scientific Reports.* 2015;5(1):1-12.
249. SF C, PIH MMA, L M, and HM N. Identification of Schizosaccharomyces pombe in the Guts of Healthy Individuals and Patients With Colorectal Cancer: Preliminary Evidence From a Gut Microbiome Secretome Study. *Gut Pathogens.* 2018;10.
250. Chassaing B, Koren O, Goodrich J, Poole A, Srinivasan S, Ley RE, et al. Dietary emulsifiers impact the mouse gut microbiota promoting colitis and metabolic syndrome. *Nature.* 2015;519(7541):92-6.
251. Earle KA, Billings G, Sigal M, Lichtman JS, Hansson GC, Elias JE, et al. Quantitative Imaging of Gut Microbiota Spatial Organization. *Cell Host Microbe.* 2015;18(4):478-88.
252. Tropini C, Earle KA, Huang KC, and Sonnenburg JL. The gut microbiome: Connecting spatial organization to function. *Cell Host Microbe.* 2017;21(4):433-42.
253. Cong Y, Brandwein SL, McCabe RP, Lazenby A, Birkenmeier EH, Sundberg JP, et al. CD4+ T cells reactive to enteric bacterial antigens in spontaneously colitic C3H/HeJBir mice: increased T helper cell type 1 response and ability to transfer disease. *J Exp Med.* 1998;187(6):855-64.
254. Sorini C, Cardoso RF, Gagliani N, and Villablanca EJ. Commensal Bacteria-Specific CD4+ T Cell Responses in Health and Disease. *Front Immunol.* 2018;9.
255. Muller S, Lory J, Corazza N, Griffiths GM, Z'Graggen K, Mazzucchelli L, et al. Activated CD4+ and CD8+ cytotoxic cells are present in increased numbers in the intestinal mucosa from patients with active inflammatory bowel disease. *Am J Pathol.* 1998;152(1):261-8.
256. Nancey S, Holvoet S, Graber I, Joubert G, Philippe D, Martin S, et al. CD8+ cytotoxic T cells induce relapsing colitis in normal mice. *Gastroenterology.* 2006;131(2):485-96.
257. Punit S, Dube PE, Liu CY, Girish N, Washington MK, and Polk DB. Tumor Necrosis Factor Receptor 2 Restricts the Pathogenicity of CD8(+) T Cells in Mice With Colitis. *Gastroenterology.* 2015;149(4):993-1005 e2.

258. Westendorf AM, Fleissner D, Deppenmeier S, Gruber AD, Bruder D, Hansen W, et al. Autoimmune-mediated intestinal inflammation-impact and regulation of antigen-specific CD8+ T cells. *Gastroenterology.* 2006;131(2):510-24.
259. Li Q, Teitz-Tennenbaum S, Donald EJ, Li M, and Chang AE. In vivo sensitized and in vitro activated B cells mediate tumor regression in cancer adoptive immunotherapy. *J Immunol.* 2009;183(5):3195-203.
260. Lundy SK. Killer B lymphocytes: the evidence and the potential. *Inflamm Res.* 2009;58(7):345-57.
261. Brandtzaeg P, Carlsen HS, and Halstensen TS. The B-cell system in inflammatory bowel disease. *Adv Exp Med Biol.* 2006;579:149-67.
262. Castro-Dopico T, Dennison TW, Ferdinand JR, Mathews RJ, Fleming A, Clift D, et al. Anti-commensal IgG Drives Intestinal Inflammation and Type 17 Immunity in Ulcerative Colitis. *Immunity.* 2019;50(4):1099-114.e10.
263. Gopalakrishnan V, Spencer CN, Nezi L, Reuben A, Andrews MC, Karpinets TV, et al. Gut microbiome modulates response to anti-PD-1 immunotherapy in melanoma patients. *Science.* 2018;359(6371):97-103.
264. Routy B, Le Chatelier E, Derosa L, Duong CPM, Alou MT, Daillere R, et al. Gut microbiome influences efficacy of PD-1-based immunotherapy against epithelial tumors. *Science.* 2018;359(6371):91-7.
265. Chaput N, Lepage P, Coutzac C, Soularue E, Le Roux K, Monot C, et al. Baseline gut microbiota predicts clinical response and colitis in metastatic melanoma patients treated with ipilimumab. *Ann Oncol.* 2017;28(6):1368-79.
266. Gong J, Chehrazi-Raffle A, Placencio-Hickok V, Guan M, Hendifar A, and Salgia R. The gut microbiome and response to immune checkpoint inhibitors: preclinical and clinical strategies. *Clin Transl Med.* 2019;8.
267. Yu AI, Zhao L, Eaton KA, Ho S, Chen J, Poe S, et al. Gut Microbiota Modulate CD8 T Cell Responses to Influence Colitis-Associated Tumorigenesis. *Cell Rep.* 2020;31(1):107471.